THE SPATIOTEMPORAL STUDY

OF

ZEBRAFISH INTESTINAL EPITHELIUM RENEWAL

SAHAR TAVAKOLI

(M. Eng., IUT)

(B.Eng., IUT)

A THESIS SUBMITTED

FOR THE DEGREE OF DOCTOR OF PHILOSOPHY

DEPARTMENT OF BIOLOGICAL SCIENCES

NATIONAL UNIVERSITY OF SINGAPORE

2013

Declaration

I hereby declare that this thesis is my original work and it has been written by me in its entirety. I have duly acknowledged all the sources of information which have been used in the thesis.

This thesis has also not been submitted for any degree in any university previously.

_____

Sahar Tavakoli

23 August 2013

Acknowledgements

One of the joys of completion is to look over the past journey and remember all professors, friends, and family who have helped and supported me along this long but fulfilling road.

Give a man a fish and you feed him for a day. Teach a man to fish and you feed him for a lifetime. I would like to express my heartfelt gratitude to my supervisor, Professor Paul Matsudaira for his patience, knowledge, insight, involvement, and supports. I could not be prouder of my academic roots and hope that I can in turn pass on the research values and dreams that he has given to me.

I would also like to thank my thesis committee, Professor Zhiyuan Gong and Professor Christoph Winkler, who have given unsparing help not only in encouraging and giving constructive feedback, but also in giving me the chance to be a part of their lab. Thank you.

Hereby, I would like to thank my international scientist collaborators: Dr. Albert Pan, Dr. Stefan Hans, and Dr. Vladimir Korzh for gifting me the zebrafish transgenic lines; and, Dr. Kiyoshi Naruse, and Dr. Nick Barker for gifting the fosmid and plasmid constructs.

To the staff and students in CBIS and MBI: Tong Yan, Dipanjan, Siew Ping, Keshma, Bee Ling, Hadisah, Al, Victor, Yosune, Bai Chang, Mas, Nikhil, Nicolas, Utkur, Duane, Zainul, Ai Kia, Shiwen, Ting Yuan, Gushu, Yuhri, Jiyun, Cheng Han, Jingyu, Cynthia, and Carol; In DBS: Reena, Pricilla, Laurence, Joan, Yan Tie, Flora, Zhengyuan, Shi Min, Li Zhen, Weiling, Huiqing, Anh Tuan, Zhou Li, Tina, Caixia, Grace, Joji, Xiaoqian, Xiaoyan, Zaho Ye, Yan Chuan, Divya, and Jianzhou; I am grateful for the chance to be a part of the department and lab. Thank you for welcoming me as a friend and helping to develop the ideas in this thesis. Also, I would like to thank Mr.

Balan, Mr. Qing Hua and Mr. Alex in the department's aquarium facility for their assistance whenever required

I would not have contemplated this road if not for my parents, Azam and Ali, who instilled within me a love of creative, pursuits, science, and patience—all of which finds a place in this thesis. To my parents, thank you. To my siblings: Sima, Sina and Soheil and sweet niece Tina, I would like to thank you for your continuous love and their supports on when times were rough. Without you, I could not have made it. This thesis would also not be possible without the love and support of my Iran-based family here, Bahar, Sepideh, Mahnaz, Shahrzad, Elham, Khatereh, and Shabnam, who gave me a home away from home.

Additionally, I would like to express my appreciation for Singapore International Graduate Award (SINGA), National University of Singapore (NUS), Centre for BioImaging Sciences (CBIS), and Mechanobiology Institute (MBI), for providing me the graduate research scholarship.

Table of Contents

SUMMARY

Specific characteristics of the intestine, such as fast self-renewal and its two-dimensional structures, provide a good opportunity to study adult stem cells and tissue renewal. The absence of a specific marker for zebrafish intestinal stem cells (ISCs) has left unanswered questions regarding intestinal epithelial renewal. Also, the absence of a stereotypic villus-crypt organization in this early vertebrate prompted us to investigate the nature of the zebrafish intestinal epithelium—its renewal in the spatiotemporal orientation and in a microscopic scale. We designed a series of different experimental techniques with specific advantages and limitations, concerning zebrafish intestinal epithelium renewal. First, we generated both the chimeric and mosaic zebrafish to examine the renewal pattern in the intestinal epithelium. To cope with the limitations of these techniques (temporal analysis), we designed the label retention experiments and studied the renewal duration and cell migration rate. Finally, to study the zebrafish intestinal epithelium renewal spatiotemporally (at the desired time and region), the Zebrabow transgenic line has been generated. We confirmed that the zebrafish ISCs are inhabited by the intervillus pockets. A group of ISCs at the intervillus bottom and

parallel to the villus tip reproduce new cells. The ribbons of the newly reproduced cells start their travel toward both flanking intestinal villi by completing their migration to the intestinal villus tip by 48 hours. As the sides of the adjacent intestinal villi flanking an intervillus pocket share the ISCs at the intervillus bottom, the adjacent intestinal villi show the similar recombination pattern. These ribbons of newly reproduced cells are temporarily reproduced by progenitor cells at the intervillus bottom. Interestingly, these ribbons later decreased in number and increased in width (with several rows of cells). These observations suggest the permanent reproduction of intestinal epithelial cells by dominant ISCs. Also, the interactions between the signaling pathways in an intestinal villus and the ISCs at the intervillus bottom induce the intestinal epithelium renewal pattern and migration rate, which will be discussed in detail in this thesis. Moreover, the results obtained through this project answered the questions regarding zebrafish intestinal epithelium renewal and introduced the future works for a better understanding of the zebrafish intestinal epithelium renewal and regeneration.

LIST OF TABLES

LIST OF FIGURES

Figure 4-12: Stripes of labeled cells travel toward the tip. Vertical stripes of labeled cells show the location of stem cells and their paths of migration to the ridge. Images A, B, C, D, E and F are the same frame but from sequential Z stacks. β-actin: GFP (Green) and β-actin: DsRed (Red). Scale bar = 50 μm.109

LIST OF ABBREVIATIONS

+ve	Positive
-ve	Negative
4-OHT	4-hydroxy-tamoxifen
Ascl1	Achaete-scute homolog 1
Bmi1	polycomb ring finger oncogene
BrdU	5-bromo-2'-deoxyuridine
CFP	Cyan Fluorescent Protein
CS	chromosome segregation
EdU	5-ethynyl-2´-deoxyuridine
dpf	day post fertilization
dpt	day post treatment
EMS	Ethyl methanesulfonate
ENU	*N*-ethyl-*N*-nitrosourea
f.o.i	fragment of interest
FP	Fluorescent Protein

GFP	Green Fluorescent Protein
hpf	hour post fertilization
hpt	hour post treatment
IACUC	Institutional Animal Care and Use Committee
IB	Intestinal Bulb
ISC	Intestinal Stem Cell
Lgr5	leucine rich repeat containing G protein coupled receptor 5
mGFP	membrane-localized Green Fluorescent Protein
px	pixel
RFP	Red Fluorescent Protein
SEM	Scanning Electron Microscope
TAC	Transit Amplifying Cell
TAM	Tamoxifen
YFP	Yellow Fluorescent Protein
YS	Yolk Sac
Wnt	wingless-type

Chapter 1

Introduction

The constancy of the internal environment is the condition for a free and independent life.

—Claude Bernard (1813 – 1878)

The concept of homeostasis (from the Greek *hómoios*, "similar," and *stásis*, "standing still") was first explored by Claude Bernard; subsequently, it was expanded by Walter Bradford Cannon (1871–1945) in his book T*he Wisdom of the Body* published in 1932:*"A condition which may vary, but which is relatively constant"* (Maton et al., 1993). Homeostatic imbalance causes many diseases and problems such as diabetes, gout, dehydration, and different types of cancers as well.

1. 1. Homeostasis studies in zebrafish

This simple animal model of a zebrafish provides an excellent platform for both molecular and structural homeostasis studies. The zebrafish, *Danio rerio* (a tropical freshwater fish) (Froese & Pauly, 2011), belongs to the Cyprinidae family of the order Cypriniformes. This early vertebrate animal model

becomes useful in developmental and cancer studies because of its numerous advantages (Mayden et al., 2007):

- Easy and cheap maintenance
- Full sequenced genetic code (Sachan, 2009)
- High fecundity
- Short generation interval (3–4 months)
- Rapid embryonic development
- Translucent embryos
- External fertilization (Dahm, 2006)
- Available zebrafish mutant strains

These unique features of zebrafish encourage scientists to model molecular mechanism of cancer using the zebrafish as a model species. External fertilization, as one of the most important traits, causes the production of a large number of eggs. In addition, this early vertebrate animal model eases developmental, gene function, stem cell, and structural homeostasis studies during the embryogenesis as well as adult stages. Adult stem cells, which are limited to their originated tissue, play a critical role in tissue homeostasis. As an example, the abnormal proliferation of intestinal stem cells (ISCs) causes the imbalanced intestinal epithelium (the inner layer of intestine and most digestive systems) homeostasis and consequently causes intestinal cancer.

1. 2. Intestine: architecture, function, and foundation for homeostasis

The intestine, compared with other organs, is an easy organ to study tissue renewal and adult stem cells because of its characteristics; first, intestinal epithelium turnover is fast. Whole epithelial cells are replaced by new cells every 3–5 days in different species (Barker, van de Wetering, & Clevers, 2008; Barker, van Oudenaarden, & Clevers, 2012; Dalal & Radhi, 2013; Langnas, Goulet, Quigley, & Tappenden, 2009; Lundgren, Jodal, Jansson, Ryberg, & Svensson, 2011). To support this fast renewal, stem cells of a crypt should generate at least 300 new cells per day in mice (Y. Q. Li, Roberts, Paulus, Loeffler, & Potten, 1994; Marshman, Booth, & Potten, 2002; Pinto & Clevers, 2005). Second, intestinal tissue has a two-dimensional structure, which forms villus-crypt structures (Heath, 1996; Sancho, Batlle, & Clevers, 2004; Schmidt, Garbutt, Wilkinson, & Ponder, 1985). In other words, intestinal epithelial is mostly like a sheet that shapes the villus structure with the help of other layers (H. J. Snippert et al., 2010).

The human intestine (or bowel or hose) is a part of the alimentary canal that starts from the stomach and continues to anus (Dorland, 2011). Mammalian intestines can be divided into the small (consists of duodenum, jejunum, and ileum), and large intestine (consist of the cecum and colon) according to their length, function and anatomical structure (H. Hans & Hedrich, 2004; Tank & Grant, 2012). Overall, the intestine plays a critical role in food digestion and subsequently in the absorption of released nutrients during digestion. Nutrients

are used by the body to provide energy, minerals, vitamins, and water for growth, body maintenance, metabolism, and injury recovery (Goldberg & Williams, 1991; Maton et al., 1993; Starr, 2013). To increase the absorption efficiency by increasing the overall surface, finger-like structures are developed from the mucosa and substantially by the epithelial layer, whereas these finger-like structures are absent in the large intestine. Also, the microvilli are present at the lumen surface of most of the intestinal epithelium cells to increase the absorption surface (Matsudaira & Burgess, 1982) (refer to 1. 3. 1. for detailed descriptions).

Crypts of Lieberkühn inhabit the ISCs and show a niche's features. The niche which provides a suitable microenvironment for stem cell activity, has a tight interaction with stem cells to regulate the newly reproduced cells' fate (Erturk et al., 2012) and subsequently regulate and maintain the tissue homeostasis (Chung et al., 2013).

The dominant signaling pathways along the crypt base to the villi tip are BMP, HH, and Wnt. The HH signaling at crypt induces the BMP signaling pathway in villus mesenchyme (Fig. 1-1). The negative feedback of BMP inhibits the Wnt signaling pathway, which is necessary for cell proliferation. However, presence of Noggin at the crypt base frustrates the BMP feedback at the crypt base region and defines the cell proliferation region at the crypt base (Clarke, 2006; Crosnier, Stamataki, & Lewis, 2006; Pinto & Clevers, 2005; Theodosiou & Tabin, 2003).

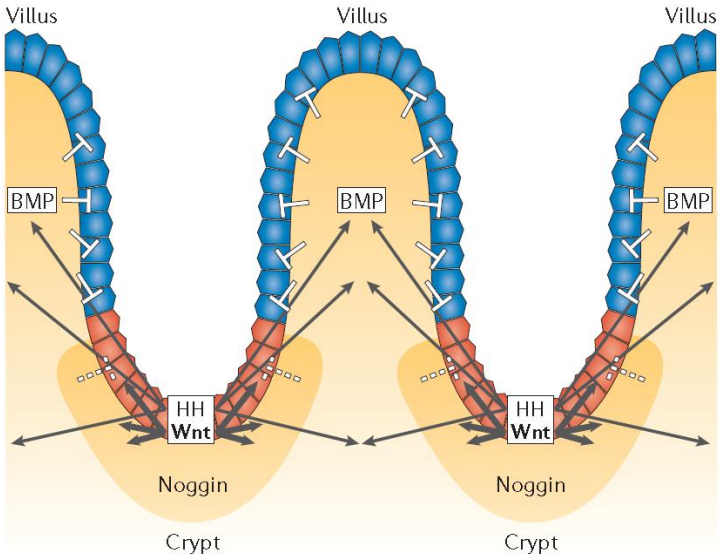

Figure 1-1: Interaction of signaling pathways along the villi base-to-tip axis (Crosnier et al., 2006). The only BMP signaling inhibitor in intestinal epithelial layer, Noggin, determines where the ISCs' niche is.

In summary, the intestinal epithelium life cycle is as follows:

1. Reproduction of new cells by progenitor cells at their intestinal niche, which is regulated by the Wnt signaling pathway
2. Differentiation of the newly reproduced cells to each of 4 epithelial differentiated cells based on cell fate decision, which is governed by the HH signaling pathway
3. Involvement of differentiated epithelial cells in food digestion and nutrient absorption during their short lifetime
4. Completion of translocation of the differentiated cells to the tip of the villus ridge in 3–5 days and shedding off to the intestinal tube by apoptosis

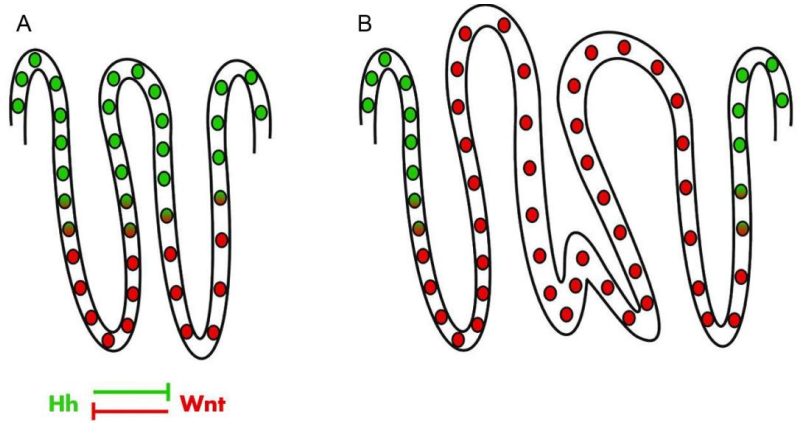

Figure 1-2: Active signaling pathways in an intestinal crypt. (A) A normal interaction between 2 signaling pathways regulates the proliferation and differentiation region in a crypt. (B) Abnormal activation of the Wnt signaling pathway in colon cancer causes nonstop cell proliferation (van den Brink & Hardwick, 2006).

Mutations in the Wnt signaling pathway disturb the balance between proliferation and death, which causes intestinal cancer formation (Fig. 1-2). In addition, as stem cells and transit amplifying cells are the only cells that divide in crypts, the mutation mainly affects these 2 batches of cells, which causes the continuous proliferation of transit amplifying cells (Humphries & Wright, 2008). Consequently, a mass of cells that are not able to leave the crypts and differentiate forms a large adenoma (Barker et al., 2008).

Different statistics reviews have been published regarding the incidence and death rate due to intestinal cancer based on race, country, age, sex, and culture (Table 1). However, intestinal cancer is rated among the top 3 most frequent cancers and as the second cancer killer after lung cancer (Hama et al., 2011).

Table 1-1: Incidence and death rate in 2005–2009 of all races from 18 geographic areas in the United States (Howell & Wells, 2011; Howlader et al., 2013).

		Male	Female
Incidence Rates	Small Intestine	2.4 per 100,000	1.7 per 100,000
	Colon and Rectum	54.0 per 100,000	40.2 per 100,000
Death Rates	Small Intestine	0.4 per 100,000	0.3 per 100,000
	Colon and Rectum	20.2 per 100,000	14.1 per 100,000

The intestine is the only source of nutrient absorption and, on the other hand, the intestinal cancer is among the most frequent cancers. Therefore, the lack of knowledge in this field encourages scientists to study the intestinal tissue. Therefore, we need to know the zebrafish intestine in detail and identify its differences with the intestines of other species. As the function and formation of the intestine in different species have been covered, below is a review on previous works to clarify the remaining gaps of knowledge on zebrafish intestinal renewal.

1. 3. Zebrafish intestine development

In most species, during embryogenesis, 3 different groups of cells develop the germ layers during gastrulation, from where the future organs originated (Dahm, 2006; Livet et al., 2007; Mundlos, 2009). However, gastrulation in

zebrafish starts 5 hours post fertilization (hpt) and with the formation of 2 layers of cells, the ectoderm and mesendoderm (Kimmel, Ballard, Kimmel, Ullmann, & Schilling, 1995; Thisse, Thisse, Schilling, & Postlethwait, 1993; Woo, Shih, & Fraser, 1995). Gradually, the mesendoderm gives rise to endoderm and mesoderm (Kimmel & Law, 1985). These 3 primary germ layers later give rise to all tissues and organs via organogenesis during the late developmental stages.

The endoderm, as the innermost layer (Gilbert, 2003), is the source of the entire gastrointestinal tract, a part of respiratory tract (trachea, bronchi, andalveoli), endocrine glands (the thymus and thyroid gland follicles), auditory system (the epithelium cells), and urinary system (the urinary bladder and a part of the urethra) (Woo et al., 1995; Zaret, 2001). Embryonic fate mapping in zebrafish demonstrates that predominantly endodermal cells at the dorsal and margin of the blastoderm form the future intestine (Warga & Nusslein-Volhard, 1999).

At day 1 after fertilization, a thin layer of endodermal cells continues from the mouth position to anus position. The intestinal lumen forms by epithelial development, and subsequently, so do the intestinal folds. In mammals, some finger-like structures (villi) form during the embryonic stages. Later, during the postnatal development, crypts are formed at the base of the villi in developed species such as mouse and human. In contrast to the stereotypic villus-crypt organization of the bird and mammalian intestines, the zebrafish

intestinal epithelium is developed into the intestinal ridge-shaped villi (Fig. 1-4C), and villus-crypt organization is absent (Crosnier et al., 2005; Faro, Boj, & Clevers, 2009; Muncan et al., 2007; Ng et al., 2005; Wallace, Akhter, Smith, Lorent, & Pack, 2005). However, it has been shown that similar to birds and mammalians, the dividing cells are still located at the base of the intestinal villus, and cell death occurs at or near the villus tip (Wang, Du, et al., 2010).

Figure 1-3 shows the multilevel folding to increase absorptive surfaces. The finger-like villi, are inhabited by circular folds. The third microscopic level of folding is represented by the microvilli, which are cellular membrane bulges and also exist in zebrafish intestinal epithelium (Pack, Solnica-Krezel, et al., 1996). The intestinal epithelium foldings slow down the passage of food and also increase the absorptive area of the intestine (P. Insel, 2010; P. M. Insel, Ross, McMahon, & Bernstein, 2013; Sherwood, 2010; Starr, Evers, & Starr, 2008; Walker, 2004). Figure 1-4 shows the scanning electron microscope (SEM) images of anterior part of zebrafish intestine. Interior view of zebrafish intestine shows the villi projection similar to those of mammals and birds (Fig. 1-4A). However, the villus has a different structure in zebrafish and shows a ridge-shaped structure (Fig. 1-4C). These ridge-shaped villi are oriented in different directions and usually in the form of a peak, which appear finger shape structure in vivo and in an unopened intestinal tube (Fig. 1-4A).

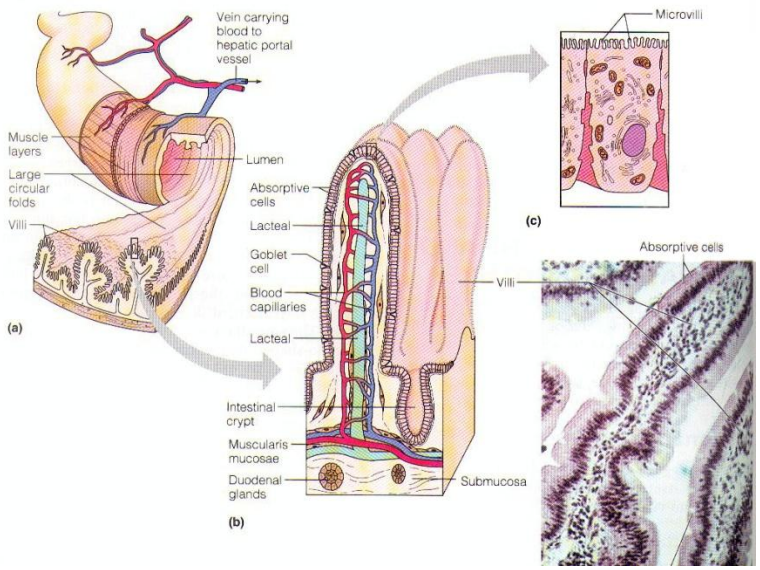

Figure 1-3: The structural layers of the mammalians small intestine: finger-like villi are inhabited by circular folds to increase the absorptive surfaces (http://jw1.nwnu.edu.cn/jpkc/jwc/2009jpkc/rtkx/jp.htm).

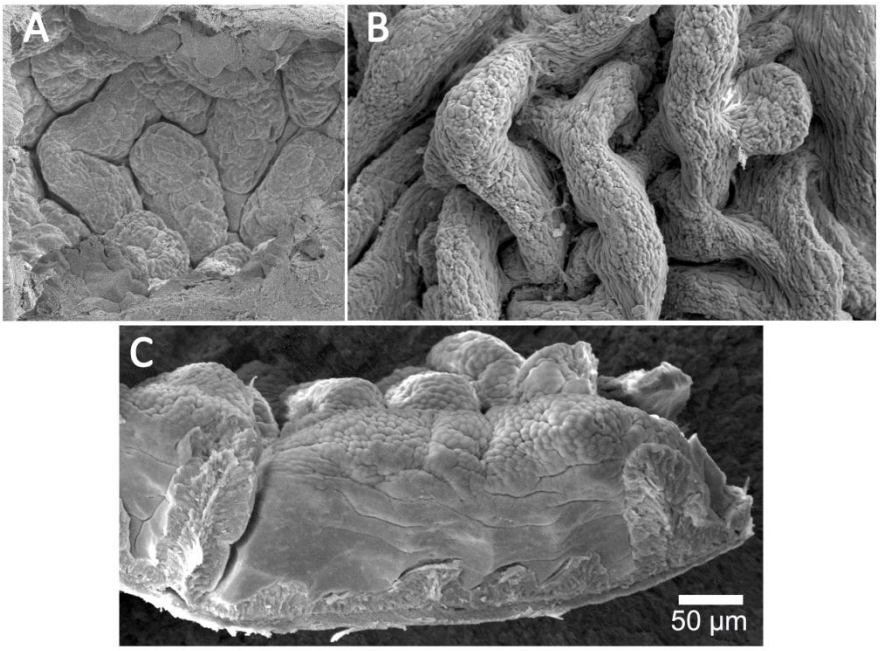

Figure 1-4: Scanning Electron Microscope (SEM) of anterior zebrafish intestine. (A) Interior view of zebrafish anterior intestine. The villar ridges usually form a peak on top and exhibit finger-shaped projections in a compact intestine. The villar ridges extend in random directions. (B) Top and (C) lateral view of zebrafish intestinal villi.

1. 3. 1. Developmental differences between zebrafish and other species

The zebrafish, an early vertebrate, shows basic differences in its digestion system. Being stomachless and having a short and simple Z-shaped intestine, which is hardly recognizable as the small or large intestine, are some of those differences at first glance (Kapoor, Smit, & Verighina, 1975; Pack, SolnicaKrezel, et al., 1996; Wang, Du, et al., 2010). Looking deeper, we can see another difference, which is the anatomical structure of the epithelial layer. As it has been explained previously, in most species, villi have a finger-like structure to increase the surface area. In contrast, the villi structure in zebrafish is absent.

Grey in 1972 and Burgess in 1975 examined chick embryo's duodenum and found it has a ridge-shaped structure in its initial structure. They found the previllus structures during the first 2 weeks of embryogenesis, which are formed from the intestinal villi too (Burgess, 1975; Grey, 1972). Twenty days later, the first projection of villi was observed in duodenum, and one day after hatching, the villi were well developed (Grey, 1972).

Besides, crypts of Lieberkühn, as the ISCs niche, are absent in zebrafish intestinal epithelium (Pack, SolnicaKrezel, et al., 1996; Sakamori et al., 2012; Wallace et al., 2005). Harder in 1975 for the first time reported the lack of crypts in zebrafish. Later in 1984, Rombout found that the zebrafish intestinal epithelium lacks the Paneth cells in neighboring proliferation cells (Rombout,

Stroband, & Tavernethiele, 1984). The 4 main types of mammalian intestinal epithelium cells are the enterocyte cells (absorptive cells), goblet cells (glandular and columnar epithelial cells that secrete mucin to form mucus by dissolving in water), enteroendocrine cells (a type of endocrine cells that produce different types of hormones), and Paneth cells (adjacent to ISCs to protect them) (Sancho, Batlle, & Clevers, 2003; Schonhoff, Giel-Moloney, & Leiter, 2004; Yang, Bermingham, Finegold, & Zoghbi, 2001); Meanwhile,the Paneth cells are absent in the zebrafish (Rombout et al., 1984; Wallace et al., 2005; Wallace & Pack, 2003).

Zebrafish intestine development during embryogenesis has been studied by Annie Ng et al. in 2005. They have divided the process into 3 steps and highlighted the developmental differences from other species (Ng et al., 2005):

1. 3. 2. Zebrafish temporal intestine development

I. **Lumen formation:** A thin layer of endoderm cells continue from the mouth position to anus during 0–52 hpf. Digestive tract development is initiated in the esophagus region and intestinal bulb and later ends in the intestinal tract. At the end of the first stage, the swim bladder and liver are differentiated from the ventral foregut endoderm (Fig. 1-5).

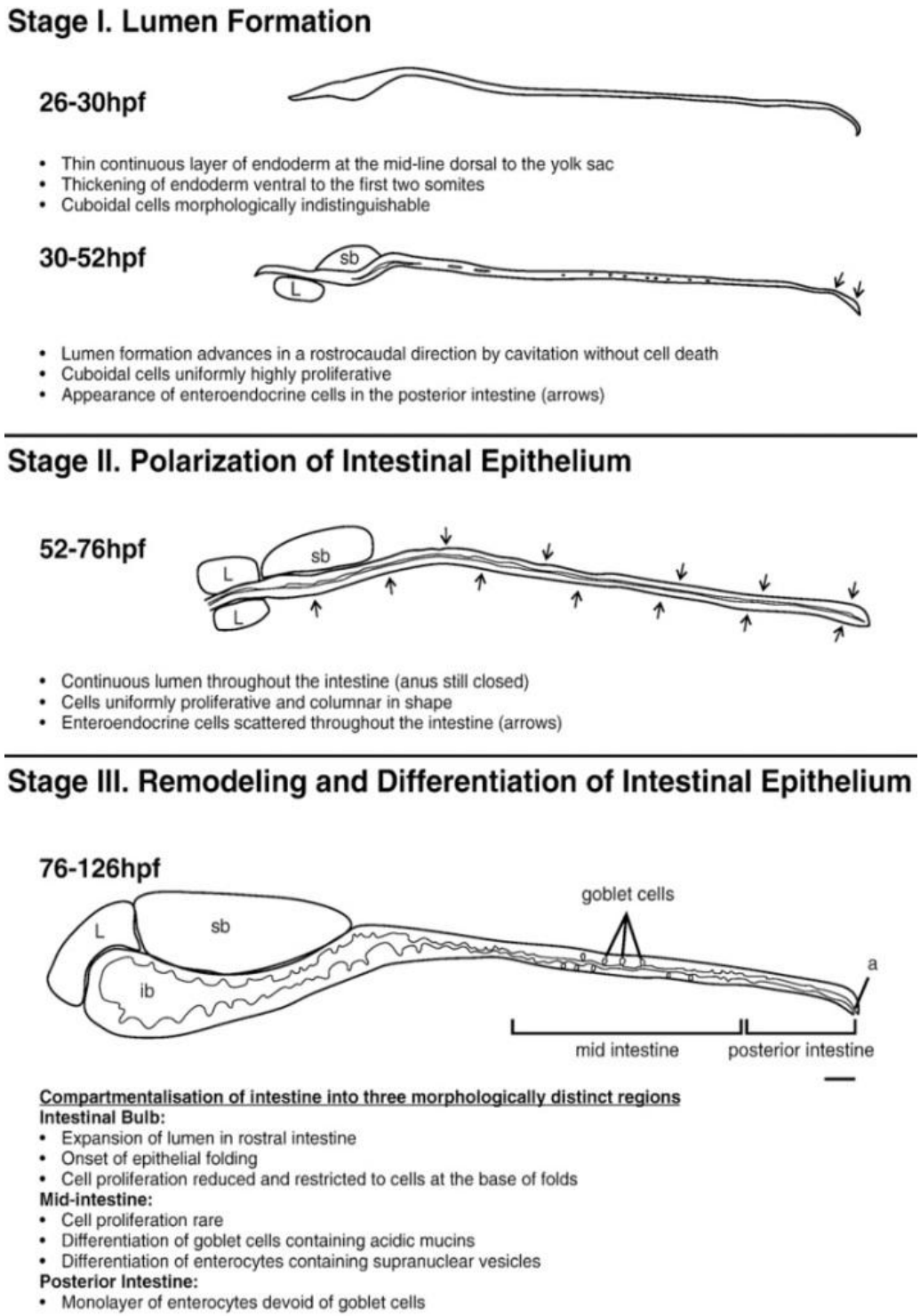

Figure 1-5: Zebrafish intestinal development during embryogenesis (Ng, de Jong-Curtain et al. 2005).

II. **Intestinal epithelium polarization:** The lumen converts to a columnar structure by the polarization of epithelial cells during 52–76 hpf. During 26–76 hpf zebrafish intestine exists in the peak of proliferation, and at the end of this stage, the intestinal tract is a hollow tube. However, the anus is still closed. The nuclei polarize at the base of the cells, and a thin layer of mesenchymal cells surrounds the intestinal tube.

III. **Remodeling and differentiation of intestinal epithelium:** During 76–126 hpf, cell proliferation decreases, and the epithelium layer forms the primary folds. In this stage, by opening the anus, the intestinal tube would be an open-ended tube and prepared for functioning. At the end of this stage, 3 different parts of the intestine (anterior, middle, and posterior) are recognizable. However, the epithelium layer is folded in the anterior part of the intestine,. In contrast, there is a single layer of cells in the posterior part, while the middle part is still undergoing cell differentiation (Ng et al., 2005).

1. 3. 3. Zebrafish intestine develops along rostrocaudal axis

Later in 2010, Wang et al. studied the zebrafish intestinal characters along the rostrocaudal axis and tried to analyze both the morphological and molecular

features of the different parts of the intestine. They divided the intestinal tube into 7 segments, which were equal in length and named S1–S7 (Fig. 1-6), and confirmed the lack of crypts in the zebrafish intestine (Wang, Du, et al., 2010). They discovered that the intestinal villi are intensely populated in the anterior intestine with highly organized extensions of intestinal villi. Toward the anus, the intestinal villi decrease in height, intensity, and the extensions appear shorter. The intestinal villi are completely absent in S7 (Fig. 1-6).

The DNA microarray analysis identified 2,558 active genes along the intestinal tube. Interestingly, Wang et al. at 2010 reported the hierarchical clustering that sorted the entire 7 segments consistency with their natural order of S1–S7 (Fig. 1-7A). The gene overlap analysis also confirmed these results (Fig. 1-7B). The first 5 segments showed a significant intersection and features of the mammalian small intestine. The transition segment, S5, appeared to be more similar to the anterior segment, S4. Finally, S6 (analogous to cecum) and S7 (analogous to rectum) intersect only 45.2% of genes. Even though the zebrafish intestine does not show any significant differences in appearance along the rostrocaudal axis to recognize the different parts of the intestinal tube similar to the small intestine and large intestine of mice and humans, it still carries different molecular makeup in its different parts along the rostrocaudal axis.

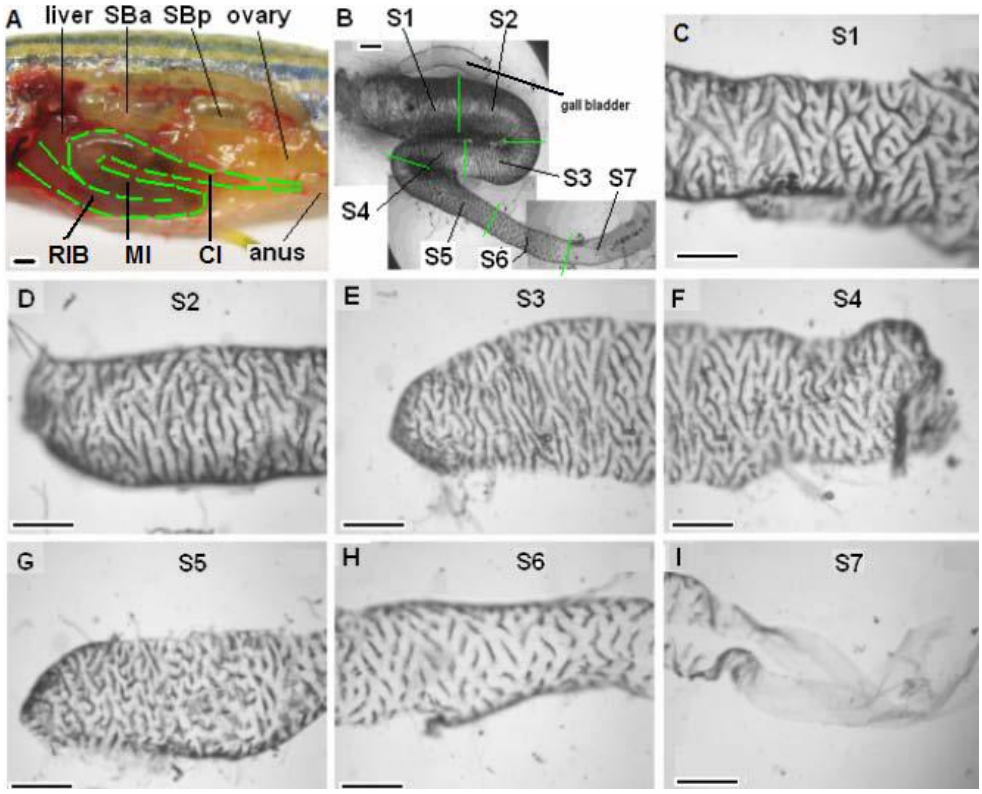

Figure 1-6: Morphology of 6-month-old zebrafish intestine. This figure also shows the segmentation pattern of S1–S7. RIB: rostral intestinal bulb; SBa/p: anterior/posterior swim bladder, MI: mid-intestine, CI: caudal intestine,scale bar = 500 μm (Wang, Du, et al., 2010).

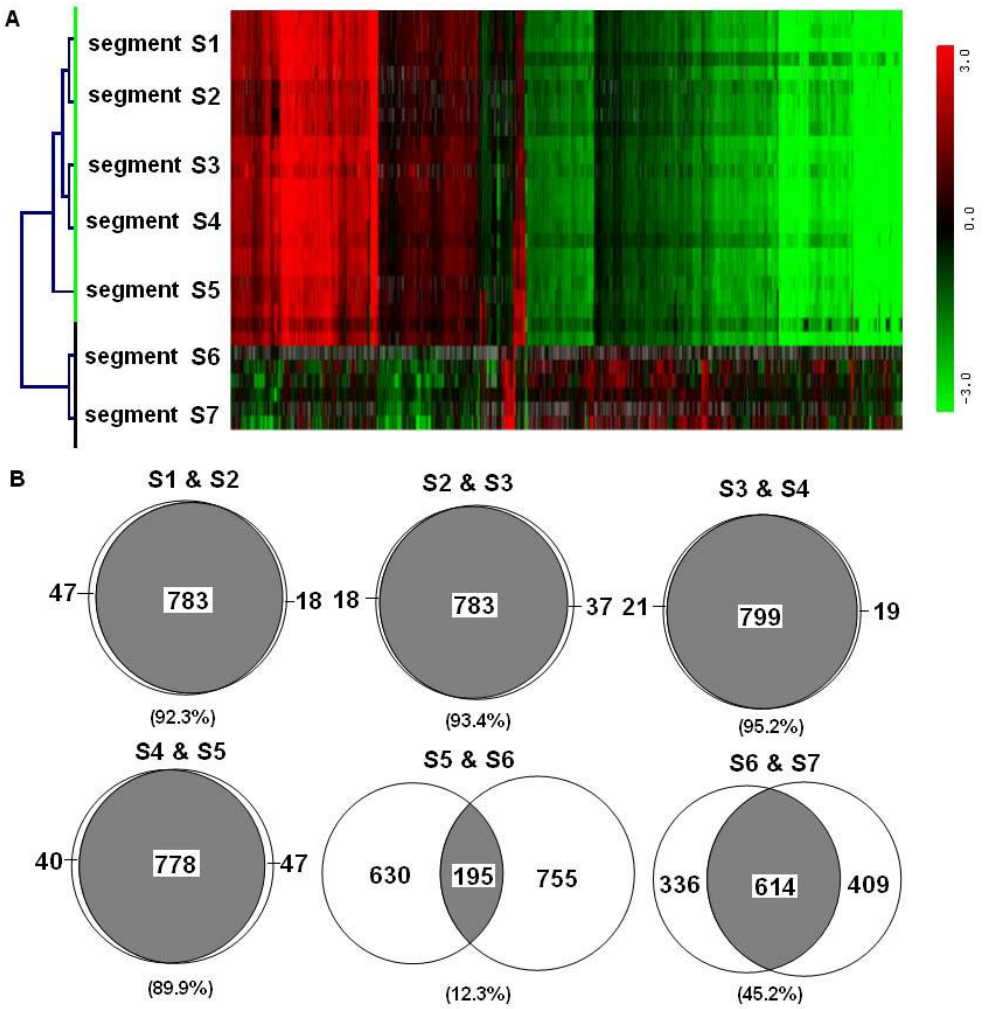

Figure 1-7: The DNA microarray analysis of S1–S7: (A) hierarchical clustering of the segments and (B) overlap analysis of the tandem segments (Wang, Du, et al., 2010).

Once the studies on embryonic stages of zebrafish intestinal development and on adult stages along the rostrocaudal axis were reviewed, next we review the Intestinal epithelium renewal.

1. 4. Intestinal epithelium renewal along the base-to-tip axis

Mammalian intestinal stem cells undergo dividing to reproduce the transit amplifying cells, which are the origin of all 4 types of the differentiated intestinal epithelial cells. The differentiated cells migrate along the crypt-villus Axis to reach to the villus tip and shed off (Bjerknes & Cheng, 1981b; van der Flier & Clevers, 2009). Similar to zebrafish, crypt is absent in amphibian too (Fig. 1-8). Also similar to those of mammalian the renewal is along the base-to-tip axis and the cells locating at the tip of the villus, which are old differentiated cells will shed off (Ishizuya-Oka, 2007).

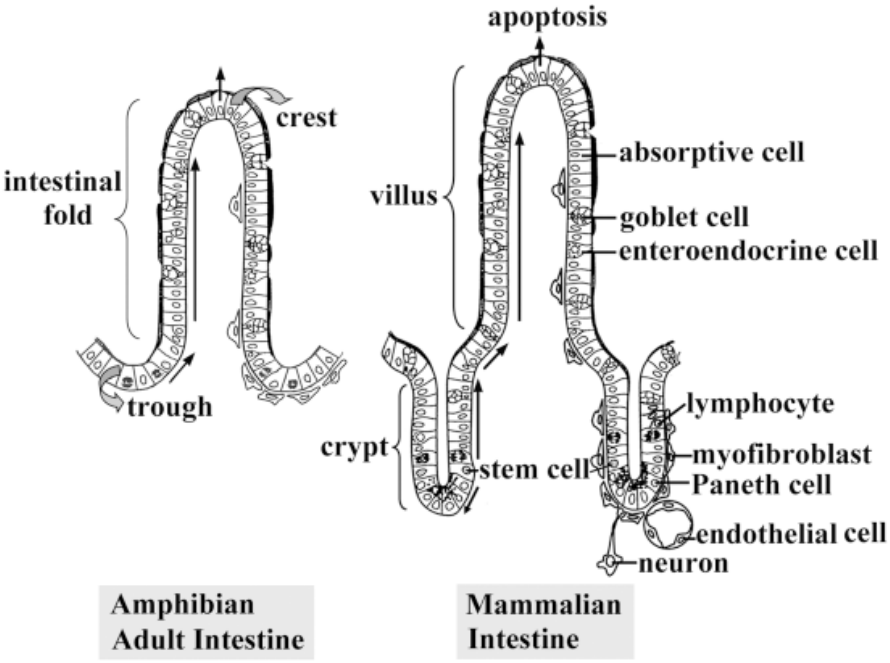

Figure 1-8: Intestinal epithelium renewal in adult amphibian and mammalian intestine. Similar to the mammalian intestine, the epithelial cells in amphibian intestine undergoes cell-renewal along the vertical axis from the base to the tip of the villus (Ishizuya-Oka, 2007).

It has also shown in zebrafish that the progenitor cells are locating at the inter-villus spaces and the old differentiated cells shed off at the tip of the villus (Crosnier et al., 2006; Ng et al., 2005; Wallace et al., 2005). However, the lack of knowledge of the dynamics, direction and duration of renewal pattern of the zebrafish intestinal epithelium along the base-to-tip axis of the villus is obvious. Here, we review the intestinal homeostasis and the different techniques to analyze the zebrafsh intestinal homeostasis in our current study.

1. 5. Localization of intestinal stem cells (ISCs) in mammalians

Cheng and Leblond in 1974 showed that intestinal epithelium undifferentiated cells are the origin of 4 main types of cells of epithelial tissue in the intestine (Cheng & Leblond, 1974). They assumed these undifferentiated cells are ISCs. Previously, Merzel and Leblond showed that undifferentiated cells are able to renew and maintain themselves and also to differentiate to epithelial cells (Merzel & Leblond, 1969). However, they introduced them as oligomucous cells (origination of intestinal goblet cells) and not stem cells as the number of labeled cells was not enough for intestinal epithelium turnover. Later Bjerknes and Cheng approved the idea of the existence of ISCs as they showed the 2 main properties of stem cells: first, the ability of 4 main differentiated intestinal epithelial cells to reproduce; and second, the ability of self-renewal

over the organism's life time (Bjerknes & Cheng, 1981a, 1999). However, there are different hypotheses about the exact location and number of the stem cells (Fig. 1-9). The "+4 position," or LRC (label-retaining cells model), and "stem cell zone," or CBC (crypt base columnar cell model), are the most accepted models up to the present time. The former hypothesis assumes that Paneth cells are located in the crypt basis, while the stem cells are located just above the Paneth cells and at the +4 position. The latter hypothesis states that ISCs are intermingled with the Paneth cells in the crypt basis (Barker et al., 2008; Barker et al., 2012; Freeman, 2008). These 2 schools of thought contend regarding the ISCs position; but the conclusion is remained unclear yet. Therefore, extending knowledge by studying the ISCs *in vivo* is inevitable.

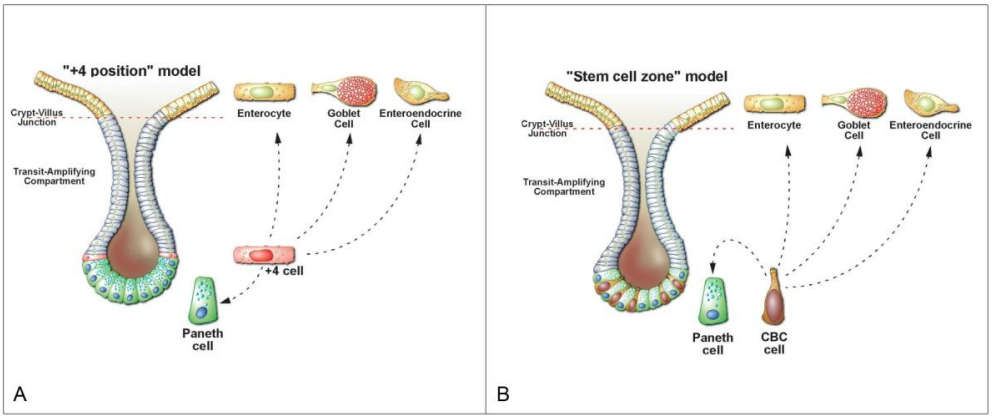

Figure 1-9: ISCs' location in (A) "+4 position," or LRC, vs. (B) "stem cell zone," or CBC model (Barker et al., 2008).

1. 6. Intestinal stem cells (ISCs) studies

As it has been discussed, ISCs play a critical role in the maintenance of tissue homeostasis, where the ISCs are located in mammalian intestine and which signaling pathways are dominantly active in the intestinal epithelium and mesenchymal layer have been covered. However, our current knowledge of zebrafish ISCs and the renewal pattern is little. Here, we describe the optional techniques for tissue renewal and adult stem cell studies. According to the animal model, type of study, study stage, and the location of stem cells, different techniques have been developed for adult stem cell studies.

1. 6. 1. Lineage tracing

Lineage tracing is a technique that marks the stem cells and subsequently its daughter cells by a biomarker. It helps to study the stem cells, behavior in their physiological context (*in vivo*). Insertion of a reporter gene (like fluorescent proteins [FPs]) helps in the isolation of cells carrying the marker. However, besides the stem cell some other cells may carry the marker too. *Lgr5*, *Bmi1*, and *Ascl1α* are among the most important ISCs marker:

Lgr5 has been known as the most proper marker for ISC in mice and humans up to the present time (Barker et al., 2007; Sato et al., 2009; Yui et al., 2012). It seems Lgr5 plays a key role in growth control and differentiation of specific

embryonic tissues (Barker & Clevers, 2010).

Bmi1, a component of a polycomb repressing complex, plays a key role in the maintenance of chromatin silencing in the neural system and hematopoietic stem cells (Lessard & Sauvageau, 2003). Both Bmi1^{+ve} cells and Lgr5^{+ve} cells are able to generate new differentiated cells and self-renew. However, these 2 markers mark different cells in a single crypt. In other words, Bmi1^{+ve} cells are located in the +4 position from the base of the crypt (LRC), while Lgr5^{+ve} cells are restricted to the crypt base (CBC) (Sangiorgi & Capecchi, 2008). These evidences suggest that *Lgr5* and *Bmi1* mark different ISCs in a single crypt.

Ascl2 is one of the genes that is controlled by the Wnt signaling pathway and expressed in the Lgr5^{+ve} cell. *Ascl2* encodes a basic helix-loop-helix (bHLH) transcription factor that expresses in extra-embryonic tissues and in the intestinal epithelium. It has been demonstrated that Ascl2 plays a key role in the maintenance of adult ISCs, as gain and loss of function of the *Ascl2* gene result in crypt hyperplasia and the disappearance of the Lgr5^{+ve} stem cells, respectively (van der Flier et al., 2009).

Some of these genes are represented in zebrafish by pairs of orthologous that evolved due to partial duplication of the bony fish genome. Until now there are no studies detailed enough to demonstrate expression of these genes in the intestinal epithelium of zebrafish at a level of single cell.

1. 6. 2. *In vitro* culture

This technique helps to study and imaging the live stemness potential in a controlled environment. Scientists have shown that a single $Lgr5^{+ve}$ cell and a single crypt have the potential to form multiple crypts and villus domain *in vitro* , which carry all 4 differentiated epithelium cells (Koo et al., 2012; Sato et al., 2011; Sato et al., 2009). As the isolation of either a stem cell or a stem cell niche is needed for *in vitro* culture, and the zebrafish ISC's marker is not known yet, this technique is not considered as an option for zebrafish ISC studies.

1. 6. 3. Label retention (BrdU and EdU)

Studying cell proliferation by labeling its daughter cells could be a fundamental method for quantitative analysis of tissue turnover and renewal. BrdU and EdU are 2 main DNA nucleoside analogues of thymidine that incorporate into the new synthesized DNA molecule during cell division. As a result, a marked cell could be a stem cell that is labeled with the label retention molecules during mitosis. However, some other non-stem cells (progenitor cells) divide frequently too and would be labeled by label retention molecules. Because of the absence of effective methods to study the zebrafish intestinal tissue, questions about the tissue renewal patterns remain. Even though the label retention technique targets dividing cells by marking the newly

synthesised DNA strand, we took advantage of this technique as an alternative to tissue renewal analysis by multiple administrations of EdU. In chapter 3, we will discuss this technique in details.

1. 6. 4. Mosaic generation

I. Cell Transplantation and chimera generation

The cell transplantation of adult tissue stem cells provides an opportunity to study their stemness behavior *in vivo*. On the other hand, the transplantation of embryonic stem cells helps the generation of chimera to study the different cells with different genetic makeups *in vivo*. Cell transplantation and mosaic generation are among the alternative techniques for studying tissue renewal in the absence of a tissue-specific stem cell marker. In chapter 2, we will discuss the cell transplantation technique to generate chimera zebrafish embryos and study the intestinal epithelium homeostasis and renewal pattern in zebrafish. However, this technique needs knowledge of the isolation and transplantation of embryonic stem cells. Moreover, a single cell at its early developmental stages is a derivative and divides fast to form a part of a tissue or several tissues. The same happens for the transplanted cell at embryonic stages too. It proliferates rapidly like the host cells to increase the number of cells. These cells develop a part of an organ or several organs based on their location and interaction with the adjacent cells. In addition, cell transplantation during the

early developmental stages will not aid in the study of the intestinal epithelium renewal temporally as it is impossible to mark the cells at the start point and track the path of the cells. However, chimera generation gives the opportunity to observe and study the intestinal epithelium renewal pattern *in vivo* as we can observe the path of cells with different origination.

II. Random mutation in intestinal epithelium cell's genetic makeup

Ethyl methanesulfonate (EMS) and *N*-ethyl-*N*-nitrosourea (ENU) are 2 mutagen components that cause damages in DNA molecule. ENU treatment in mice showed that all the cells of a crypt are originated from a single and dominant ISC, while the villus epithelial cells are reproduced in different crypts and consequently from different ISCs (Winton, Blount, & Ponder, 1988). In chapter 2, we will test the cells migration in zebrafish intestinal epithelium. A brief EMS treatment of a heterozygote GFP gene under a ubiquitous promoter mutates random epithelial cells and ISCs resulting in a heterogeneous expression of GFP along the villus base-tip axis.

The administration of the EMS component in tissue renewal studies is straightforward but has a major limitation: EMS affects all the cells regardless of proliferation population or differentiated population at the start point. This causes a mixture of normal cells adjacent to mutated cells at the start point and the frustration of a temporal study on the migration of intestinal epithelial cells. To cope with this limitation, we designed the label retention experiments

(chapter 3), which provide the chance to analyze the intestinal epithelium renewal temporally too.

III. Cre-regulated recombination

The Brainbow is a new strategy to label the cells by different FPs (YFP, RFP, and BFP) resulting from a random recombination (Pan, Livet, Sanes, Lichtman, & Schier, 2011). The Brainbow construct carries several FP genes in a single construct followed by a single promoter. These FP's genes are flanked by loxP sites. Basically, the first FP gene would be transcribed into mRNA, and then transcription would be stopped by the stop codon of first FP's gene. Therefore, protein synthesis will not proceed to the next FPs in the construct. However, the construct would be cut and modified at the loxP sites once the Cre enzyme is activated. Consequently, some FPs genes are randomly deleted from the construct by the Cre recombinase enzyme, and as a result, different expression patterns of FPs would be observed in different cells because of the independent activity of Cre recombinase in any cell. The Cre recombinase enzyme plays a key role in creating the recombination expression pattern. Therefore, besides a Brainbow cassette, we need to activate the Cre recombinase enzyme in the cells too. However, the potential of recombination generation for the desired gene at the desired time and location suits this technique for renewal studies to cope with the previous technique's limitation. In chapter 4, the generation of the Zebrabow transgenic line and the random recombination by heat shock will be reviewed.

As it has been reviewed above, zebrafish intestine has a different anatomical structure. Even though it provides a highly significant case of study, relatively little work has been done on the zebrafish intestine, and none of the previous studies conducted detailed analysis to consider the procedure of intestinal epithelium renewal. As renewal and homeostasis both are dependent on stem cells behavior, marking the stem cells paves the way to study these 2 processes. However, as discussed earlier, there are no studies detailed enough to demonstrate expression of these genes in the intestinal epithelium of zebrafish at a level of single cell. Therefore, absence of a reliable and specific marker for zebrafish ISCs has made it difficult to prove their localization at the inter-villus spaces.

Some of these genes are represented in zebrafish by pairs of orthologous that evolved due to partial duplication of the bony fish genome. Until now there are no studies detailed enough to demonstrate expression of these genes in the intestinal epithelium of zebrafish at a level of single cell.

The main aim of this thesis is to produce a detailed study and analysis of the zebrafish intestinal epithelium renewal pattern to operate a balanced homeostasis. As one of the prominent differences between the zebrafish intestine and those of other species is the interior structure of the intestinal epithelium (the absence of finger-like structure villi and crypt of Lieberkühn), the remaining question is whether either side of a ridge originated from a single stem cell or a group of stem cells along its intervillus pocket. This may

contribute to a better understanding of the existing differences between zebrafish and other species, and it may provide the basis to study the behaviour of zebrafish ISCs.

As there is no ISC marker in zebrafish, it is beyond the scope of this study to trace the newly generated cells via cell lineage or *in vitro* culture. Therefore, first, we tried to analyze the intestinal epithelium renewal pattern by mosaic generation. In chapter 2, mosaic generation via both chimeric zebrafish creation and induced mutation will be discussed. In chapter 3, marked progenitor cells have been examined, and the intestinal epithelium renewal studies in the temporal dimension by the label retention technique has been studied. In chapter 4, details regarding the spatiotemporal studies of zebrafish intestinal epithelium renewal by Cre-regulated recombination in the intestine are explained. These experimental techniques complementary help to study, analyze, and understand the nature of zebrafish intestinal epithelium.

Chapter 2

The spatial orientation of zebrafish intestinal epithelium renewal

2. 1. The spatial orientation of zebrafish intestinal epithelium renewal– *by positive marking of epithelial cells*

2. 1. 1. Background

The cell transplantation of adult tissue stem cells gives the chance to study their stemness behavior *in vivo* and eases an application of the regenerative medicine manifestation of stemness (V. S. W. Li & Clevers, 2012). On the other hand, the transplantation of embryonic stem cells helps the generation of chimera to study the different genetic makeups *in vivo*. The cell transplantation and mosaic generation are among the only suitable techniques for studying tissue renewal in the absence of a tissue-specific stem cell marker. Chimera refers to a creature that contains a mixture of cells with different genetic makeup from different parents. A normal embryo originates from a pair of parental germ cells. A chimera carries different cells with different origins. A chimeric zebrafish is generated by cell transplantation from a donor embryo to a host embryo. Based on the purpose of experiments, it can be done at different stages (blastula, gastrula, and even late developmental stage). Therefore, a chimera's cells have originated from at least 2 different embryos. It is in contrast to mosaicism too. Mosaicism refers to an embryo with cells with the same genetic makeup initially. The mosaic

expression pattern has been induced by a genetically altered genome. Cell transplantation, the technique for generating chimera, provides the chance to mix cells from 2 separate zygotes or organisms. These 2 groups of cells express different phenotypes because of their different genotypes and cause heterogeneous expression patterns in an organism. The different expression patterns, as markers, ease studying renewal patterns in a tissue. Here, we are trying to use cell transplantation to generate chimeric zebrafish embryos and understand intestinal epithelium renewal in zebrafish.

2. 1. 2. Materials and Methods

In this study, Tg(β-actin:mGFP) was used as the donor embryo, and the host embryos were wild type embryos. The donor embryos were microinjected with fluorescein dextran at 1–2 cells stage to enable tracing them during the transplantation procedure. The dechorionated embryos were kept in Danieau solution at 28.5°C until 3 hpf (blastula stage) to 6 hpf (shield stage). The donor and host embryos were located and oriented with the yolk up and yolk down, respectively, in the agarose wells (Fig. 2-1).

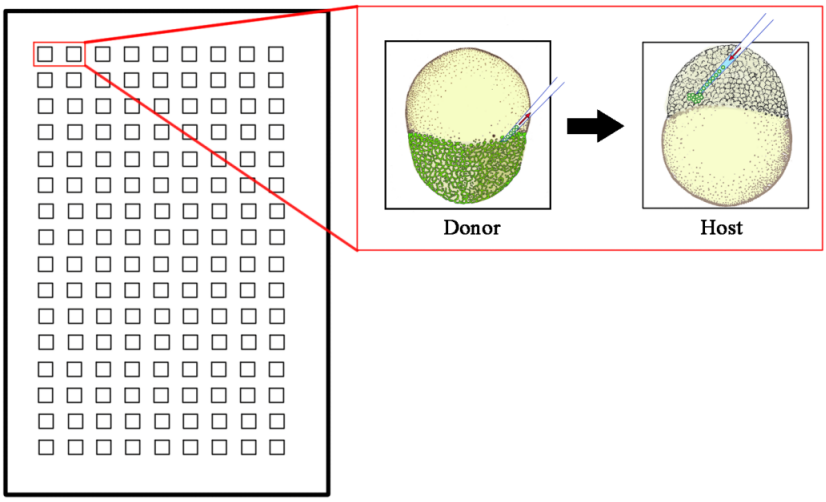

Figure 2-1: Schematic figure of the cell transplantation mold and the orientation of the donor and host embryos during the cell transplantation.

As the cell size gradually decreases by frequent and fast cell divisions, the needle opening hole size should be customized by polishing the edges on a microforge (55–65 μm, 40–50 μm, and 25–35 μm for early blastula, late blastula, and gastrula, respectively). The needle is inserted into the cell mass, close to the yolk sac margin, of the donor embryo, and then an adequate number of cells (50–100 cells) are drawn. The cells are transplanted to the same position in the host embryo. Finally, the embryos are transferred to the Danieau solution. During the next 48 hours, the Danieau solution and petri dish are carefully changed regularly.

Tissue sampling

The dissected intestine of the adult chimeric fish was fixed in 4% paraformaldehyde, followed by cryoprotection embedding in 2% agarose and 5% sucrose solution at 4ºC overnight. The tissue specimen was embedded with a tissue freezing medium (Leica 14020108926) and rapidly frozen in liquid nitrogen and sectioned at a thickness of 8 μm in a cryostat at −25°C (Leica CM1850). The sections were mounted on a room temperature superfrost plus microscope slide after 1 minute and air-dried for 3–5 hours. Sections were cell demembranated, decalcified, blocked, and stained with 0.5% Triton X-100, 0.5 M EDTA (pH 7.4), 4% blocking reagent and DAPI, respectively. The sections were protected by embedding in vectashield h-1400 mounting medium (Vector Laboratories) and covered with a coverslip. The mounted slides stored in a light-protected condition at 4°C to preserve the fluorescence before imaging.

Imaging

Images were acquired using a PerkinElmer Ultraview Vox Spinning Disk, with the laser line 405 and 488. The captured images were processed by Volocity software.

2. 1. 3. Results and discussion

Mesodermal and endodermal derivatives share their location in the blastoderm margin (Warga & Kimmel, 1990); where it is impossible to distinguish them based on morphological at early stages. Warga et al. coinjected 2 fluorescent dyes into the embryos of 1K–4K cells embryo to analyze the fate map of the zebrafish embryonic cell (Warga & Nusslein-Volhard, 1999). Based on fate mapping, we tried to transplant donor cells from Tg(β-actin:mGFP) to the margin of the host embryo. Even though the donor cells were transplanted at the margin, this would not vouch for the mosaic expression pattern in the intestine because at this stage, the dorsal and ventral parts are not distinguishable. Hence, most of the chimera embryos showed positive GFP expressions in their somites (muscles) as well (Fig. 2-2B and C). On the other hand, an autofluorescent yolk sac masks the intestinal tube for both screening and imaging (Fig. 2-2). Therefore, the chimeras were screened at larval stages for GFP expression in the intestinal tube and studied in later developmental stages. The screened fish were kept under standard conditions (Westerfield, 2007).

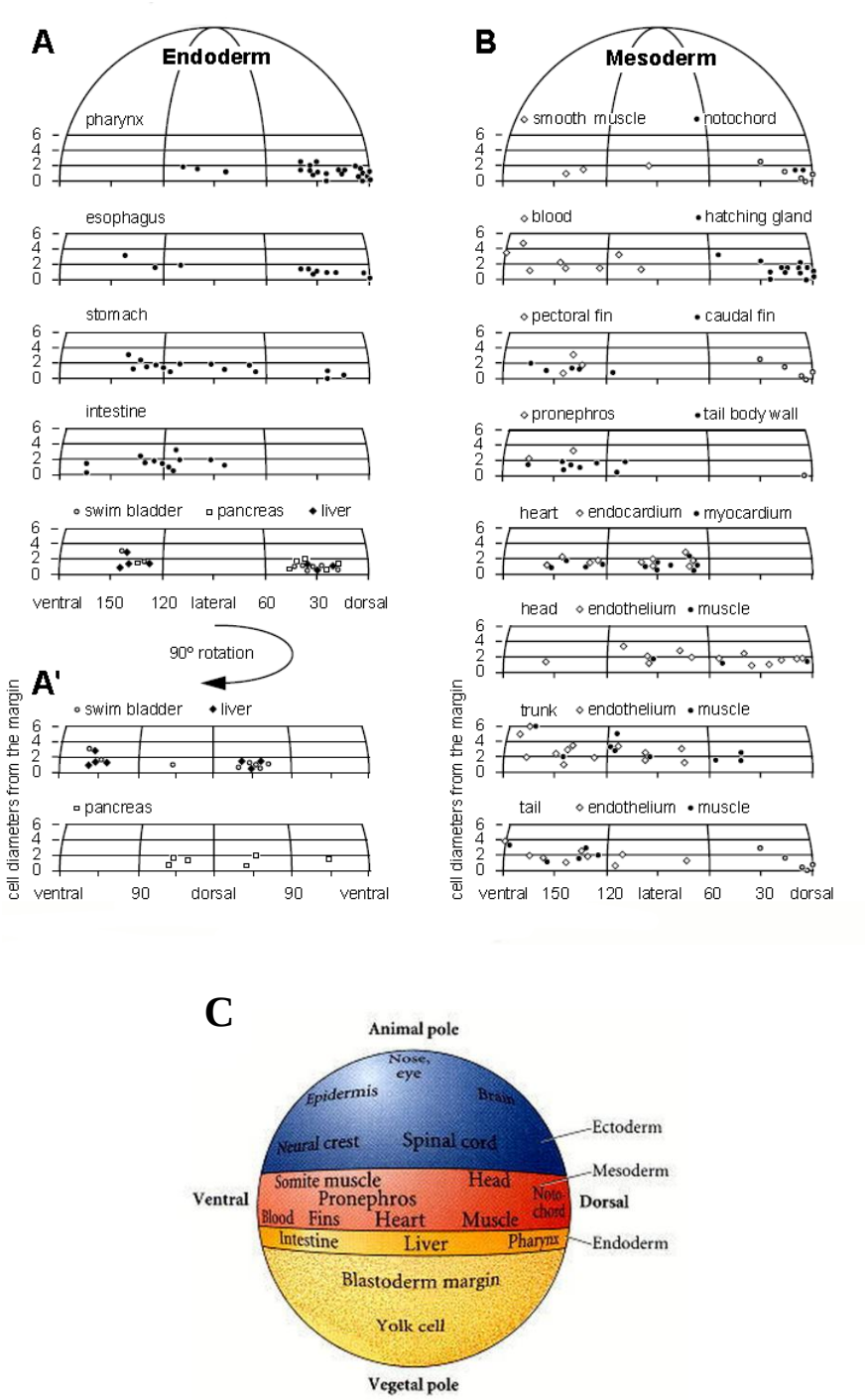

Figure 2-2: Fate mapping of future (A) endodermal and (B) mesodermal organs' derivatives. Intestinal derivatives showed colocalization with mesodermal organs' derivatives like smooth muscles, blood cells, heart, fin, trunk, and tail. Because the ventral and dorsal parts are not distinguishable at this stage, the cells were transplanted anywhere at the margin of the host embryo (Warga & Kimmel, 1990). (C) Cartoon figure of deep cell fate mapping after stopping cell mixing during embryogenesis (Gilbert, 2003).

Figure 2-3E shows the dissected intestinal tube at 7 dpf. Because the separation of adult ISCs without biomarkers is impossible, cell transplantation has been carried out prior to cell differentiation and organ development. A single cell at early developmental stages divides fast to form a part of a tissue or several tissues. The same happens for the transplanted cell at embryonic stages. It proliferates rapidly like the host cells to increase the number of cells with GFP expression. These cells develop a part of an organ or several organs based on their location and interaction with the adjacent cells (Warga & Kimmel, 1990). As shown in figure 2-3E, a part of the intestinal tube is entirely expressing GFP, while, other cells originate from the host embryonic stem cells and do not carry the GFP gene in their genome. Therefore, it is not possible to study intestinal epithelium renewal at the cellular scale level (single cell renewal). Moreover, cell transplantation during early developmental stages will not yet aid in studying intestinal epithelium renewal temporally too. However, chimera generation gives the opportunity to observe and study intestinal epithelium renewal pattern *in vivo*. This technique helps to study the potential stemness of cells rather than their actual stemness. Intestinal dissection and imaging at adult stages, besides our previous results, reveal new findings (Fig. 2-4). It has been previously showed that the dividing cells are located at the base of the intestinal villus, while cell death occurs at or near the intestinal villus tip (Wang, Du, et al., 2010). Now I have found that ISCs in this simple organization repopulate the intestinal villi epithelial cells along a base-to-tip axis.

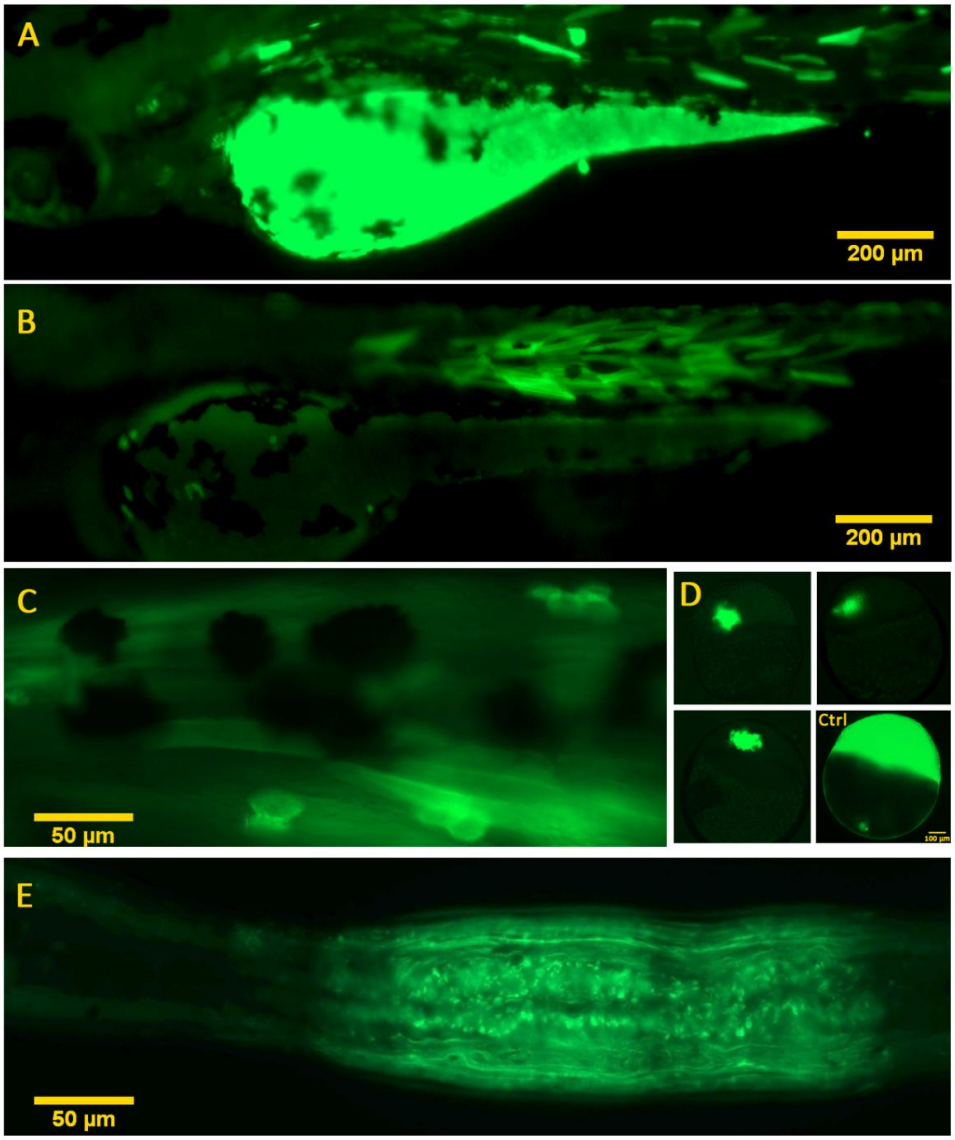

Figure 2-3: Mosaic expression pattern in a 7 dpf chimeric zebrafish. (A) Autofluorescent yolk sac. (A, B, and C) Mesodermal and endodermal derivatives share their localization in early embryonic stages; therefore, the mosaic pattern is observed both in somites and in the intestine. (D) Three chimeric zebrafish embryos vs. a donor embryo. (E) Mosaic expression pattern in the intestinal tissue.

Table 2-1 shows the total number of intestinal villi counting. Out of 194 intestinal villi, only 41 intestinal villi are originated from the donor embryos entirely and show the fluorescent expression pattern. While 127 are entirely non-fluorescent, and originated from the host embryos (wild type). Only 26 intestinal villi (13.40%) express both fluorescent and non-fluorescent cells on either side of the intestinal villus. Figure 2-4B shows the 50 % GFP^{+ve} intestinal villi are located between the 100 % GFP^{+ve} and 0% GFP^{+ve} intestinal villi domains.

Figure 2-4A, B, and C show the intestinal villi cross sections of an adult chimeric zebrafish foregut. These figures show the continuous villi of the intestinal epithelium that form the ridge-shaped structures in contrast to finger-like villi in mice and humans. These observations also reveal that the zebrafish intestinal epithelium does not only harbor the crypt of Lieberkühn but also lacks the villi on the intestinal villi.

This chimeric tissue harbors 2 batches of cells with different origins and genetic makeup. The GFP^{+ve} cells originated from the donor transplanted cells that carry the β-actin:mGFP cassette in their genome. On the other hand, the cells with no GFP expression originated from the wild type host embryonic stem cells.

Table 2-1: Number of intestinal villi with different expression pattern in the chimeric tissues. 100 % GFP^{+ve}: Fluoresent expression pattern at both sides of the intestinal villus (originated from donor embryos). 0% GFP^{+ve}: Non-fluorescent expression pattern at both sides of the intestinal villus (originated from host embryos). 50 % GFP^{+ve}: One side shows fluorescent expression while the other side is non-fluorescent (originated from both the donor and host embryos).

	Positive Marking	
	Number of villi (#)	**%**
100 % GFP^{+ve}	41	21.14
50 % GFP^{+ve}	26	13.40
0% GFP^{+ve}	127	65.46
Total	**194**	**100**

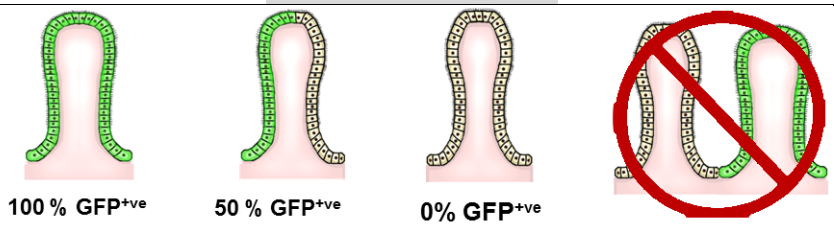

Figure 2-4A also proves the presence of more than one ISC at the bottom of the intestinal villus. This figure shows the mosaic expression pattern in a cross-section of the intestinal villi. As it is obvious, the expression pattern of one side of the intestinal villus may change along with it too (Fig. 2-4A). Later, in chapter 3, we will also confirm this result through a label retention experiment. Figure 3-2 shows the dividing cells labeled with click-iT EdU and located at the bottom of the intestinal intervillus, which will be discussed in chapter 3.

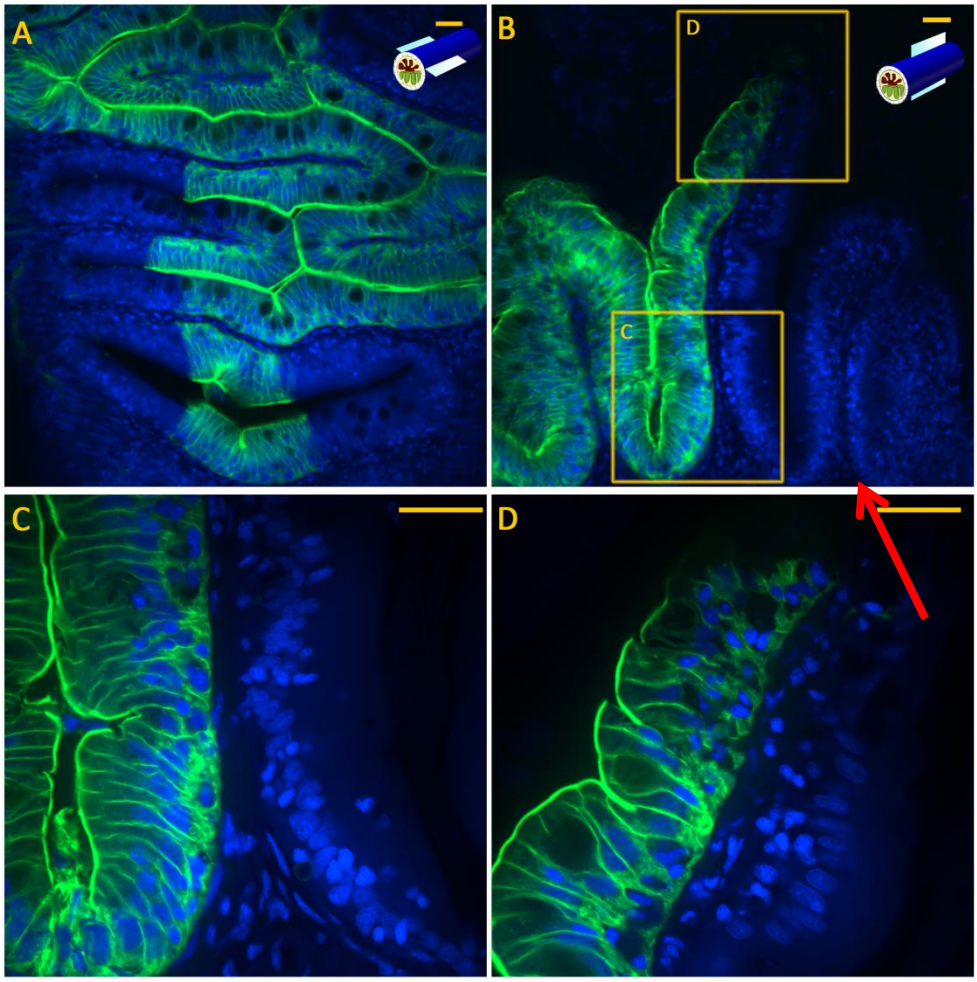

Figure 2-4: (A) Mosaic expression pattern in a cross-section of the intestinal villi. (B, C, and D) Mosaic expression patterns of either side of an intestinal villus that is located at the margin of the donor embryo's and host embryo's derivatives. (C) The bottom of the intervillus (proliferation region) and (D) the intestinal villus tip (apoptosis region). β-actin:mGFP (Green), DAPI (Blue). Scale bar = 20 μm.

Figure 2-4B, C, and D show the lateral section of the ridge shaped intestinal villi and intervillus of an adult chimeric zebrafish foregut. The entire intervillus and the sides of the villi flanking the intervillus pocket were either fluorescent or nonfluorescent (Fig. 2-4B and C). In contrast, the phenotype of 2 sides of a single villus can be different because either side of a villus originates from different stem cells at the bottom of the intervillus (Fig. 2-4). The young and newly reproduced cells migrate toward the villi flanking the intervillus pocket, as the phenotype of the intestinal villi flanking an intervillus pocket is always similar. These observations confirm that the dividing cells occupy the intervillus pocket, while cell death occurs at or close to the villus tip. A similar behavior was observed in mice and humans too (Barker et al., 2008; Leblond & Stevens, 1948; Merzel & Leblond, 1969; Schmidt, Winton, & Ponder, 1988; van der Flier & Clevers, 2009).

In 2005, scientists focused on the zebrafish intestinal epithelium development extensively (Crosnier et al., 2005; Ng et al., 2005; Wallace et al., 2005). They found the location of ISCs in zebrafish and pointed out that the location the cells were shed off is at or close to the intestinal villus tip. However, it was the first time that the intestinal villi were analyzed specifically. With its specific features, the zebrafish provides the opportunity to study renewal and cell migration of the epithelial layer in intestinal villi.

Here, I show the symmetric renewal pattern of the intestinal villi. In other words, even though the Wnt, HH, and BMP signaling pathways control the

cell fate of a single intestinal villus (Crosnier et al., 2005), the cells at either side of a villus originate from different stem cells at the bottom (See P. 54).

2. 2. The spatial orientation of zebrafish intestinal epithelium renewal– *by negative marking of epithelial cells*

2. 2. 1. Background

Even though cell transplantation as well as EMS treatment caused a mosaic expression pattern, it does not provide the chances to analyze with a single cell resolution. Cell transplantation refers to cell exchange during embryonic stages (or adult stages). The cells are not differentiated at this time, and undergo fast division. Therefore, a single transplanted cell gives rise to large populations of cells. In addition, chimera refers to a creature that contains a mixture of cells with different genetic makeup from different parents. However, as discussed earlier in the case of mosaic generation, all cells of the embryos are of the same genetic makeup. A point mutation of a reporter gene in those cells helps to mark some cells. We expected to see similarities and comparable results when analysing the chimeras and mosaics.

EMS and ENU are 2 mutagens that cause DNA damage. Winton et al. (1988) used ENU to generate a mutation in the ISCs of mice. They found that all cells of a crypt that harbor the mutated ISCs express the mutated gene. On the other hand, a part of the villus, which originates from the same crypt, showed the

expression of a mutated gene, while the other parts of the villus, which originate from other surrounding and unmutated crypts, revealed normal expression patterns. They suggested that all cells of a crypt originate from a single and dominant ISC, while the villus epithelial cells are reproduced from different crypts and consequently from different ISCs (Winton et al., 1988).

Therefore, we tried to generate mosaic intestine tissues to test whether cells migrate from the base to the tip of the villi. A brief EMS treatment of a heterozygote GFP gene under a ubiquitous promoter mutates most epithelial cells and ISCs, resulting in a heterogeneous expression of GFP along the villus base-tip axis.

2. 2. 2. Materials and methods

In vivo labeling of proliferating intestinal epithelium cells

Adult heterozygote Tg(β-actin:mGFP) fish were chosen for the experiment. The fish were kept in water at 28.5˚C as recommended (Westerfield, 2007). The fish were anesthetized by gradually decreasing water temperature 12ºC over several minutes. To limit the effects of EMS to the intestine only, it was orally administrated. Three different amounts of EMS (3 μl, 6 μl, and 9 μl) with 2 repeats were orally administrated to the anesthetized fish via bypassing the shortened microloader tip (Eppendorf 930001007) through the mouth and esophagus. The EMS solution was drenched in the beginning portion of the foregut. Finally, the fish were returned to 28.5ºC water after 30 seconds.

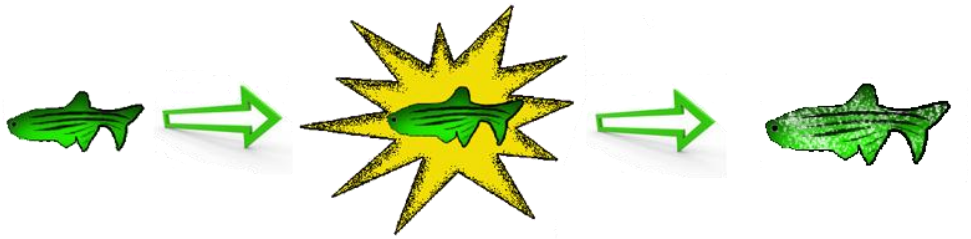

Figure 2-5: Schematic figure of EMS treatment of a heterozygote reporter gene transgenic line.

Tissue sampling

The zebrafish were killed at 3, 24, 36, 48 and 72 hpt. The dissected intestines were fixed in 4% paraformaldehyde, followed by cryoprotection embedding with 2% agarose and 5% sucrose solution at 4ºC overnight. The tissue specimen was embedded with a tissue freezing medium (Leica 14020108926) and rapidly frozen in liquid nitrogen and sectioned by the cryostat at −25°C (Leica CM1850). The sections were mounted on room temperature superfrost plus microscope slide after 1 minute and air-dried for 3-5 hours. Sections were demembranated, decalcified, blocked, and stained with 0.5% Triton X-100, 0.5 M EDTA (pH 7.4), 4% blocking reagent and DAPI, respectively. The sections were protected by embedding in a mounting medium (vectashield h-1400) and covered with a coverslip. The mounted slides were stored in a light-protected condition at 4°C to preserve the fluorescence before imaging.

Imaging

Images were acquired using a PerkinElmer Ultraview Vox Spinning Disk, with the laser line 405 and 488. The captured images were processed by Volocity software.

Deactivation of EMS

Equal volumes of 10% sodium thiosulfate and 1% sodium hydroxide were added to 30 EMS solutions to inactive the EMS in 1.4 hours at 20°C. However, for safety issues it was suggested to keep it under the hood for 24 hours (Westerfield, 2007).

2. 2. 3. Results and discussion

EMS as a mutagen causes genomic DNA damages as well as reporter gene (GFP gene) damages. Therefore, it would deactivate the GFP expression in intestinal epithelium cells of the heterozygote Tg(β-actin:mGFP) transgenic line. To observe the mutation effect, it is necessary to have a single copy of the GFP gene in the genome. Having two or more GFP genes in the genomic material decreases the chance of mutation observation because the possibility of a point mutation in all the GFP genes of a genomic material is small; therefore, the unmutated GFP gene in the genome would mask the effect of

mutation in the mutated GFP fragments.

To find the optimal concentration (with minimal damage to intestinal epithelium renewal and minimal mortality rate), we tried three different amounts of EMS (3 µl, 6 µl, and 9 µl) with two repeats. The fish that were injected with 6 µl and 9 µl of EMS died after the second and first EMS oral administration, respectively. Therefore, the experiments proceeded with 3 µl EMS oral administrations. The adult heterozygote fish were first orally administrated with EMS mutagen. Next, the fish were killed according to the scheduled time course.

Table 2-2 shows the total number of intestinal villi counting. Out of 366 Intestinal villi, 169 villi were not affected by this treatment. 112 villi are entirely non-fluorescent and flanked with the 50% GFP^{+ve} intestinal villi. Also in figure 2-6D and E it is clearly visible that the 100 % GFP^{+ve} or 0% GFP^{+ve} intestinal villi are flanked by 50 % GFP^{+ve} intestinal villi. Only 85 intestinal villi (23.22%) contained both fluorescent and non-fluorescent cells at either sides of the intestinal villus.

Table 2-2: Number of intestinal villi with different expression pattern in the mutated tissues. 100 % GFP^{+ve}: Fluoresent expression pattern at both sides of the intestinal villus. 0% GFP^{+ve}: Non-fluorescent expression pattern at both sides of the intestinal villus. 50 % GFP^{+ve}: One side shows fluorescent expression while the other side is non-fluorescent.

	Negative Marking	
	Number of villi (#)	**%**
100 % GFP^{+ve}	169	46.18
50 % GFP^{+ve}	85	23.22
0% GFP^{+ve}	112	30.6
Total	**366**	**100**

In figure 2-6 has been shown that some parts of the intestinal epithelium are GFP^{-ve} expression, while the rest are still fluorescent regardless of treatment durations.

Changes of expression pattern were studied in five groups of treated fish (3, 24, 36, 48, and 72 hours post treatment) (Fig. 2-6). At time 0, the fish were orally administrated with 3 µl EMS. Three hours after oral administration, the first group was killed, and the intestinal tissue was dissected to be prepared for imaging. The procedure was the same for the other groups. Group 1 (3 hpt) showed that patches of fluorescent are non-fluorescent cells populate the valley between the intestinal villi as well as the bottom of the intervillus,with the remaining sides and ridge of the intestinal villi displaying heterogeneous GFP expression (Fig. 2-6).

Therefore, we successfully showed that EMS causes mutation in GFP genes in the intestinal epithelium. EMS affects the cells at the starting point regardless

of whether the cells are proliferating cells or differentiating cells. This causes presence of unmutated cells next to the mutated cells, which limits the temporal analysis of the renewal speed in the intestinal epithelium too.

The expression pattern at the intervillus bottom is homogenous (either fluorescent or non-fluorescent) by 24–36 hpt (Fig. 2-6C). This observation indicates the activation of the proliferating cells, which spread out their genetic materials (including either a mutated or an unmutated GFP gene) to the newly reproduced cells. In contrast, the old differentiated cells close to the intestinal villus tip are not replaced with the newly reproduced cells yet; therefore, the heterogeneous expression pattern, either fluorescent or nonfluorescent, is still present near the tip (Fig. 2-6B, arrowheads).

However, by 48–72 hpt, the entire valley and the sides of the intestinal villi flanking the valley were either fluorescent or non-fluorescent. The persistence of non-fluorescent cells along the intestinal villus axis indicates the presence of a mitotic population of non-fluorescent stem cells located in the intervillus pocket between a pair of villi. In another words, the villus ridges that flank a common intervillus pocket show similar expression patterns (Fig. 2-6D and E, red arrowheads). In contrast, both sides of a villus may not show similar expression patterns (Fig. 2-6D and E yellow arrowheads). Previously, we showed that the dividing cells are located at the base of the intervillus pockets, while cell death occurs at or close to the intestinal villus tip (Wang, Du, et al., 2010). The previous observations and the recent results suggest that the

dividing cells at the base of intervillus pockets produce new cells for both villus ridges flanking the intervillus pocket. Therefore, the expression patterns of the valley flanking the villus ridges are always similar. On the other hand, the expression patterns at both villus ridges of an intestinal villus is not necessarily similar, which indicates that 2 separate populations of dividing cells generate a single intestinal villus. In addition, as the expression patterns of either side of a villus change at the tip of the villus ridge, it would confirm the previous results, which showed that apoptosis takes place at the villus tip.

We have successfully showed that mosaic generation via mutagenesis can be used for cellular studies in tissue renewal. In addition, these results are in conformity with those of the cell transplantation experiments too. The ISCs that are inhabited by the intervillus bottom reproduce the new cells. The new cells migrate toward the flanking intestinal villus tip.

In 1988, Ponder's team tried to use the *in vivo* system to examine the ISCs' behavior in a single crypt via the ENU mutagen component and in the Dlb-1 locus in SWR mice. They found the monoclonal behavior of ISCs in a crypt and a ribbon of mutated cells that migrated up the villus (Schmidt et al., 1988; Winton et al., 1988). Later in 1999, Bjerknes and Cheng also used ENU to introduce somatic mutation in the same transgenic line and detected the mutated cells both in crypts and villi (Bjerknes & Cheng, 1999).Winton's team confirmed their previous results from mutagenesis by β-naphthoflavone and tamoxifen induction in a $CreER^{T2}$ transgenic mice (Lopez-Garcia, Klein,

Simons, & Winton, 2010). Clever's team recently explored murine intestinal epithelium renewal *in vivo* by generation of a transgenic line. They identified Lgr5 as the ISC marker and showed that the crypt and the surrounding villi is lined with a ribbon of marked cells too (Barker et al., 2007; Simons & Clevers, 2011; van der Flier & Clevers, 2009).

From previous findings in another species and our observations, which have been demonstrated for the first time in zebrafish, we suggest that the renewal of the zebrafish epithelium is similar to those of birds and mice with the newly divided cells at the base completing their translocation to the tip of the intestinal villus by 48 hours. The results indicated that this technique, regardless of its limitation, could help to disclose more information regarding tissue renewal and be an alternative to lineage tracing when there is lack of knowledge on tissue-specific stem cell markers. The administration of the EMS component in tissue renewal studies is straightforward but has a major limitation: EMS affects all cells regardless of proliferation population or differentiated population at the start point. This causes formation of a mixture of normal and mutated cells adjacent to each other at the start point and the frustration of a temporal study of intestinal epithelial cells' migration. To cope with this limitation, we designed the label retention experiments (chapter 3), which provide the chance to analyze intestinal epithelium renewal temporally.

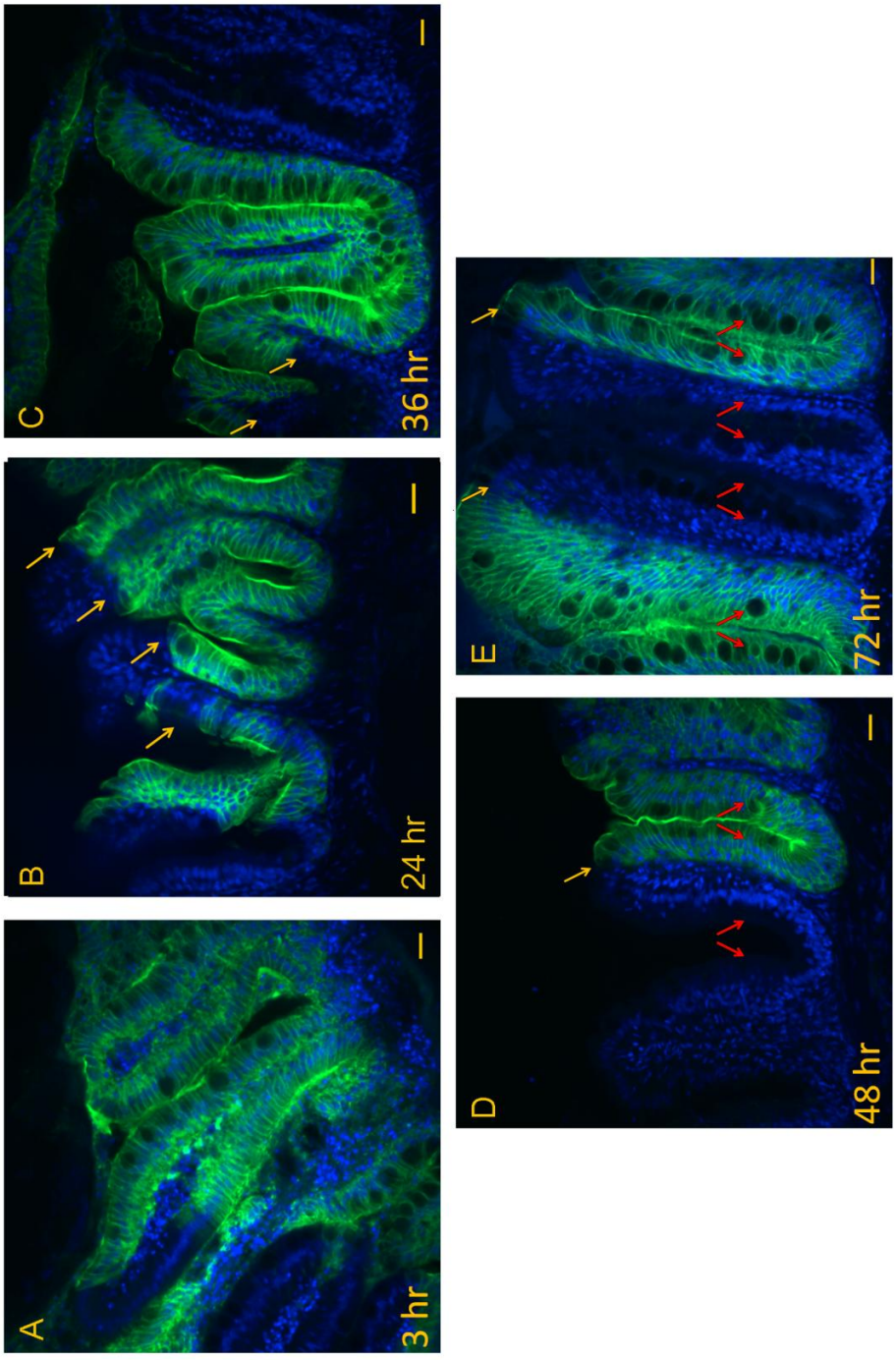

Figure 2-6: Mosaic generation by EMS treatment of Tg(β-actin:mGFP) heterozygote zebrafish in a time course experiment. The yellow arrows show the progress of cell migration along the base to tip axis. The red arrows show the similar expression pattern of two adjacent sides of two villi. mGFP, DAPI. Scale bar = 20 μm.

2. 3. Conclusions

Because there is no specific ISC marker, we used alternative options of lineage tracing. As has been described in chapter 1, mosaicism, by either chimera generation or mosaic generation, is considered as an option with advantages and disadvantages. In this chapter, chimera generation and mosaic generation studied. Mosaic generation not only reveals and confirms the cell transplantation's results, but also yields further insight into the intestinal epithelium renewal pattern. In summary:

1. Differentiated cells originated from the stem cells located at the bottom of the inter-villus.

2. The 2 sides of an individual intestinal villus epithelium are renewed from different ISCs, as the mosaic intestinal villi show different expression patterns on 2 sides of the villus.

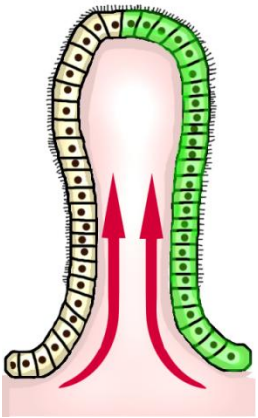

3. The 2 adjacent sides of the intestinal villi, flanking an inter-villus pocket, share the ISCs at the intervillus bottom.

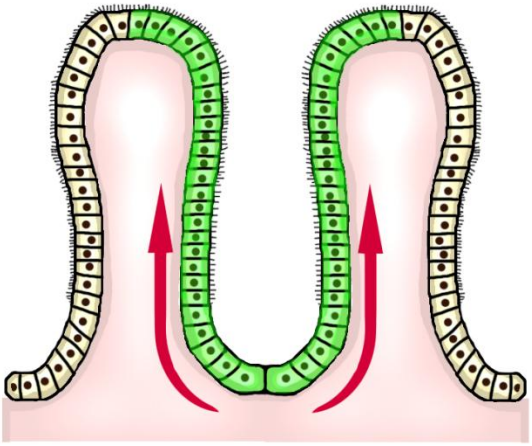

4. Either of lateral walls of the intestinal villus are renewed from more than one ISC, as the cross-sections of chimeric tissue showed changes in the expression pattern on one side of the intestinal villus.

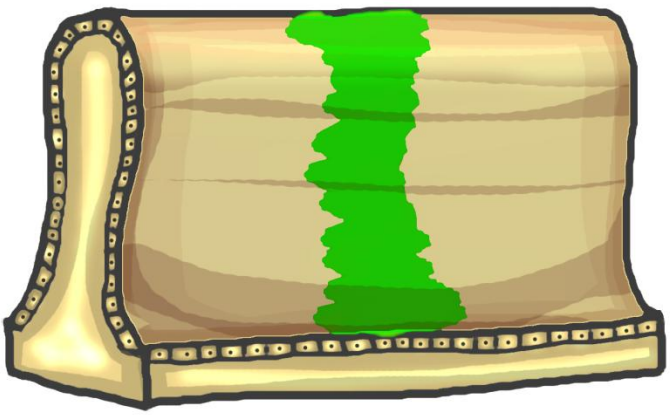

5. The old cells are replaced by younger cells at or close to the villus tip, where apoptosis of old cells takes place.

6. Renewal of the zebrafish epithelium is similar to those of birds and mice with the newly divided cells at the base completing their translocation to the tip of the intestinal villus by 48 hours.

Chapter 3

The temporal dimension of zebrafish intestinal epithelium renewal

3. 1. Background

Studying cell proliferation by labeling its daughter cells could be a fundamental method for the quantitative analysis of tissue turnover and renewal. Because of the absence of effective methods to study the zebrafish intestinal tissue, questions about the tissue renewal patterns remain. The lineage tracing technique via a specific ISC marker helps to study tissue renewal in mice and humans. The other alternative to mark the dividing cells is label retention technique. The two conventional label retention techniques [^{3}H]thymidine (^{3}HTdR) autoradiography and 5-Bromo-2′-deoxyruidine (BrdU) are used for marking the dividing tissues *in vitro* and *in vivo* (Fig. 3-1A). Both are incorporated into a newly synthesized DNA strand while cells are dividing. The [^{3}H]thymidine could be detected by autoradiography, and BrdU could be stained through immunohistochemistry. [^{3}H]thymidine labeling is relatively easy to perform but the technique is cumbersome because of the use of radioactivity. Using the BrdU was more convenient before emergence of EdU, but the limitation is in necessity of the DNA denaturation step by either heating or a chemical assay as the anti-BrdU antibody does not fit spaces between the 2 DNA strands in a DNA helix to conjugate with the incorporated BrdU in the DNA strand (Rakic, 2002). This harsh BrdU staining both elongates the staining process and denatures the specimen morphology (Zeng et al., 2010).

5-ethynyl-2´-deoxyuridine (EdU) is another of nucleoside analogs of thymidine incorporated into the new synthesized DNA strand (Buck et al., 2008; Cappella, Gasparri, Pulici, & Moll, 2008; Salic & Mitchison, 2008). EdU could be detected through a copper-catalyzed reaction between the EdU molecule and a fluorescent azide. Because of the small size of the fluorescent azide, it can easily diffuse in the DNA helix and react with incorporated EdU molecules in the newly synthesized DNA strand (Fig. 3-1B and C). So unlike the conventional BrdU label retention, EdU is easily detectable without heating or a chemical assay (Yu, Arora, Min, Roifman, & Grunebaum, 2009); so the sample morphology remains preserved better comparing to BrdU labelling.

It has been estimated that a murine ISC divides about a thousand times to renew the intestinal epithelial layer in its lifetime and still carries an intact genome with a rare carcinogenic mutation, suggesting the presence of a well-developed genome protection pattern among these cells (Potten, Owen, & Booth, 2002). Mitotic division is an essence of tissue renewal. Therefore, measuring the proliferating cells provides further insights into the unknown factors of tissue renewal. Even though label retention technique targets the dividing cells via marking the immortal DNA strand, we took advantage of this technique as an alternative to tissue renewal analysis by multiple administrations of EdU. As EdU is incorporated with the newly synthesized DNA strand, the new generations of cells are marked if the EdU is accessible.

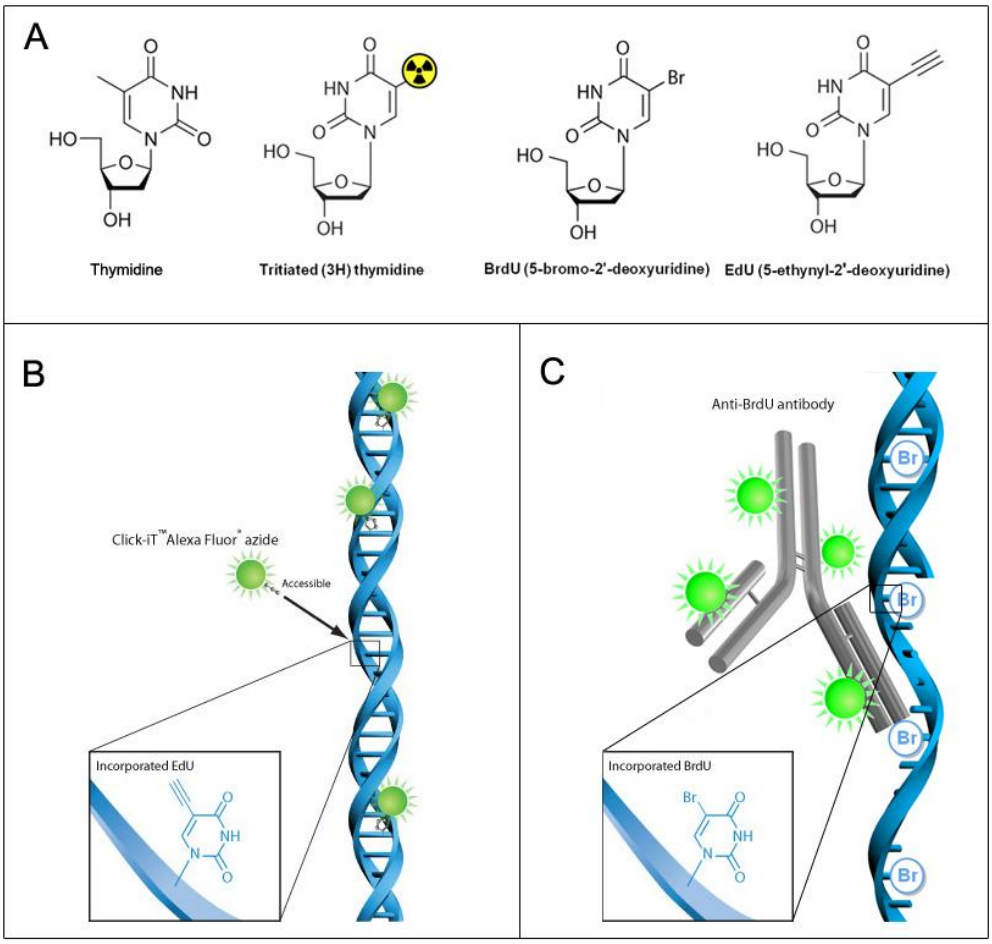

Figure 3-1: Label retention assay components: (A) thymidine molecule: a DNA nucleoside; ^{3}HTdR ([^{3}H]thymidine): a thymidine analog used in the original assay for marking the dividing cells; BrdU (5-Bromo-2′-deoxyruidine); and EdU (5-ethynyl-2´-deoxyuridine): the other thymidine analog. (B) Click-iT EdU vs. anti-BrdU antibody staining of thymidine analog. The small size of Click-iT EdU eases the penetration into the DNA double strands' spaces. Therefore, the DNA molecule morphology is conserved, and it has been blocked from other antibodies binding (http://www.invitrogen.com/site/us/en/home/brands/Molecular-Probes/Key-Molecular-Probes-Products/Click-iT-Detection-Assays/Click-iT-EdU.html).

3. 2. Materials and Methods

3. 2. 1. *In vivo* labelling of proliferating intestinal epithelium cells

Adult wild type male zebrafish (Danio rerio) at close age and weight (0.7 ± 0.05 gram) were randomly chosen for the experiment. The fish were kept at a water temperature of 28.5ºC based on conventional conditions (Westerfield, 2007). The fish were fed 1 hour before the oral administration of EdU to keep the EdU solution in the intestinal tube for a longer time. Next, the fish were anesthetized by gradually decreasing in water temperature to 12ºC over several minutes. 10 µl of 10 mM EdU in 1 X phosphate-buffered saline (PBS) was orally administrated to the anesthetized fish via bypassing the shortened microloader tip (Eppendorf 930001007) through the mouth and esophagus. The EdU solution was drenched in the beginning portion of the foregut. The fish were returned to 28.5ºC water after 30 seconds. EdU administration was repeated every 12 hours to label the proliferating cells that were not in the S phase during previous administrations.

3. 2. 2. Tissue sampling

The zebrafish were killed, and the dissected intestines were fixed in 4% paraformaldehyde, followed by cryoprotection with 2% agarose and 5% sucrose solution at 4ºC overnight. The tissue specimen was embedded with a

tissue freezing medium (Leica 14020108926) and rapidly frozen in liquid nitrogen and sectioned at a thickness of 8 μm thick in the cryostat at −25°C (Leica CM1850). The sections were mounted on room temperature superfrost plus microscope slide after 1 minute and air-dried for 3–5 hours. Sections were demembranated, decalcified, blocked and stained with 0.5% Triton X-100, 0.5 M EDTA (pH 7.4), 4% blocking reagent and click-iT EdU Alexa Fluor 488 (Invitrogen), respectively. The sections were protected by embedding in a mounting medium (vectashield h-1400) and covered with a coverslip. The mounted slides were stored in a light protected condition at 4°C to preserve the fluorescence before imaging.

3. 2. 3. Imaging and statistical analyzes

Images were acquired using a Leica TCS SP5X with the laser line 405, 488, and 568. The captured images were processed quantitatively using the Imaris software.

The intestinal villi length and migration rate in each group (treatment duration) were analyzed using Matlab software. Pixels with low signal intensity (smaller than one-quarter of the brightest signal in each image) were recognized as noise and removed. The intensity of EdU signals was analyzed to determine the migration level of EdU^{+ve} cells from the villus base. The border of 83% cumulative EdU signals from the villus base was considered as the migration indicator (Fig. 3-8).

The migration level and the intestinal villus length are recorded for each treatment and analyzed. The average of migration distances and standard deviations is depicted in table 3-1 and figure 3-7 for both original images and standardized images.

The images from each treatment were merged in the middle and at the villus base. The average signal intensity for any specific pixel was depicted in a raw image. The brightest pixels in the raw image were maximized in the final merged image; the rest of the signals were increased proportionally as well.

3. 3. Results and discussion

Figure 3-3 shows the bottom of the intervillus at 16 hpt. In this figure, it is clearly visible that the intervillus pockets are occupied with dividing cells. Therefore, it can be concluded that each intestinal villus harbors several stem cells at the base. The presence of different signal intensities of the click-iT EdU at intervillus pockets reveals different mitotic division stages among the dividing cells. Those with strong intensities are slow in division and keep the high concentration of EdU in their genomes. In contrast, those cells with weak signals have less concentration of EdU in their genomic material as the cells divide fast and the EdU has spread out in the daughter cells. However, it does not give a clue if the zebrafish ISCs divide symmetrically or asymmetrically. Different studies in past have deduced different conclusions: because adult tissue stem cells and ISCs are fast dividing cells, some authors have proposed

the immortal DNA strand hypothesis which suggests that these fast-dividing cells shall keep the immortal DNA strand for themselves to minimize the mutation effect during their lifetime (Cairns, 1975; Lansdorp, 2007; Montgomery & Breault, 2008; Rando, 2007). Based on that they proposed, ISCs undergo non-random chromosome segregation (CS) or asymmetric division and reproduce one stem cell and one normal cell. In contrast, other studies showed the presence of the click-iT EdU signal after > 4 regenerations, since it is much more difficult comparing to the first chase, the random CS or symmetric division must take place here (Fig. 3-2) (Escobar et al., 2011; Kiel et al., 2007).

Also, the existence of two types of ISC (fast dividing and quiescent)(Barker et al., 2012) complicates interpretation of results. Quiescent cells divide slower than the columnar base cells and may keep the EdU strongly and for a longer time. On the other hand, the EdU concentration would be decreased during tissue renewal involving fast-dividing ISCs.

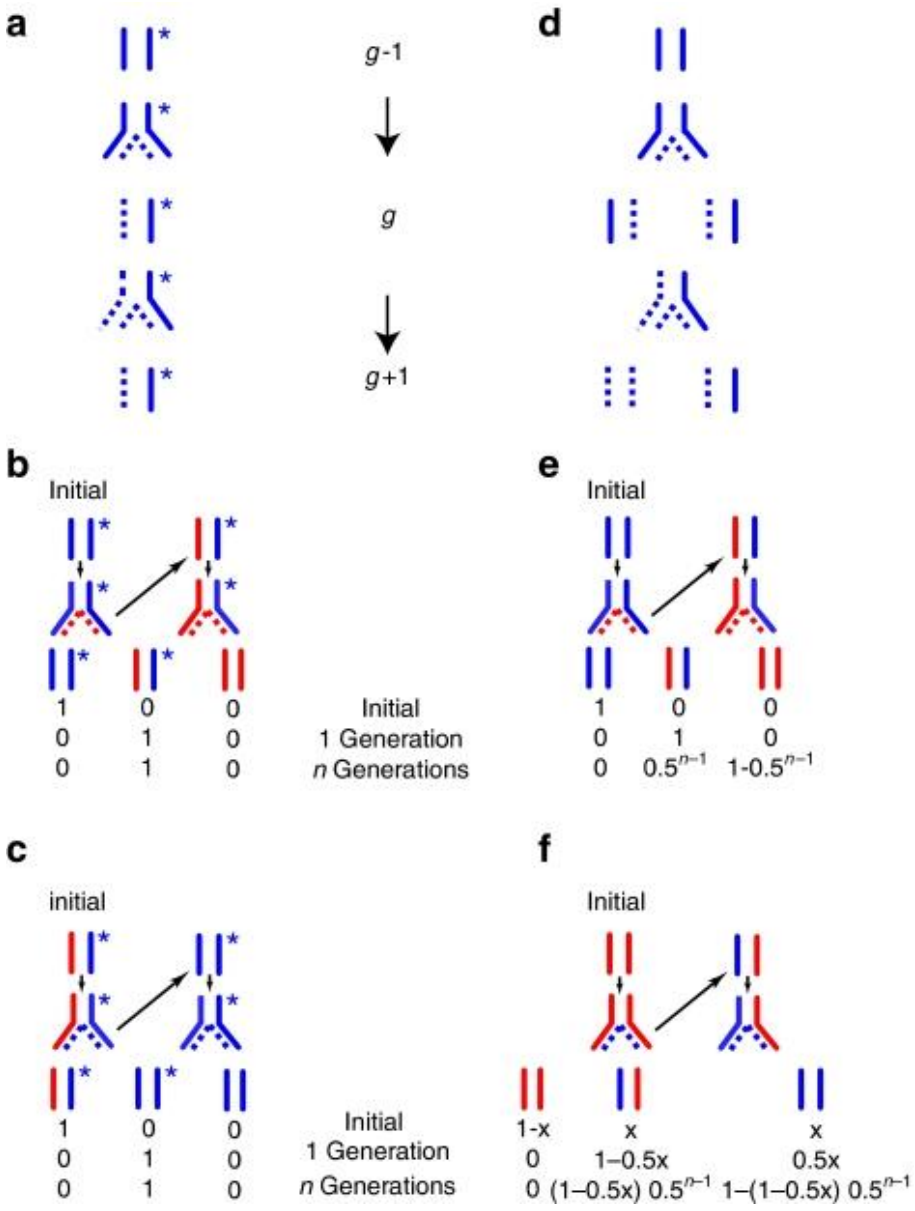

Figure 3-2: Different modes of stem cell division in either pulse chase or single chase of label affect the frequency of different types of daughter cells in each generation: (a) Non-random chromosome segregation (CS) in asymmetric stem cell division. (b) Non-random CS in asymmetric stem cell division and pulse chase of label. (c) Non-random CS in asymmetric stem cell division and single chase of label. (d) Random CS in symmetric stem cell division. (e) Random CS in symmetric stem cell division and pulse chase of label. (f) Random CS in symmetric stem cell division and single chase of label. Solid line: parental DNA strand, dotted line: new synthesized DNA strand, *: the template strand, red line: the labeled DNA strand (Escobar et al., 2011).

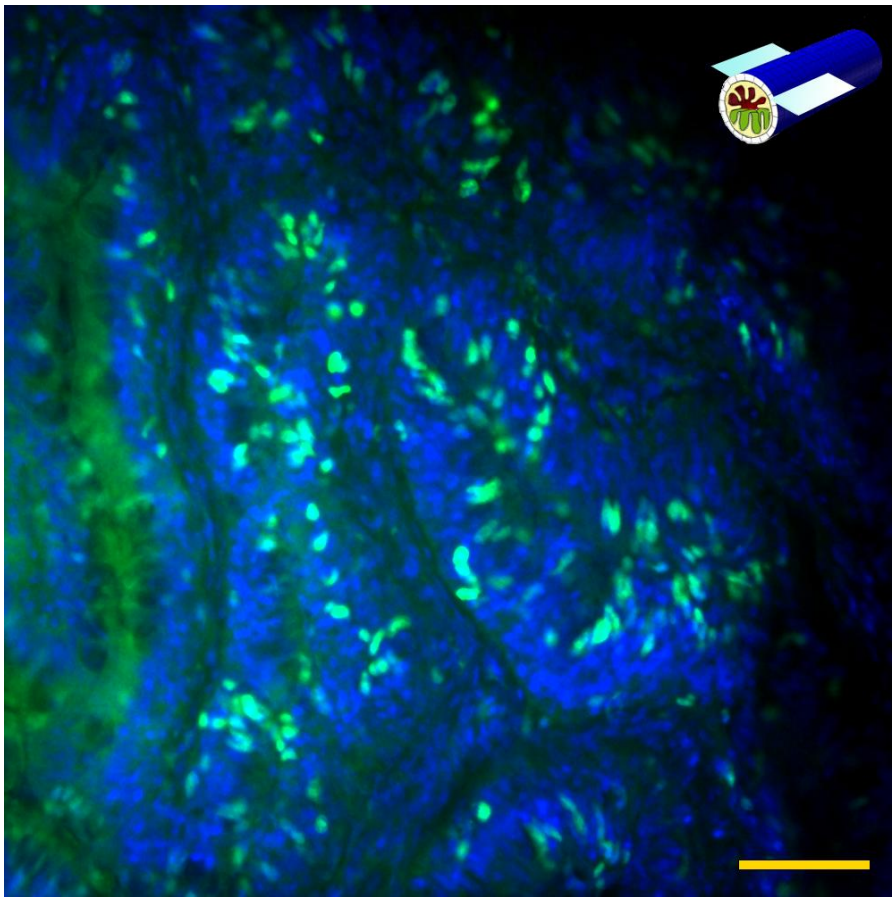

Figure 3-3: A cross-section of intervillus spaces stained by the label retention assay of zebrafish intestinal epithelium at 16 hpt. The cells incorporating in mitotic division use the available EdU molecule in the intestinal lumen to pair with deoxyadenosine (A) nucleoside in the target DNA strand. Therefore, the proliferating cells occupy the bottom of the intervillus to produce new cells for the fast tissue renewal. The concentration of EdU has been decreased during the frequent cell division in the cells with weak signals. DAPI (Blue), Click-iT EdU Alexa Fluor 488 (Green). Scale bar = 50 μm.

Figure 3-4 shows the labeled cells at 0.5 hpt. As expected, some cells at the base of intervillus pockets are EdU^{+ve}. As has been shown, there are only individual labeled cells at the spot. Regardless of random or non-random CS, both the stem cells and daughter cells must be EdU^{+ve} (Fig. 3-2).

The average cell cycle (including G1, S phase, G2, and M phase) lasts 24 hours. However, as described previously, the ISCs are among the fast-dividing cells, and in this case a cell cycle takes only 6–10 hours (Sakamori et al., 2012). As a result, I scheduled the EdU oral administrations every 12 hours. On the other hand, the cell cycle in mouse skin stem cells during rest may last more than 200 hours. In spite of the variable cell cycle length, the lengths of S phase, G2, and M phase are similar in different cell types, whereas G1 varies widely in different cell types. As G2 (gap between S phase and M phase) is about 2–4 hours (Lee, Goolsby, & Sensibar, 1994), We may conclude that these EdU^{+ve} cells are either in G2 or M Phase of mitosis (after S phase), the chromosomes are duplicated, and the new synthesized genetic materials carry EdU molecules in the DNA strands.

In addition, these EdU^{+ve} cells are often observed in +4 position (Fig. 3-4B and C vs. Fig. 3-4A); which resembles the position of +4 stem cells in mice.

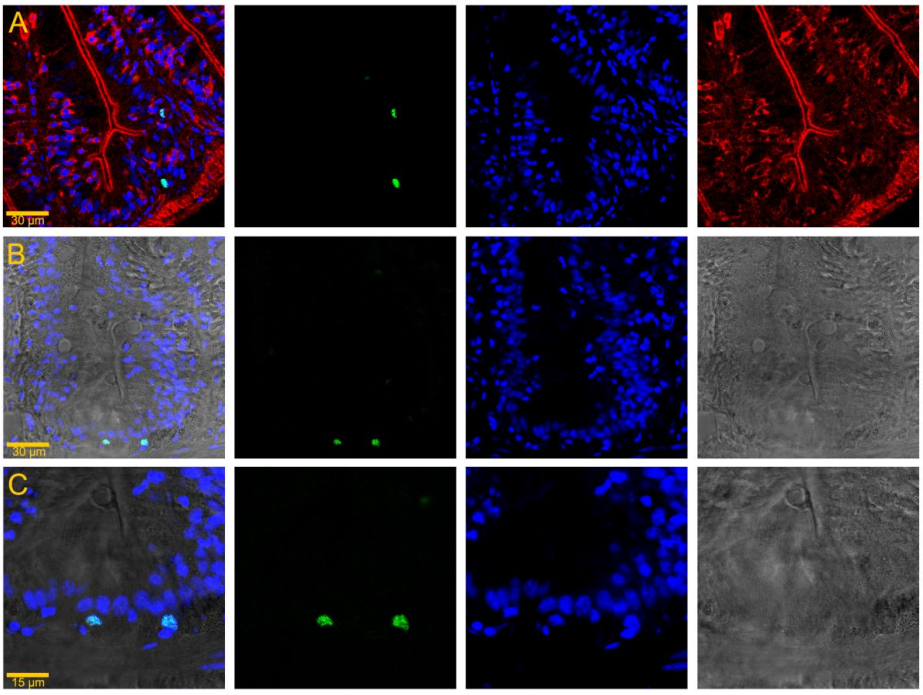

Figure 3-4: EdU^{+ve} cells early after treatment (0.5 hpt), Click-iT EdU Alexa Fluor 488 (Green), DAPI (Blue), β-actin (Red) and Bright Field. Scale bar (A and B) = 30 µm and (C) = 15 µm.

Figure 3-5 shows a ribbon of cells that are EdU^{+ve}. As expected, cells move toward the intestinal villus tip during their migration. However, as cells divide regularly, the new cells will not be marked if there is no available EdU. Therefore, we repeated the oral administration of EdU every 12 hours (Fig. 3-2B and F).

Intestinal epithelium renewal lasts 3–5 days in mice (Barker et al., 2007; Chia & Kuo, 2010; Potten & Ellis, 2006; van der Flier & Clevers, 2009). It depends on the position of newly reproduced cells in the crypt. The deeper in a crypt the cells are reproduced, the longer migration distance and time are needed (5 days) to reach the villus tip. However, no comprehensive study has been done on zebrafish intestinal epithelium renewal to compare our findings. In addition, the different features in zebrafish intestinal epithelium (the absence of villi and crypts) urged us to analyze and compare zebrafish intestinal epithelium renewal carefully.

Crosnier et al. and Wallace et al. in 2005 showed the presence of last $BrdU^{+ve}$ cells in the intestinal epithelium and at the tip of the intestinal villus 7 and 8 days after a single BrdU administration (Crosnier et al., 2005; Wallace et al., 2005). However, neither of the previous studies analyzed the intestinal epithelium renewal time course along the base to the tip axis by repeated label pulse in zebrafish. We tried to take advantage of labeling cells during mitosis and chase them in a time course experiment to study tissue renewal in the cell scale for the first time in zebrafish.

In this figure, the migration progress is clearly visible in the time course. The scheduled timing for sampling was every 2 hours; however, we have chosen these four groups (12, 24, 36, and 48 hpt) to see the migration progress clearly. In addition, we set the 12 hpt as the first group to ensure all progenitor cells (ISCs and TACs) divided at least once. Therefore, by 12 hpt, we expect to see the progenitor cells, domain marked with EdU^{+ve} cells (Fig. 3-5A).

Next, by 24 hpt, the expected result was observed: the ribbon of EdU^{+ve} cells has been stretched up toward the intestinal villus tip (Fig. 3-5B). Similarly, by 36 hpt, the ribbon of EdU^{+ve} cells is closer to the tip. The intestinal villus tip inhabits the cells that are reproduced before EdU administration and are not labeled as yet (Fig. 3-5C). However, neither at 24 hpt nor at 36 hpt, the EdU^{+ve} cells close to the tip are as intense by labelled as those in the bottom of the intervillus (Fig. 3-5B and C). An interval of 12 hours for EdU administration is long enough to allow some dividing cells to escape the EdU labeling and reproduce unlabeled cells in differentiated cells' domain (above the intervillus bottom). However, a 12-hour EdU administration interval was the optimal time to both observe the ribbon of labeled cells and minimize the fish mortality rate.

By 48 hours, the intestinal villi are occupied with EdU^{+ve} cells entirely. Similar to 24 hpt and 36 hpt, we can clearly see the intensity labelling of EdU^{+ve} cells is depressed close to the tip. In contrast, the EdU^{+ve} cells still occupy the base of the intervillus bottom (the progenitor cells' domain)

intensely.

We may conclude the average travel time from the intervillus pockets to the tip of the intestinal villus is 48 hours. As labeling the newly reproduced cells according to their location (either deep or shallow in intervillus pockets) is impossible, we consider the possibility of a longer time for travelling from the bottom base to the tip.

Figure 3-6A shows the EdU signal's average of all the intestinal villi of each group in a merged image. In other words, any single pixel in the merged image reveals the average signal intensity of all the images (the intensity of the same pixel in all the images divided by the number of images). As a result, the brighter the pixels in the merged image, the higher the possibility of the presence of the EdU^{+ve} cells in the same pixel of the images of the individual intestinal villus. In contrast, the dimmer the pixel in the merged image, the less the possibility of the presence of EdU^{+ve} cells in the same pixel of the images of the individual intestinal villus.

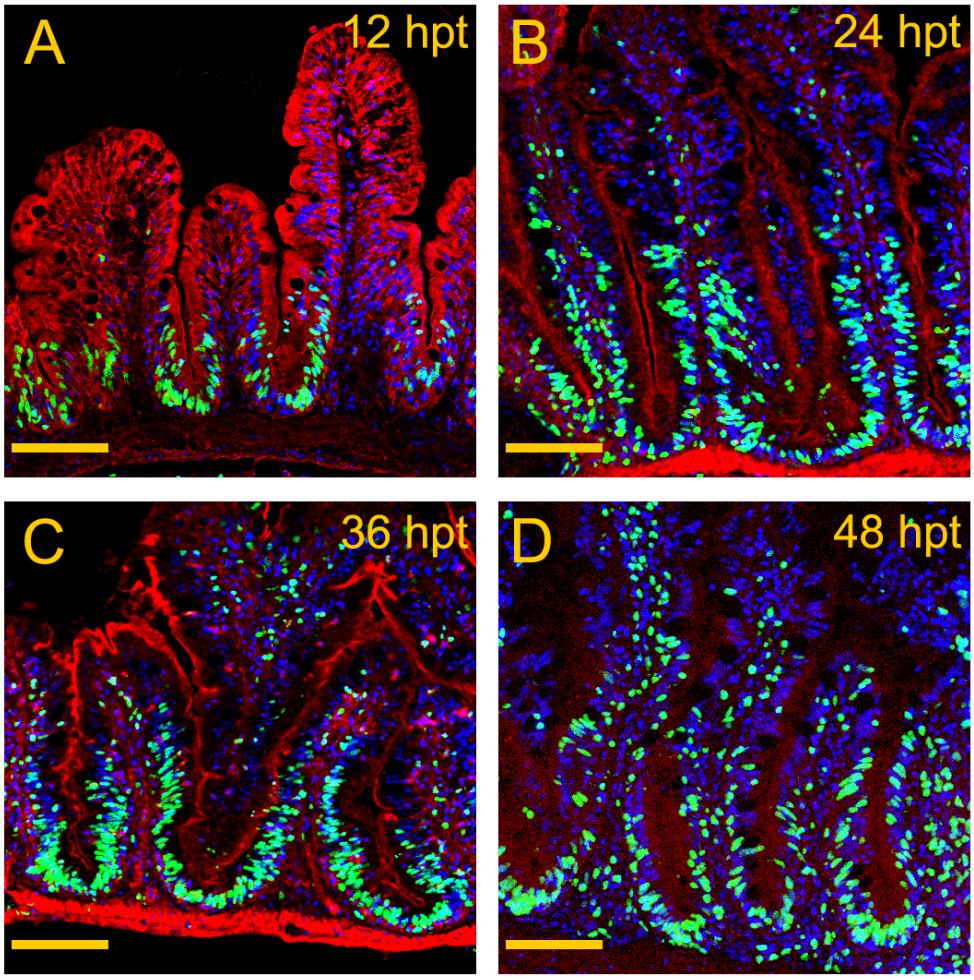

Figure 3-5: EdU^{+ve} cells migration pattern in a time course. Cross-sections of the zebrafish intestinal villus and intervillus pockets labelled by the label retention assay at (A) 12 hpt, (B) 24 pt, (C) 36 hpt and (D) 48 hpt. The cells incorporating in mitotic division use the available EdU molecule in the intestinal lumen to pair with deoxyadenosine nucleoside in the target DNA strand. DAPI (blue), Click-iT EdU alexa fluor 488 (green) and β-actin (red). Scale bar = 80 µm.

However, there is an exception regarding the 2 hpt group. As it has been shown in previous figures, there are single labeled cells after EdU administration. Hence, the 2 hpt merged image in figure 3-6 results from with merging all individual images of the intestinal villus and without getting an average.

It can be clearly observed that the EdU signals are progressively shifted towards the tip of the villus, which suggests that the cells are migrating toward the tip. By 48 hours, the migration is complete, and the entire intestinal villus is occupied by EdU^{+ve} cells with a high intensity of EdU^{+ve} cells at the base of the intervillus pockets. In contrast, the distribution of EdU^{+ve} cells is uniform in the 2 last images (4 and 8 days post treatment) regardless of the intestinal villus area. It could be due to the frequent division of cells at the base of the intervillus pockets, which causes a decrease in EdU concentration in progenitor cells too.

Figure 3-6B also shows the average distribution of EdU^{+ve} cells in the intestinal villus in a time course. However, the intestinal villus length was normalised to 200 pixels before getting the average and making the final merged image. The observations confirmed the results in figure 3-6A, and it gives an accurate estimation of cell migration in the intestinal epithelium. Here, we could successfully, and for the first time, show the traveling direction and duration of intestinal epithelium cells along the base-tip axis of the intestinal villi in zebrafish.

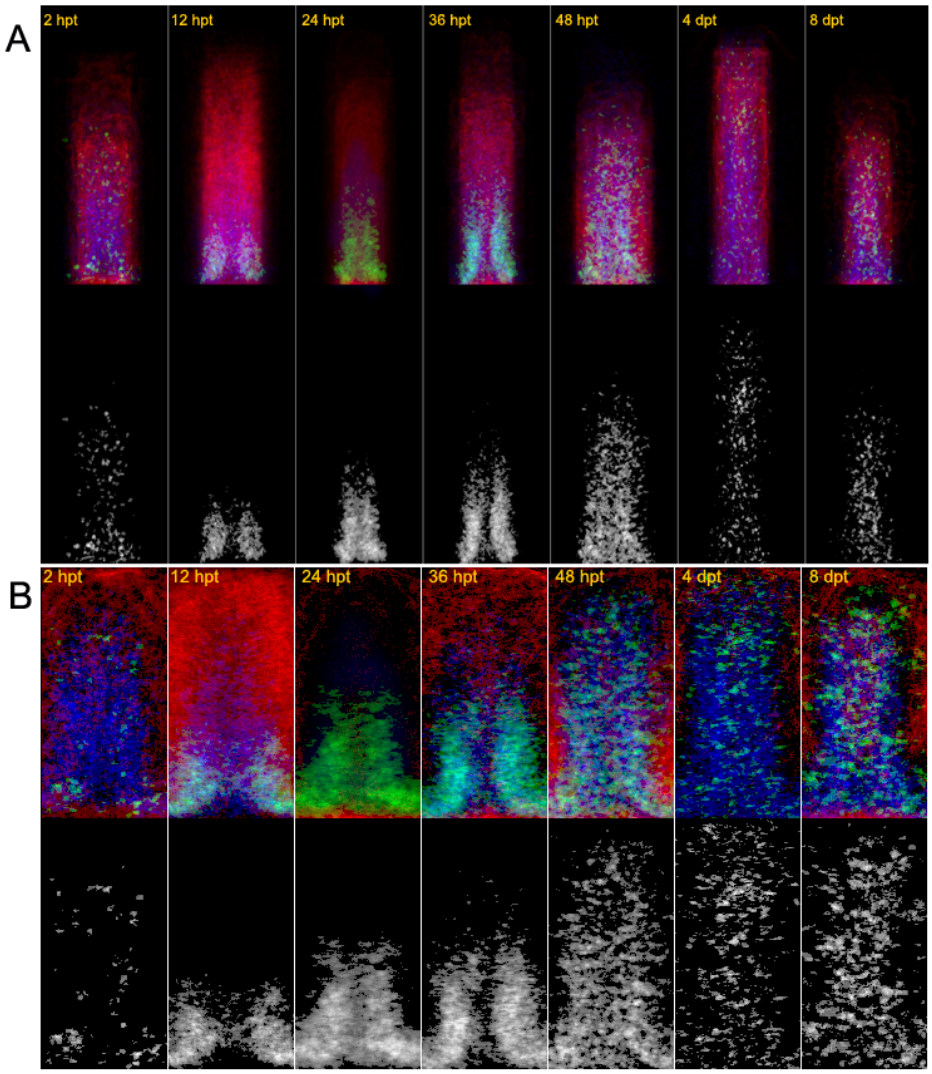

Figure 3-6: Average distribution of EdU^{+ve} in the intestinal villus during a time course in (A) a merged image and (B) standardized merged image. Distribution of EdU^{+ve} cells shows base-to-tip translocation of epithelial cells. The second row shows the Click-iT EdU Alexa Fluor 488 distribution in grey scale. DAPI (Blue), Click-iT EdU Alexa Fluor 488 (Green) and β-actin (Red).

The transit amplifying cells are located above the ISCs and divide continuously. Therefore, some of the top EdU^{+ve} pixels originate from TACs instead of ISCs. Therefore, 83% of EdU^{+ve} pixels from the villus base are considered as the newly reproduced cells by ISCs (100% -2 standard deviation $\simeq$ 83%). Table 3-1 shows the length of intestinal villi that harbor 83% of EdU^{+ve} pixels in non-normalized and normalized villi length. Figure 3-7 also shows the progress of 83% of the EdU^{+ve} cells, distribution along the intestinal villus length. By 48 hpt (when renewal is completed and the villus epithelium entirely occupied by the EdU^{+ve} cells), contrary to our expectations only 64% of the villus is covered by 83% of the EdU^{+ve} pixels. Because the distribution of the EdU^{+ve} pixels is not uniform along the intestinal villi length, the high and compact intensity of the EdU^{+ve} pixels at the base of the villi would dramatically depress the area that is covered by 83% of the EdU^{+ve} pixels. However, by 4 dpt, the intensity of the EdU^{+ve} pixels at the intestinal villus base has been decreased, and the distribution of the EdU^{+ve} pixels is uniform along the intestinal villus base-to-tip axis.

Table 3-1: Length of the villus that carries 83% of the EdU signal in nonstandardized villi length and standardized villi length.

EdU treatment duration	Non-normalized intestinal villus length (px)	Normalized intestinal villus length (px)
12 hpt	101.04±24.52	47.02±11.19
24 hpt	148.87±48.25	76.454±15.60
36 hpt	184.32±47.40	89.70±12.30
48 hpt	249.12±50.74	128.78±16.72
4 dpt	346.66±52.13	148.51±13.99
8 dpt	223.11±59.40	138.11±18.57

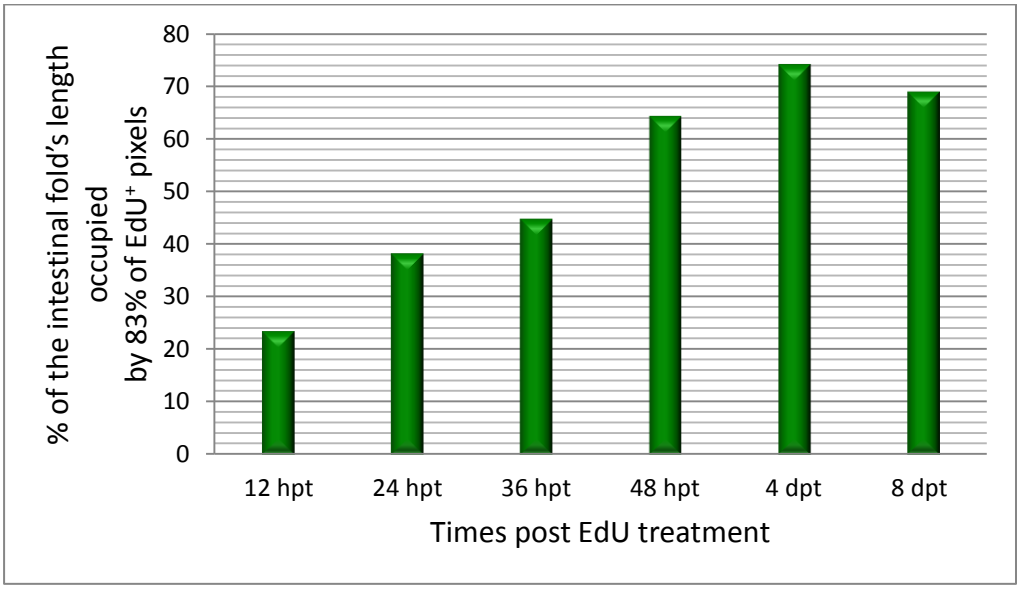

Figure 3-7: Percent of the intestinal villus length occupied by 83% of the EdU^{+ve} pixels.

Migration rate at the either side of an intestinal villus is similar as at both sides the EdU^{+ve} cells travel to an equal distance from the villus bottom (Fig. 3-8). On the other hand, the migration pattern of EdU^{+ve} cells at the adjacent intestinal villus side flanking an intervillus pocket is almost similar too. In other words, the ribbons of the EdU^{+ve} cells' length at the adjacent sides of the intestinal villi flanking an intervillus pocket are similar (Fig. 3-8). Migration rate of 83% of the EdU^{+ve} cells has been shown in normalised and non-normalised villi length groups (appendix A).

Wnt and Bmp signaling pathways control the proliferation at the villi base and differentiation at the villi tip, respectively (Crosnier et al., 2006; Gregorieff & Clevers, 2005; Radtke & Clevers, 2005). Our symmetric migration pattern observations in a villus confirm the activation of the signaling pathways in a villus that affect both sides of the villus.

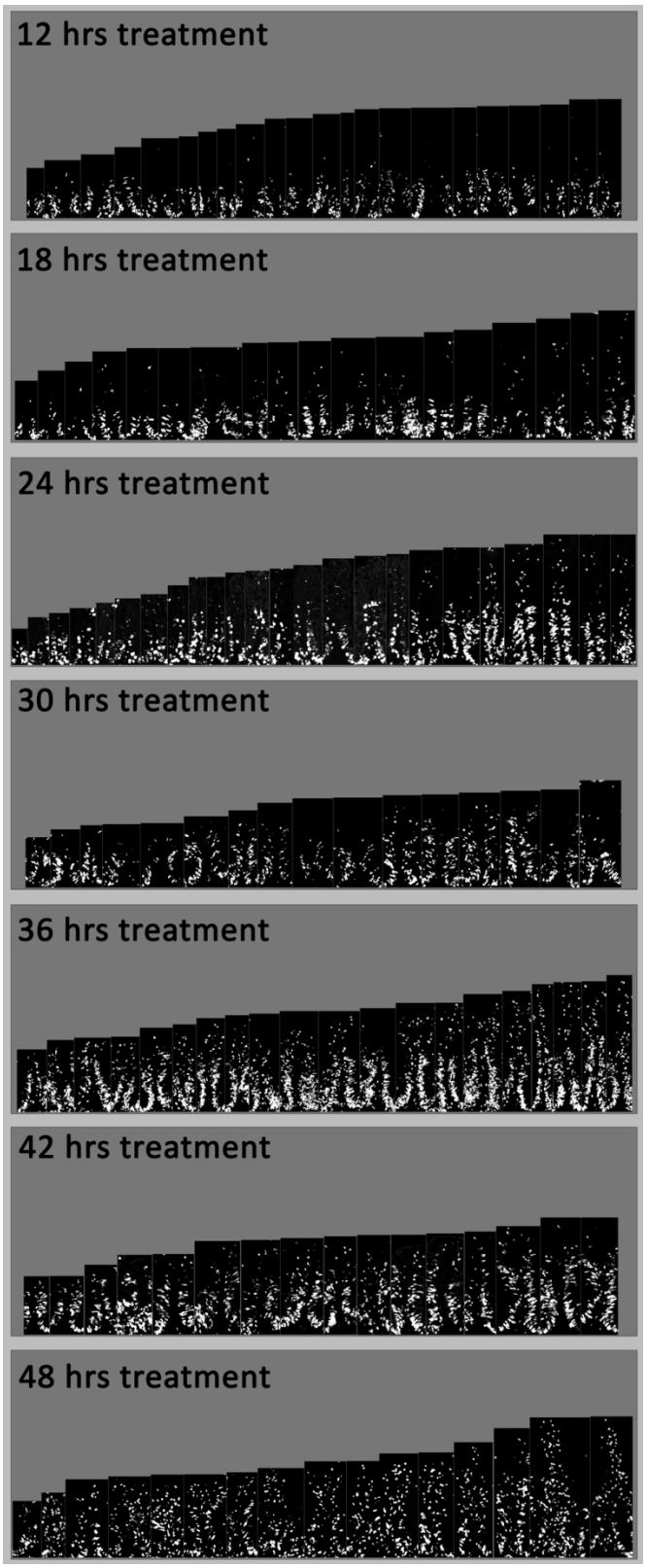

Figure 3-8: EdU^{+ve} cells distribution at different treatment duration.

STORM (STem cell mediated Optimal Renewal of epithelium Model)

Using STORM, a two-dimensional model, it is possible to predict the number of stem cells at each intervillus pocket. This model requires knowledge of the number of transit amplifying cells (TACs) and differentiated cells (Wang, Matsudaira, & Gong, 2010). A reliable control to mark the TACs is anti-PCNA antibody. Using anti-PCNA antibody we marked the proliferating cells (ISCs and TACs) (Fig. 3-9A), which is equivalent to the lable retention results by 12 hpt (Fig. 3-9B). Thereafter, we measured the number of proliferating cells and differentiated cells of 12 hpt group for the stem cell's quantity calculation.

$$(\boldsymbol{s}, \boldsymbol{k_4}) = \boldsymbol{argmin}_{s,k_4|c_0,\beta,\gamma} - \frac{\boldsymbol{s(\beta+\gamma)}}{\boldsymbol{2\beta}} - \frac{\boldsymbol{1}}{\boldsymbol{2(1+k_4)}} +$$

$$\frac{\boldsymbol{1}}{\boldsymbol{2\beta(1+k_4)}}\sqrt{(\boldsymbol{s(1+k_4)(\beta+\gamma)+\beta)^2 - 4s\beta\gamma(1+k_4)(1+\frac{\beta}{\gamma}+s+sk_4)}}$$

s.t. $\boldsymbol{s(1+k_4)(\beta+\gamma)+\beta)^2 - 4s\beta\gamma(1+k_4)\left(1+\frac{\beta}{\gamma}+s+sk_4\right) \geq 0}$;

$\boldsymbol{s \geq 0}$;

$\boldsymbol{k_4} \geq 0$.

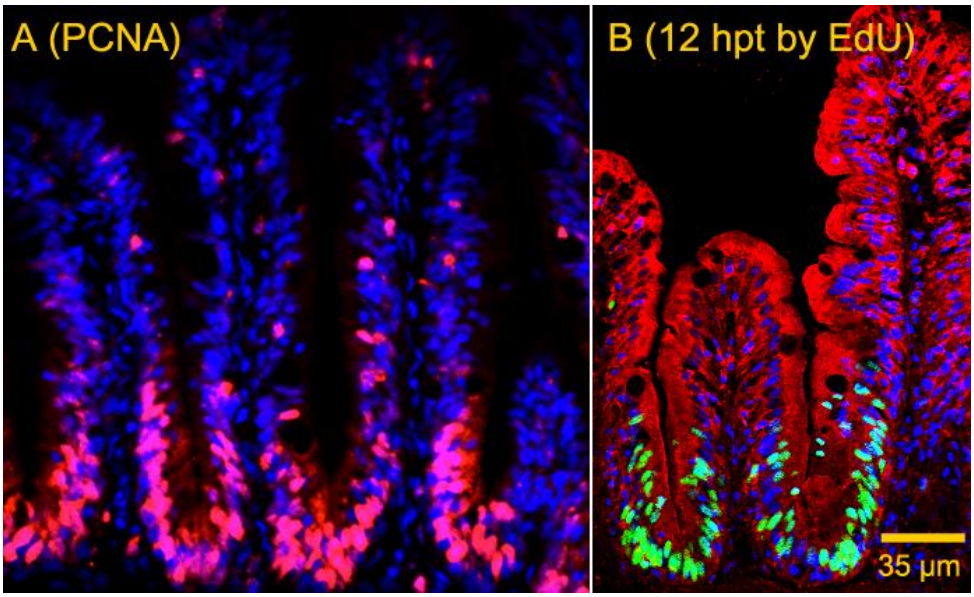

Figure 3-9: (A) Mouse monoclonal anti-PCNA [PC10] antibody (proliferation marker) immunohistochemistry on adult zebrafish intestine sections. Proliferating cells' nucleus are labeled by Alexa Fluor®568-conjugated rabbit polyclonal to mouse IgG (red), cells' nucleus are labeled by DAPI (blue). (B)

Because the EdU-tagged cells are both TACs and stem cells, the model needs to be iterated several times to calculate the accurate number of transit amplifying cells. According to our measurements and using STORM, the number of stem cells in each intervillus pocket is 3.51 if they divide only once per day and 1.75 if they divide twice per day, which shows the consistency of the STORM model using different techniques and experiments. Refere to appendix B for the complete STORM matlab code.

$$\boldsymbol{\beta = 2.050; s = \frac{c_0}{\alpha} = 0.253}$$

$$\text{Stem cell \#} = \begin{cases} \mathbf{3.51}\ \forall \boldsymbol{c_0 = 1} \\ \mathbf{1.75}\ \forall \boldsymbol{c_0 = 2} \end{cases}$$

Table 3-2: Intestinal Stem cell population in a valley calculation by two-dimensional STORM model. The similar results show the consistency of the model in number of stem cells calculation.

		Wang Zh., et al. 2010	**Our result**
Counting		200	50
Transit amplifying cells +Stem Cells		12.5	12.73
Differentiated Cells		100	95.96
β_1 *		8.0	7.53
# ISC	**1 division/day**	4.1	3.51
	2 divisions/day	2.0	1.75

*β = differentiated epithelium / transit amplifying progenitors

3. 4. Conclusions

Label retention, an alternative technique to study tissue renewal temporally, was examined and analyzed on the zebrafish intestine in this chapter. In summary, we can draw the following conclusions:

1- The intestinal villi length does not affect the migration rate.

2- Progenitor cells activity (proliferation) on either side of a single intestinal villus is often symmetric. Regardless of the intestinal villi length, either side allocates the ribbon of the EdU^{+ve} cells at an equal distance from the base.

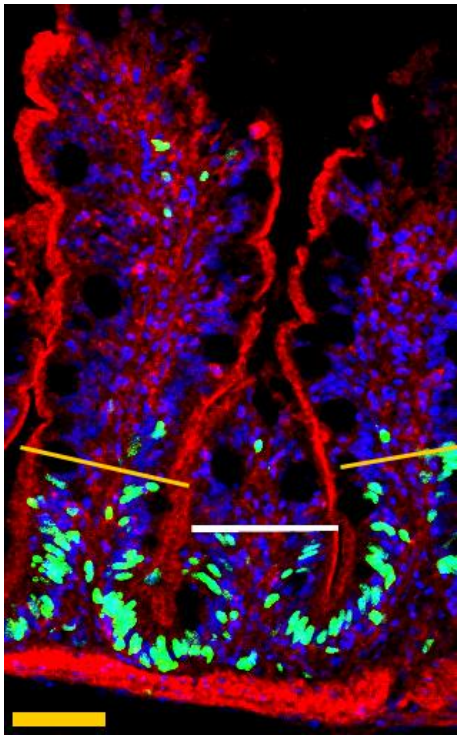

3- Renewal of the zebrafish epithelium is similar to those of birds and mice with the newly divided cells at the base, completing their translocation to the tip of the villus ridge by 48 hours (Fig. 3-10).

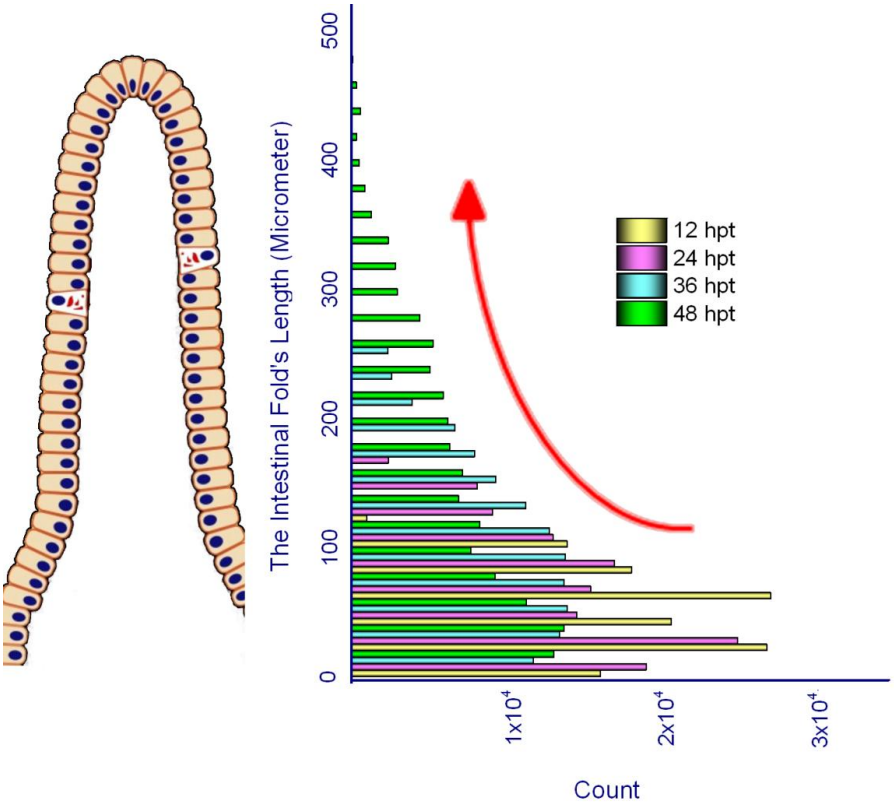

Figure 3-10: Renewal of the zebrafish epithelium with the newly divided cells at the base, completing their translocation to the tip of the villus ridge by 48 hours.

Chapter 4

The spatiotemporal orientation of zebrafish intestinal epithelium renewal

4. 1. Background

Advances in high-resolution and deep-imaging technologies and coincidentally in generation of novel transgenic lines, which carry the desired cells labeled result in increases at the contrast, ease *in vivo* studies. Brainbow is a novel and recently generated transgenic animal model that has a tandem of XFPs in its genome and are followed by the desired promoter (Livet et al., 2007). These FPs' genes are flanked by loxP sites. Basically, the first FP's gene would be transcribed into mRNA, and then the transcription would be stopped by the stop codon of the first FP's gene. Therefore, protein synthesis will not proceed to the next FPs in the construct. However, the construct would be cut and modified in loxP sites once the Cre enzyme is activated. Consequently, some FPs' genes are randomly deleted from the construct by the Cre recombinase enzyme, and as a result, different expression patterns of FPs would be observed in different cells because of the independent activity of the Cre recombinase in any cell. The Cre recombinase enzyme plays a key role in creating the recombination expression pattern. Therefore, besides the Brainbow cassette, we need to activate Cre recombinase enzyme in the cells too.

Four years later, in 2011 Pan et al. generated a zebrafish transgenic line carrying the Brainbow under a ubiquitous promoter and named it Zebrabow (Pan et al., 2011). Here, we used the β-actin promoter and a 2 colors zebrabow

construct to generate the β-actin-Zebrabow and study the spatiotemporal intestinal epithelium renewal.

4. 1. 1. β-actin:Zebrabow

As having the Brainbow cassette in the entire intestinal epithelium was necessary, the promoter of β-actin gene was chosen for expressing the Brainbow cassette.

The β-actin:LoxP-EGFP-LoxP-DsRed fosmid was a gift from Dr. Masato Kinoshita (Okazaki, Japan) (Fig. 4-3A). In this case, the Cre-mediated recombination is either EGFP or DsRed2. EGFP would be expressed under the β-actin promoter. Once the Cre recombinase enzyme is activated, the flanked gene by loxP sites would be deleted. Consequently, the DsRed2 gene (the latter gene) is liberated for expression (Fig. 4-1).

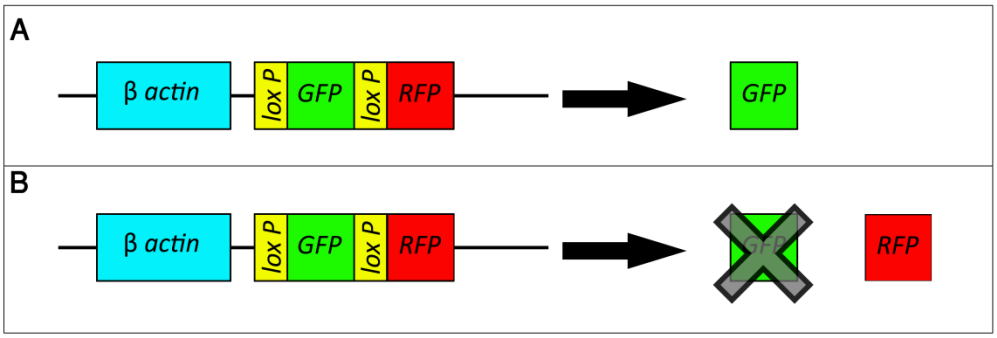

Figure 4-1: Cre-mediated recombination at loxP sites causes the permanent deletion of flanked fragment. (A) GFP the first reporter gene will express before Cre recombinase enzyme activation. (B) GFP, the loxP flanked reporter gene, is eliminated by the Cre recombinase enzyme, and DsRed is liberated for expression.

4. 1. 2. Brainbow (3 colors)

CMV-Brainbow-1.0 L plasmid was purchased from Addgene Company and has the following sequence (Fig. 4-3B):

CMV-Lox 2272-Lox P- dTomato-Lox 2272-eYFP-Lox P-mCerulean like the 2-color Brainbow, this construct will express dTomato, eYFP, or mCerulean based on Cre activity. It expresses the dTomato (former gene) constitutively and without recombination; eYFP and mCerulean (2nd and 3rd genes) are kept silent as the transcription is stopped by the stop codon of the dTomato gene (former gene). Once the Cre recombinase enzyme is activated, the flanked fragment by either lox2272 sites or loxP sites would be deleted randomly. Because dTomato is flanked by lox2272 sites, the deletion of this part regulates the transcription of next gene, eYFP. Later the transcription is

stopped by eYFP stop codon. Similarly, the deletion of loxP sites flanked fragment liberated the mCerulean for expression (Fig. 4-2A). Therefore, Cre-mediated recombination causes a random color expression in any single cell independently. On the other hand, at the time of injection and generation of the transgenic line, it is possible to insert more than 1 cassette to a cell's genome. As a result, the cells carrying 3 Brainbow cassettes in their genome have the potential to express 3 different fluorescent proteins at the same time and finally show a secondary color (Fig. 4-2B).

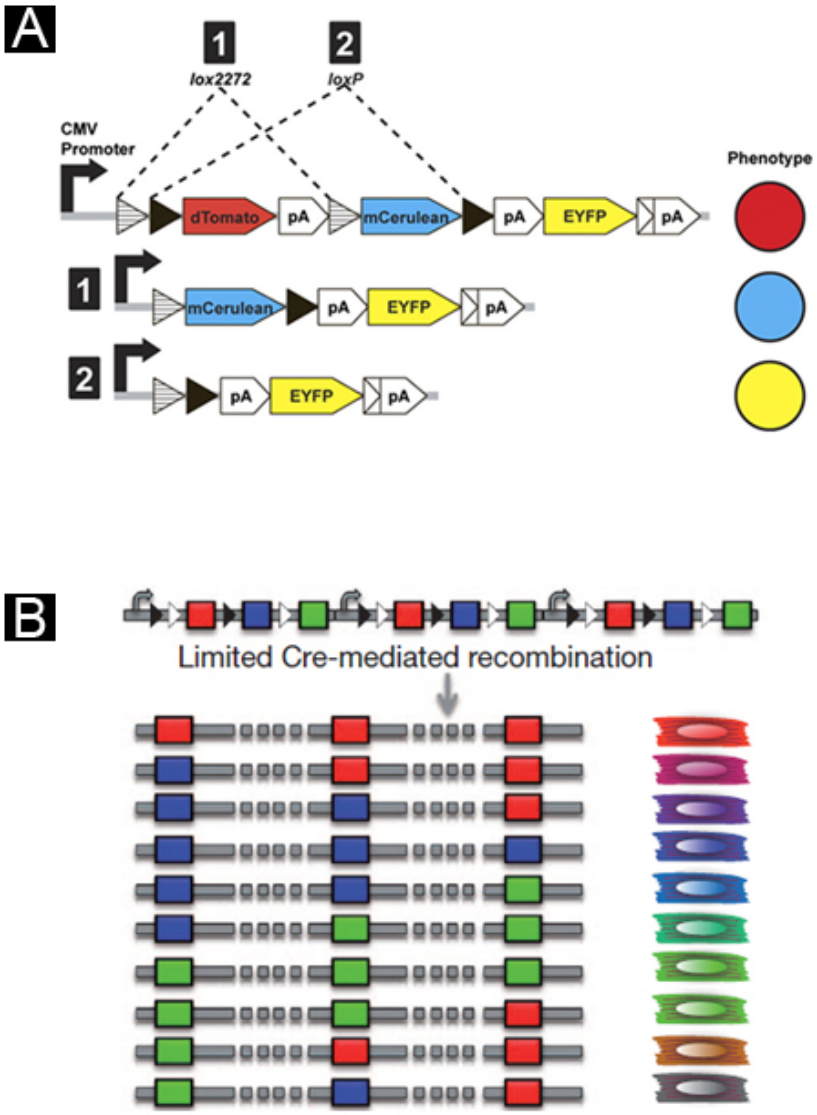

Figure 4-2: (A) Cre-mediated recombination at either lox2272 or loxP sites causes the permanent deletion of flanked fragment. (1) dTomate, the lox2272 flanked reporter gene, is eliminated by the Cre recombinase enzyme, and mCerulean is liberated for expression. (2) dTomate and mCerulean, the loxP flanked reporter genes, are eliminated by the Cre recombinase enzyme, and subsequently EYFP is liberated for expression (Card et al., 2011). (B) Cre-mediated recombination of the 3 tandem Brainbow cassettes in the genome causes the observation of secondary colors (Gupta & Poss, 2012).

4. 2. Materials and Methods

4. 2. 1. Plasmid construction and microinjection

To ease the generation of the transgenic line, the maize Ac/Ds transposable elements, as a transposon system, were used. This Ac/Ds system inserts the fragment of interest (f.o.i) to the animal genome and boosts the transgenic line generation efficiency. The commercial CMV-Brainbow-1.0 was purchased from Addgene Company. The CMV promoter was replaced by the β-actin promoter as a housekeeping gene in zebrafish. Next, the β-actin:dTomato-eYFP-mCerulean was inserted between the Ds sites into the pMDS6 plasmid as the backbone. The final construct, pMDS6:β-actin:Lox2272-LoxP-dTomato-Lox2272-eYFP-LoxP-mCerulean, and Ac mRNA were coinjected to the 1–2 cell stage zebrafish embryos. The injected embryos were incubated at 28.5ºC in an E3 medium. The positive 24-hour embryos were cultured and grown to their adult stage according to the protocol in *The Zebrafish Book* (Westerfield, 2007). Later, the adult fish were crossed with Tg(hsp70l:mCherry-CreER^{T2}), gifted by Stefan Hans from Dresden University of Technology.

A

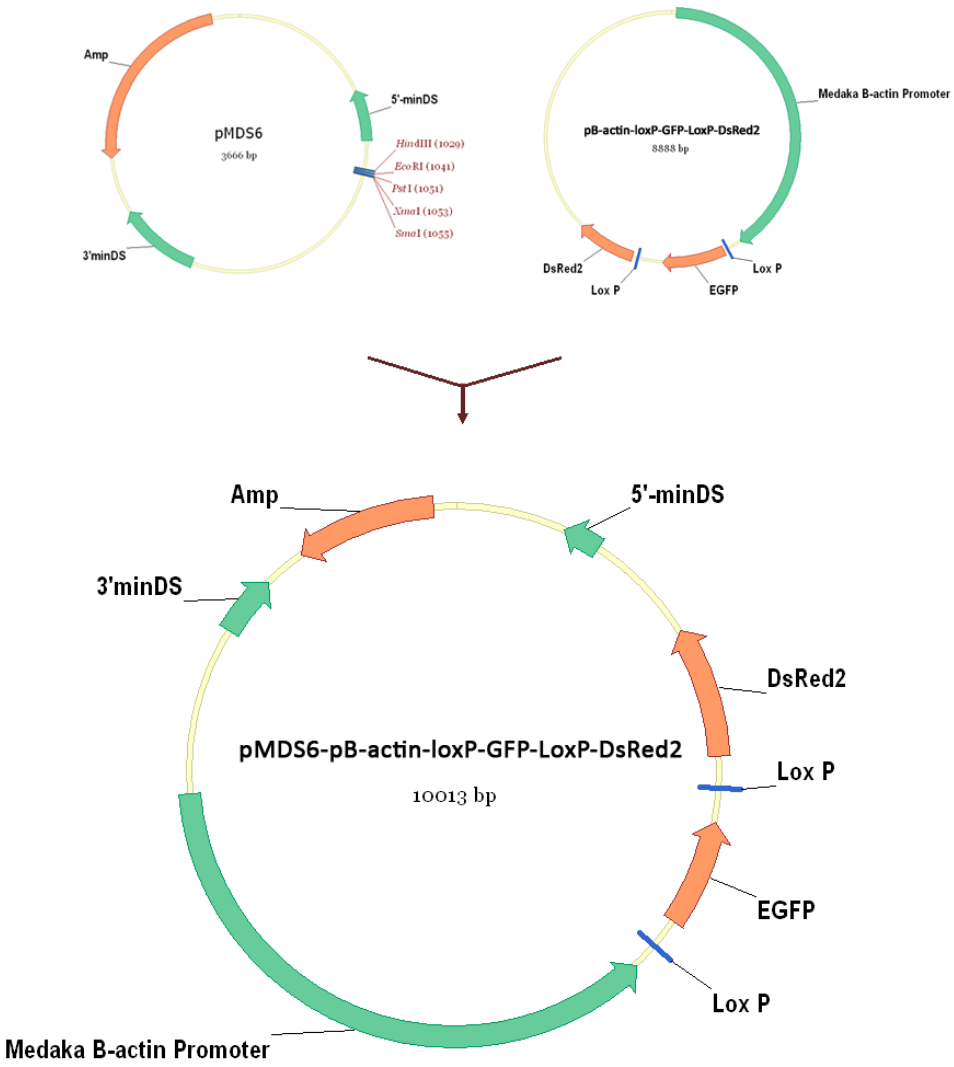
Amp
5'-minDS
pMDS6
3666 bp
HindIII (1029)
EcoRI (1041)
PstI (1051)
XmaI (1053)
SmaI (1055)
3'minDS
Medaka B-actin Promoter
pB-actin-loxP-GFP-LoxP-DsRed2
8888 bp
DsRed2
Lox P
Lox P
EGFP
Amp
5'-minDS
3'minDS
DsRed2
pMDS6-pB-actin-loxP-GFP-LoxP-DsRed2
10013 bp
Lox P
EGFP
Lox P
Medaka B-actin Promoter

B

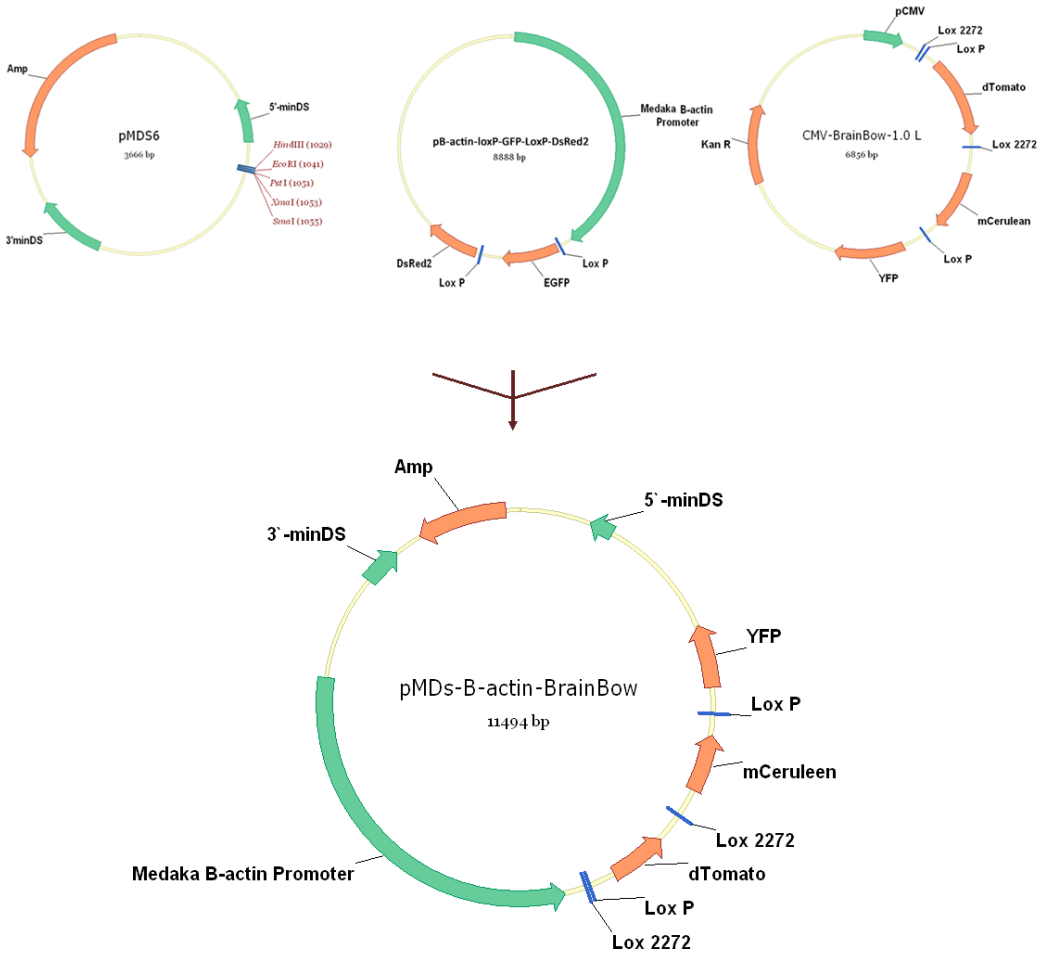

Figure 4-3: Brainbow (A) 2 colors and (B) 3 colors construct. The β-actin promoter and the flanked XFPs have been inserted between the DS sites in pMDS6 plasmid.

4. 2. 2. Heat shock and tamoxifen treatment

Embryonic stage: The embryos were heat shocked by adding 42ºC E3 medium and kept at 37ºC for 0.5–2 hours. Next, the embryos were returned to a 28.5ºC incubator. Once the $CreER^{T2}$ was expressed uniformly by heat induction, it was activated via pharmacological treatment. 50 mM tamoxifen (TAM; Sigma, T5648) in DMSO and 25 mM 4-hydroxytamoxifen (4-OHT; Sigma, H7904) in ethanol were prepared as a stock solution and stored in −20ºC in the dark. The embryos were incubated in either 5 mM TAM or 0.5 mM 4-OHT at 28.5ºC in the dark. Next, the embryos were rinsed 3 times and returned to the 28.5ºC incubator (S. Hans et al., 2011; S. Hans, Kaslin, Freudenreich, & Brand, 2009; Mosimann et al., 2011).

Adult stage: The water was gradually heated to 37ºC in 30 minutes and kept at 37ºC for 30 minutes. During the next 5–6 hours, the water temperature decrease to 28ºC. Next, the fish were either intraperitoneally injected or orally administrated 5 µl of 10 mM 4-OHT (S. Hans et al., 2009).

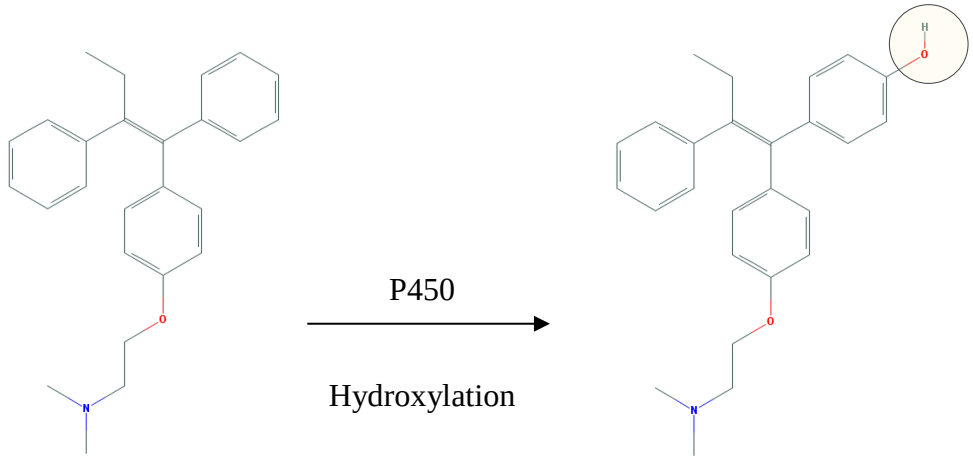

Tamoxifen

Molecular Formula: $C_{26}H_{29}NO$

Molecular Weight: 371.51

4-Hydroxytamoxifen

Molecular Formula: C26H29NO2

Molecular Weight: 387.51

Figure 4-4: Tamoxifen, a prodrug, has little affinity for the estrogen receptor. In contrast, 4-hydroxytamoxifen, the active metabolite of tamoxifen, has 30–100 times more affinity with the estrogen receptor. This hydroxylation reaction occurs in the liver and by the cytochrome P450.

4. 2. 3. Tissue sampling and vibratome sectioning

The zebrafish were killed, and the dissected intestines were fixed in 4% paraformaldehyde, followed by preparation for vibratome sectioning. The samples were embedded in 4% low-melting-point agarose (LMA) (Hugo J. Snippert, Schepers, Delconte, Siersema, & Clevers, 2011). Once the LMA block was formed, it was ready for sectioning by vibratome (Leica VT1200).The sections were mounted on a room temperature coverslip to ease the imaging from either side of the sample. The sections were protected by embedding in a mounting medium (vectashield h-1400) and a covered with a coverslip. The mounted slides stored in a light protected condition at 4°C before imaging.

4. 2. 4. Imaging

Images were acquired using a PerkinElmer Ultraview Vox Spinning Disk, with the laser line 440, 514, and 568. The captured images were processed by Volocity software.

4. 3. Results and discussion

To check whether the system works properly and efficiently, the double transgenic line from β-actin:Lox2272-LoxP-dTomato-Lox2272-eYFP-LoxP-

mCerulean and hsp70l:mCherry-CreERT2 were induced by both heat shock and 4-OHT at the early developmental stages and 6 dpf. At 1 dpf, the larval fish were fixed and prepared for imaging.

Figure 4-5 shows the Cre-regulated recombination in somites and muscle cells.

As described previously, the simultaneous existence of different FPs in a cell expresses the secondary color.

Figure 4-5 also shows both the primary and secondary colors because some cells express different FPs, which are colocalized in the cell.

Next, we examined the recombination response in intestinal epithelium. In section 1. 3. 2. it has been described that the intestinal epithelium folding has already been started at 6 dpf. Therefore, the Cre recombinase enzyme was induced by heat shock and 4-OHT treatment at 6 dpf. The next day, the fixed intestine was dissected and prepared for imaging.

Figure 4-6 shows an expanded focus of the intestinal bulb with a thickness of 32.8 µm (by merging 320 stacks with a Z-stack size of 0.1 µm).

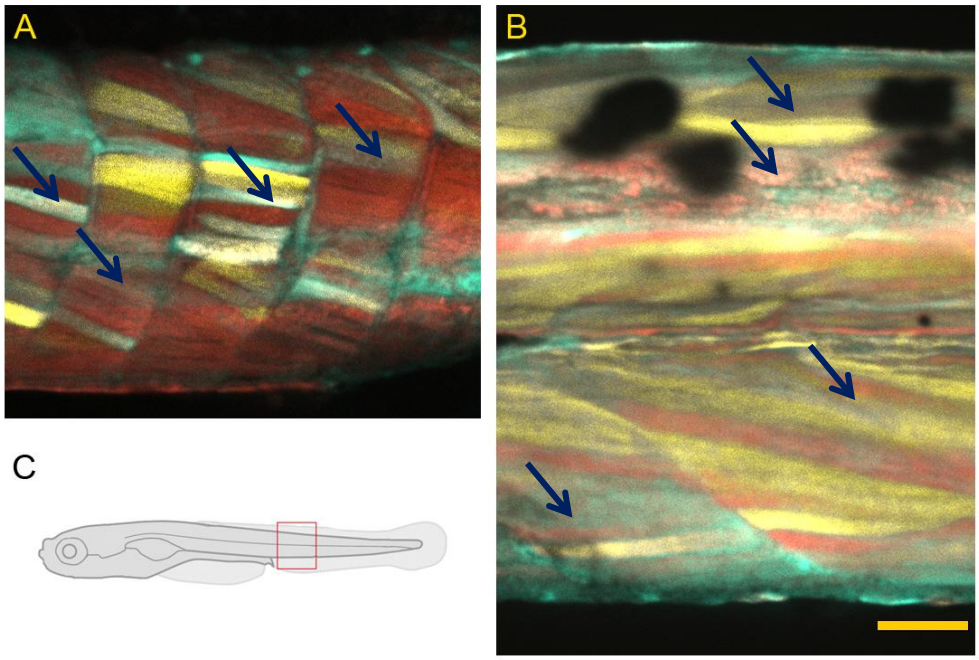

Figure 4-5: Cre-regulated recombination in (A) 24 hpt and (B) 7 dpf larval fish muscle cells. Arrows show the secondary colors. β-actin: dTomato (Red), β-actin: YFP (Yellow) and β-actin: mCerulean (Blue). Scale bar = 100 µm.

In this figure, the onset of the intestinal epithelium folding is clear (Fig. 4-6 white arrowhead) and the intestinal lumen is well developed. However, the folding has not started in the dorsal side of the intestinal bulb yet, which helps the intestinal bulb formation. The proliferation rate has been decreased at this time and is limited to the base of the intestinal villus. Therefore, the intestinal villi, which are short at this time, show a similar expression pattern with the intervillus base (Fig. 4-6 yellow arrowhead).

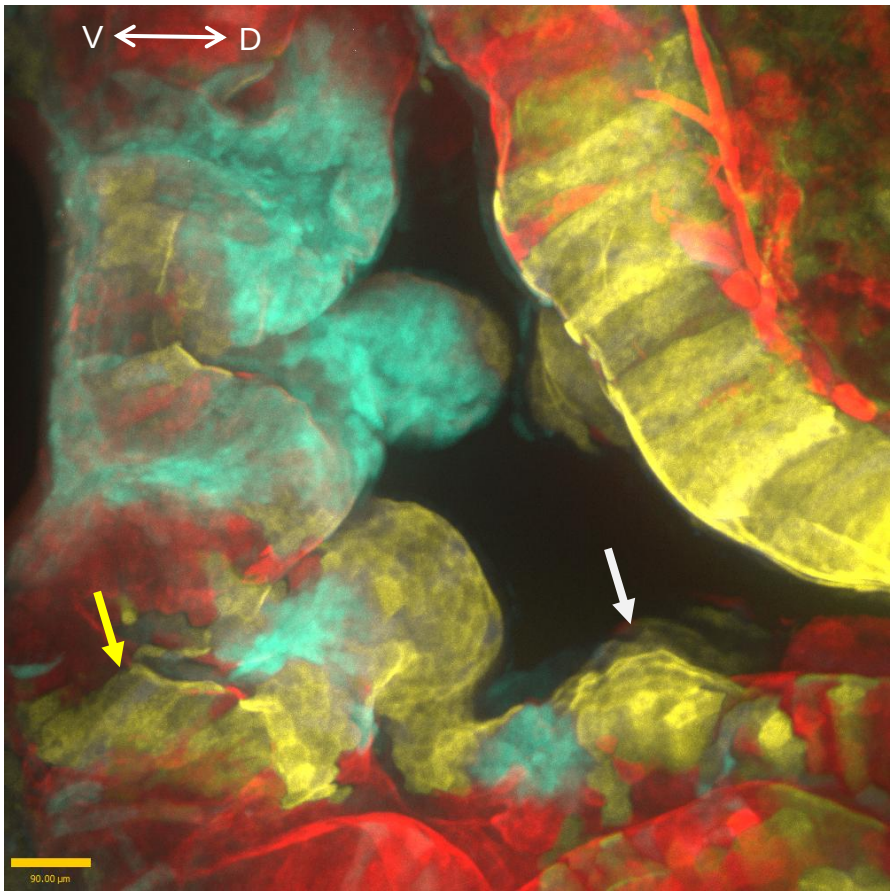

Figure 4-6: Interior view of an intestinal bulb at 7 dpf. This image is an expanded focus of 32.8 µm of Z depth (320 stacks with a Z-stack size of 0.1 µm). The intestinal folding has been started in the ventral side of the intestinal to shape the intestinal bulb (white and yellow arrowheads). The expression pattern of the epithelial cells of an intestinal villus is similar (yellow arrowhead).V: ventral. D: Dorsal. β-actin: dTomato (Red), β-actin: YFP (Yellow) and β-actin: mCerulean (Blue). Scale bar = 90 µm.

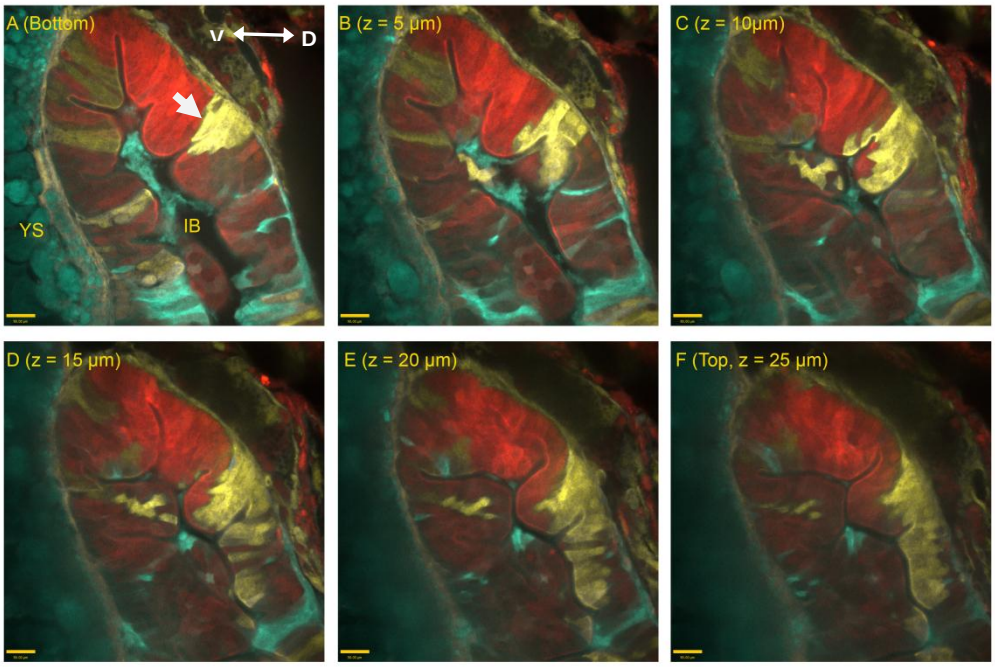

Figure 4-7: Cre-regulated recombination in intestinal bulb at 7 dpf at different Z depths (Z-stack interval distance of 5 µm). YS: yolk sac, IB: intestinal bulb. V: ventral. D: Dorsal. β-actin: dTomato (Red), β-actin: YFP (Yellow) and β-actin: mCerulean (Blue). Scale bar = 90 µm.

Figure 4-7 shows intestinal epithelium at 7 dpf, imaged at different Z depths as mentioned in the image. The interval distance of 2 sequential Z-stacks is 5 µm. This figure shows the onset of the intestinal folding at this stage. It also confirms the proliferation of the cells at the intervillus bottom to renew the intestinal epithelial cells. At the lowest plane, the yellow patch is limited to a small area at the intervillus bottom (Fig. 4-7 arrowhead). The yellow patch expanded to the intestinal villus and reached the villus tip as the Z-stacks move towards the top (Z stack 5 µm, 10 µm, 15 µm, 20 µm, and 25 µm). These observations show that the ISCs in the epithelial layer reproduce new

cells through an increase in the proliferation rate at the intervillus bottom to form the intestinal villi during intestinal development coincidentally by mesenchymal layer invagination (Savin et al., 2011). On the other hand, as the proliferation rate is limited to the intervillus bottom by 4–6 dpf (Ng et al., 2005) the only direction for cell migration is away from the ISCs at the intervillus bottom and toward the intestinal villi tips. As the cells reached the villus tip from either side of the intestinal villus, they would shed off inevitably.

Because the trial experiments showed satisfactory and efficient responses, we tried to study intestinal epithelium renewal by Cre-regulated recombination in adult stages too.

Figure 4-8 shows the top view of the intestinal villi at adult stage and at 4 dpt. The adult fish were induced by heat shock and treated by 4-OHT. Four days later, the intestines were dissected, fixed, and prepared for imaging without sectioning. The result of the Cre-regulated recombination is clearly visible. Interestingly, the recombination pattern of either side of the intestinal villi would change at the villi tip. In other words, the ribbon of cells does not continue to the opposite side of the intestinal villus. The white borders in this figure show where apoptosis happens, as the ribbons of cells traveled all the way toward the villus tips and are discontinued at the villi tips.

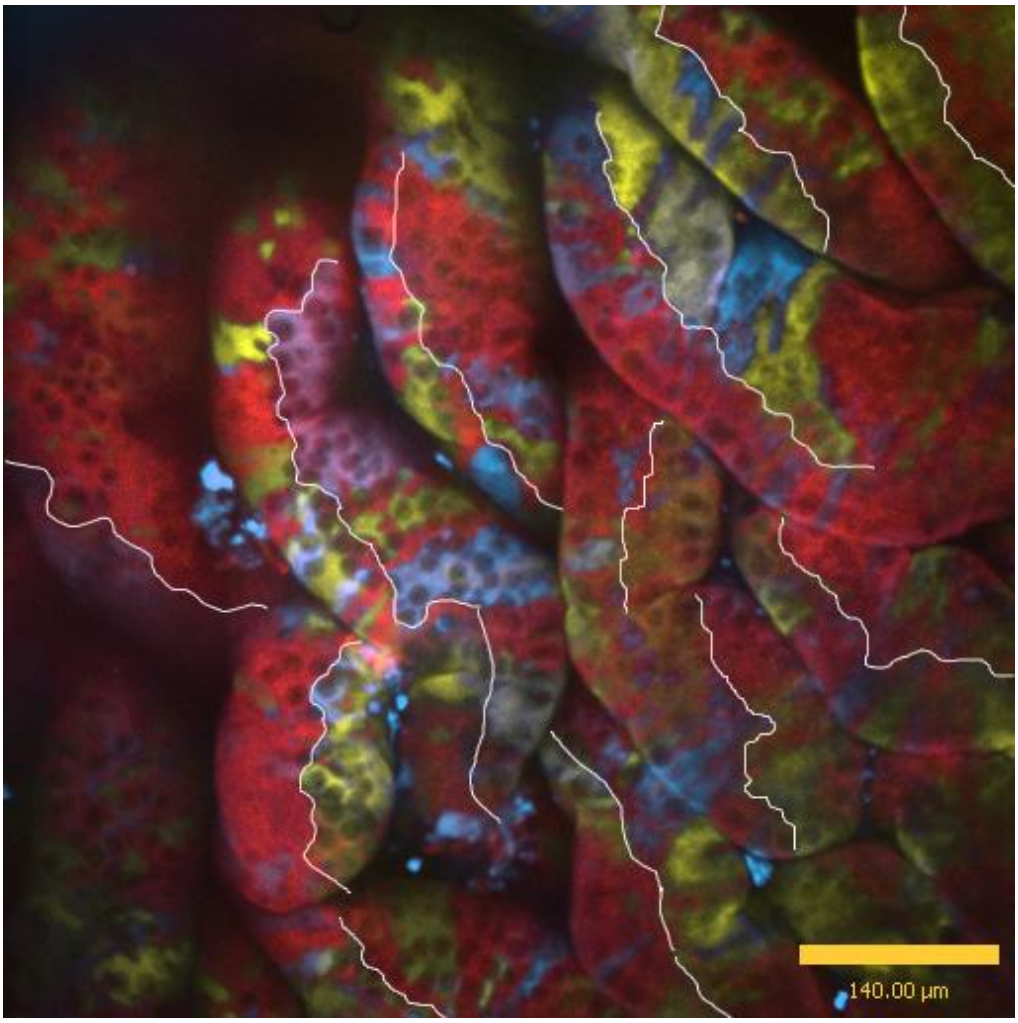

Figure 4-8: Top view of the recombinant intestinal villi at adult stage without sectioning. The white lines show the border of either side of the intestinal villi. The lines also show where apoptosis happens. β-actin: dTomato (Red), β-actin: YFP (Yellow) and β-actin: mCerulean (Blue). Scale bar = 140 µm.

Figure 4-9 shows the recombination pattern in a smaller scale. This figure shows the lateral view of a foregut cross-section. The ribbons of recombinant cells are clearly visible and can be interpreted as the traveling of cells from the intestinal villi bases toward the villi tips. Interestingly, the width of the ribbons varies from 1 row of cells (white arrowheads) to several rows of cells (pink arrowheads). These new results suggest the existence of ISCs or progenitor cells at the intervillus bottom and parallel to the intestinal villus tip. Therefore, an intestinal villus epithelium is renewed by 2 groups of ISCs, which are located at the intervillus bottoms at both sides, and parallel to the intestinal villus tip. These ISCs reproduce the new cells, which migrate toward the villus tip. In the same intestinal villus and at the adjacent positions, the other newly reproduced cells from the neighboring ISCs at the intervillus bottom travel to the villus tip too. Therefore, the intestinal epithelium layer would be renewed by the ISCs at the intervillus bottoms.

The same conclusion could be drawn from figure 4-8. The top view of the intestinal villi shows different recombinant patterns at either side of the intestinal villi, both of which are separated by the white line. This observation confirms the existence of a group of ISCs at the intestinal villus bottom that reproduced the cells' ribbons, which are parallel and travel toward the villus tip.

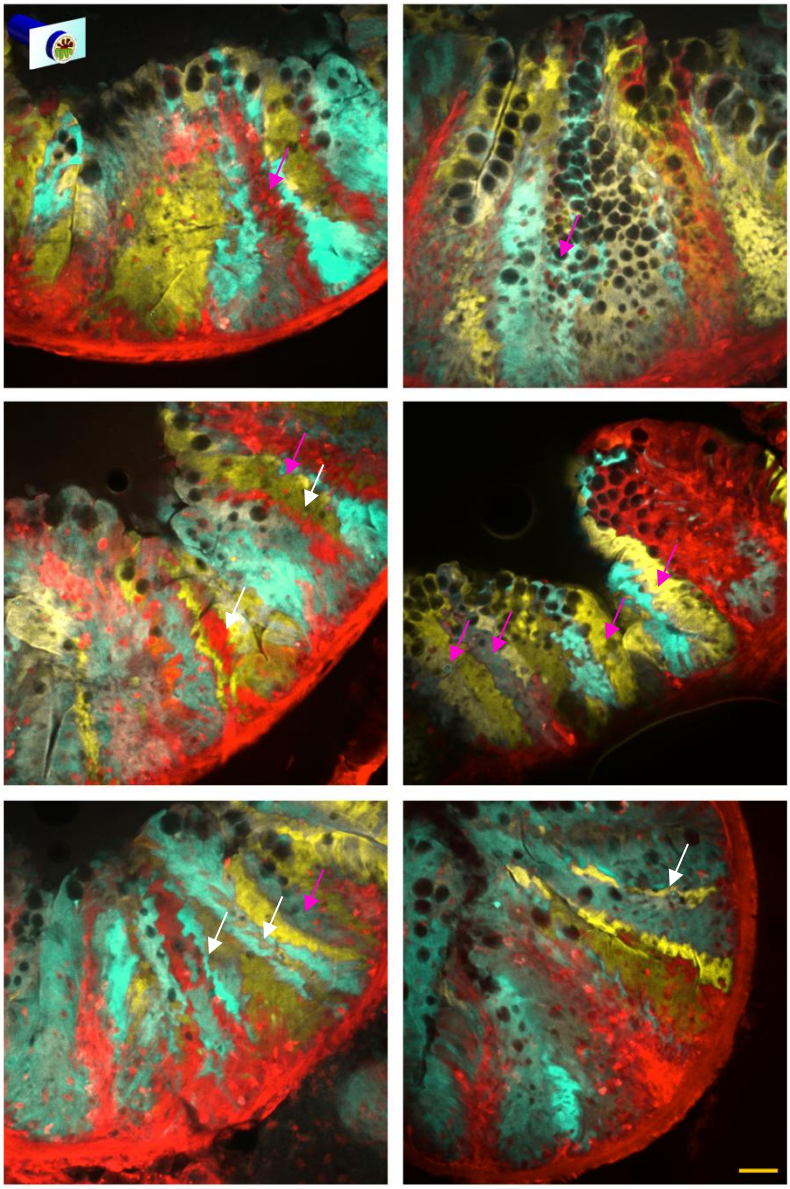

Figure 4-9: Lateral view of a recombinant foregut cross-section at adult stage and at 4 dpt. The ribbons of cells with different colors travel toward the villus tip. The ribbons' widths vary from 1 (white arrowheads) to several rows of cells (pink arrowheads). β-actin: dTomato (Red), β-actin: YFP (Yellow) and β-actin: mCerulean (Blue). Scale bar = 35 µm.

Figure 4-10 shows the lateral view of an individual intestinal villus at adult stage and 2 wpt. The intestinal villi are tightly compacted together. Therefore, imaging and analysing cell migration along the base-to-tip axis is impossible. To ease imaging, decrease the cross-talk between the adjacent intestinal villi, and liberate the lateral view of the intestinal villus for imaging, it was separated manually by 27-gauge syringe needles. Similar to previous figures of recombinant tissue, the ribbons of cells with different recombination patterns travel from the base to the villi tips. However, the ribbons of recombinant cells decreased in number but increased in width by 2 wpt. These observations suggest that some cells at the intervillus bottom proliferate temporarily to reproduce the new cells. However, after a longer time, these progenitor cells are replaced with new cells originating from the same ISC with the same Cre-regulated recombination to reproduce the new cells. As a result, the wider ribbons of cells will appear by 2 wpt. The cells that proliferate temporarily may be the progenitor cells, TACs or CBCs.

As discussed earlier, there are different types of ISCs in mice and mammalians: the +4 LRC that are quiescent and CBC that are rapidly cycling (Barker et al., 2012; Buczacki et al., 2013; Scoville, Sato, He, & Li, 2008). CBCs are frequent, active, and divide rapidly to reproduce the new cells. The quiescent ISCs, +4 LRC, are less frequent, silent and display slow activity.

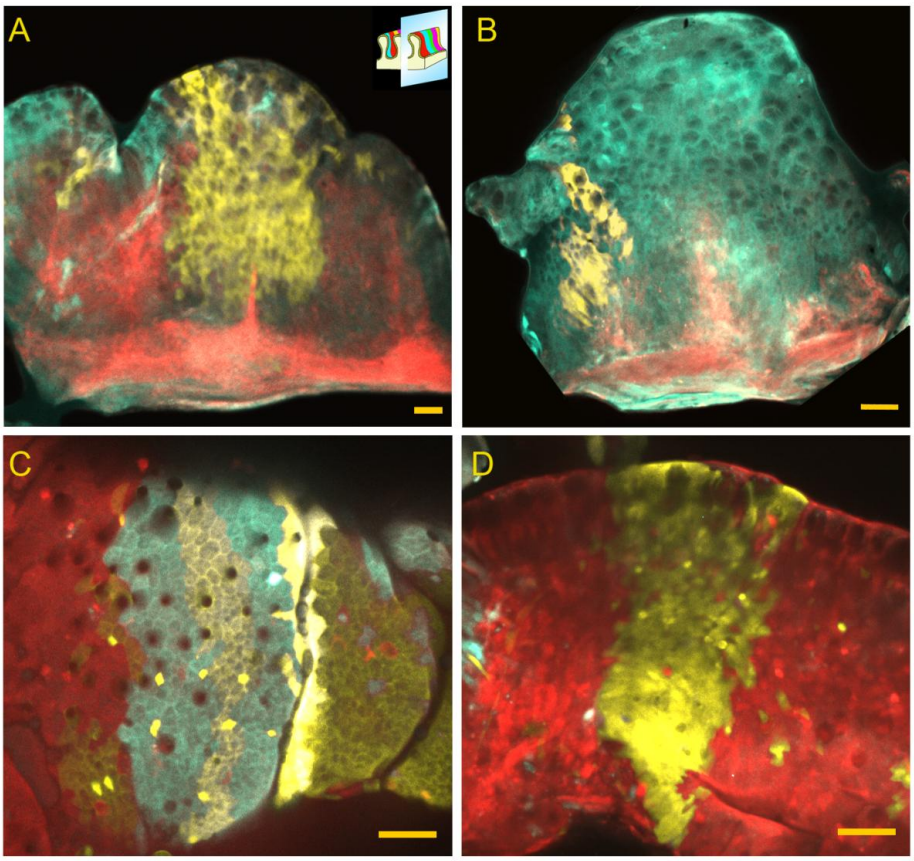

Figure 4-10: Cre-regulated recombination pattern at adult stages and at 2 wpt in (A and B) foregut and (C and D) mid-gut. The ribbons of recombinant cells decreased in number but increased in width by 2 wpt. β-actin: dTomato (Red), β-actin: YFP (Yellow) and β-actin: mCerulean (Blue). Scale bar = 30 µm.

It may be concluded that by 2 wpt, the CBCs are replaced with newly reproduced CBCs with similar recombinant genomic materials from the +4 LRC and quiescent stem cells. Consequently, the reproduced cells by the new CBCs show similar recombination patterns too. As a result, the number of ribbons decreased, while the widths of the ribbons increased.

Next, we studied the cells' migration pattern in the recombinant intestinal epithelium in 3D. Figure 4-11 shows the recombination pattern in a top view of an intestinal villus at 2 weeks post treatment. Interestingly, the villus epithelium mirrors the adjacent villus expression pattern; In other words, if the villus epithelial cells do not show recombination pattern and still are GFP-tagged, the neighbor villus is also preserved and express GFP. In contrast, if the villus epithelium has been altered to DsRed expression during the recombination the neighbor villus also shows genetic alteration and express DsRed. These observations also confirm the bilateral migration of newly reproduced cells toward the flanking villi, which we had shown in 2D renewal pattern results.

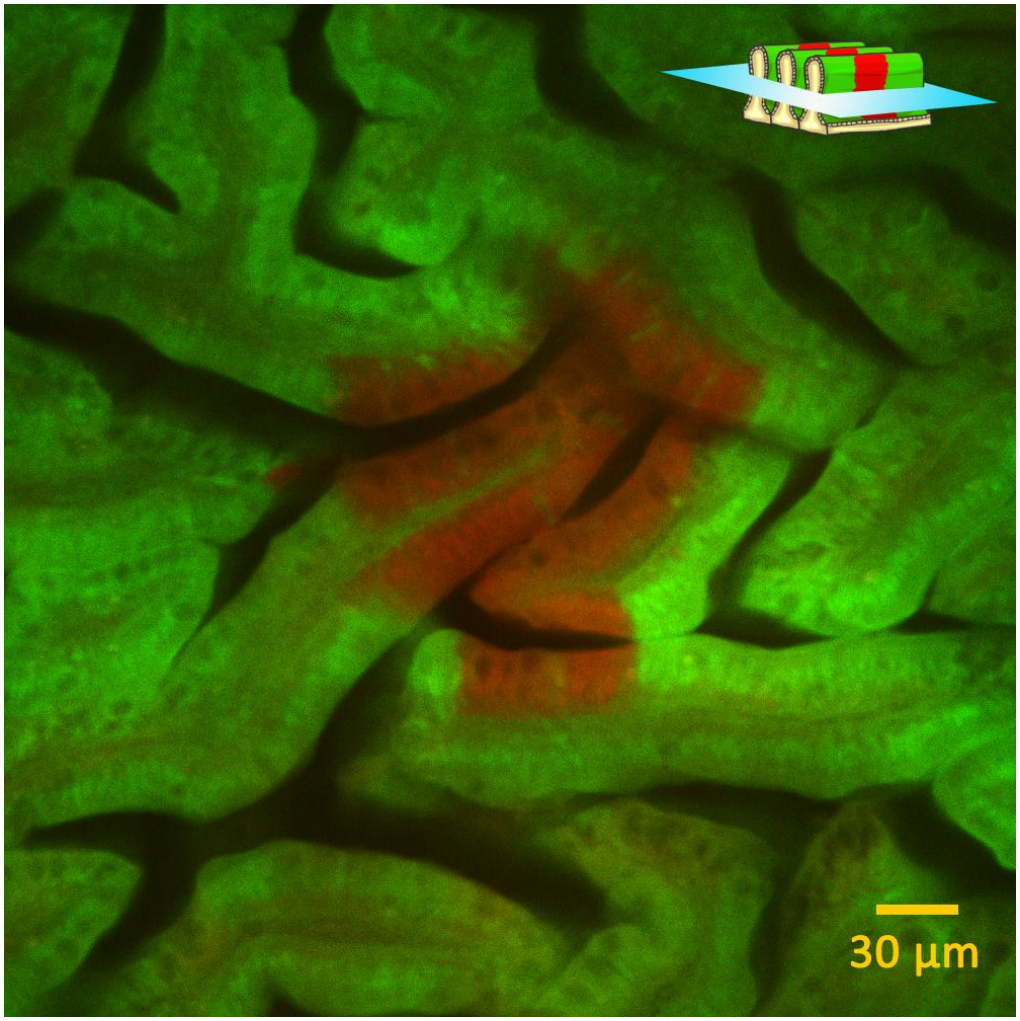

Figure 4-11: The villus epithelium mirrors the adjacent villus expression pattern. Cre-regulated recombination pattern at adult stages 2 weeks post treatment. The recombinant expression pattern marks the stem cells' path. β-actin: GFP (Green) and β-actin: DsRed (Red). Scale bar = 30 µm.

To show if the vertical stripes continue along the base-to-tip axis, we acquired a 3D image traveling in Z direction (Fig. 4-12 and supplementary movie 1) and showed the border of normal GFP-tagged cells and recombinant RFF cells continue from the base to the tip of the villus. Notably the vertical stripes of labeled cells show the location of stem cells and their paths of migration to the ridge. These observations prove the presence of more than one ISC at the bottom of the intestinal villus.

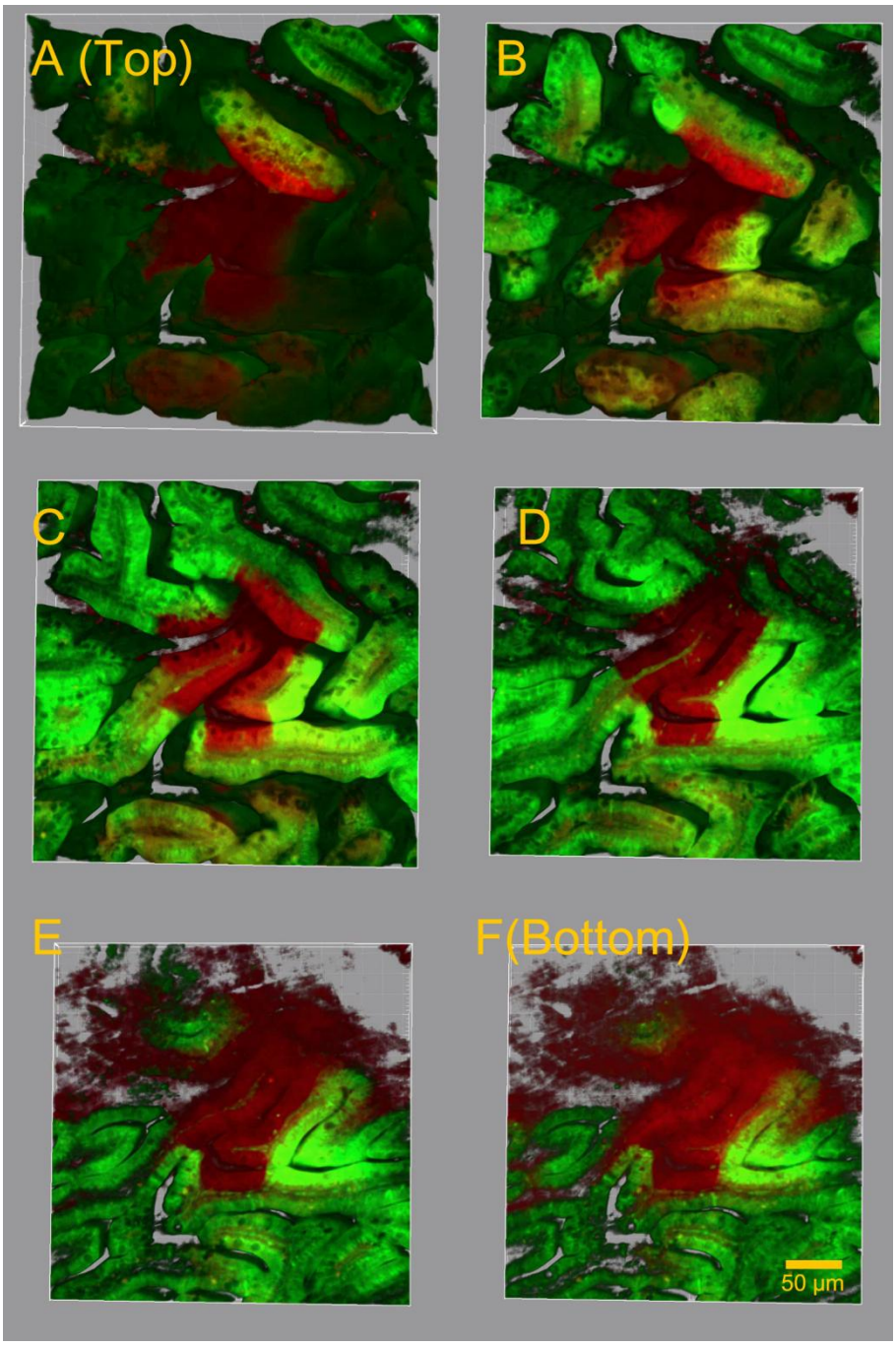

Figure 4-12: Stripes of labeled cells travel toward the tip. Vertical stripes of labeled cells show the location of stem cells and their paths of migration to the ridge. Images A, B, C, D, E and F are the same frame but from sequential Z stacks. β-actin: GFP (Green) and β-actin: DsRed (Red). Scale bar = 50 µm.

4. 4. Conclusions

Because there is no specific marker for zebrafish ISCs, we took advantage of Zebrabow to study zebrafish intestinal epithelium renewal. This novel and powerful method provides the opportunity to study tissue renewal at the desired time (in contrast to chimera generation and mosaic generation) and desired region. On the other hand, the recombination pattern in this strategy has a wide range of different colors, which provides the opportunity to study the tissue renewal spatially (in contrast to the label retention technique). Therefore, this technique, along the previous experiments, helped us to draw new conclusions:

1. Either side of an intestinal villus is renewed with a group of progenitor cells at the intervillus bottom and parallel to the villus tip.

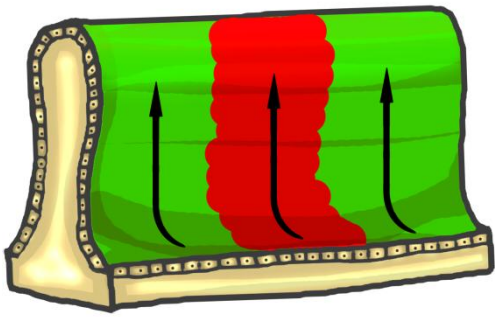

2. A limited number of dominant ISCs renew either side of an intestinal villus.

3. Adjacent sides of the neighboring intestinal villi, flanking an intervillus, share the ISCs at the intervillus bottom.

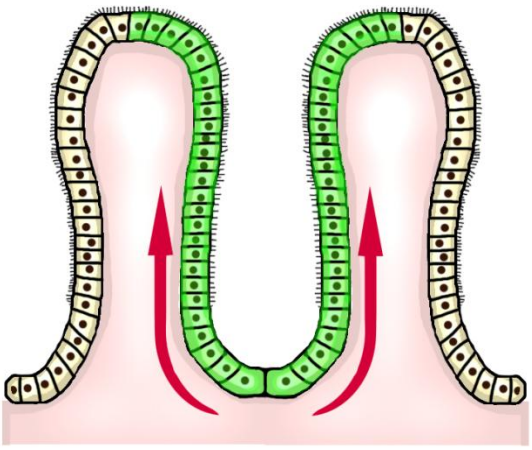

Appendix

(A) Label retention results of a time-course experiment:

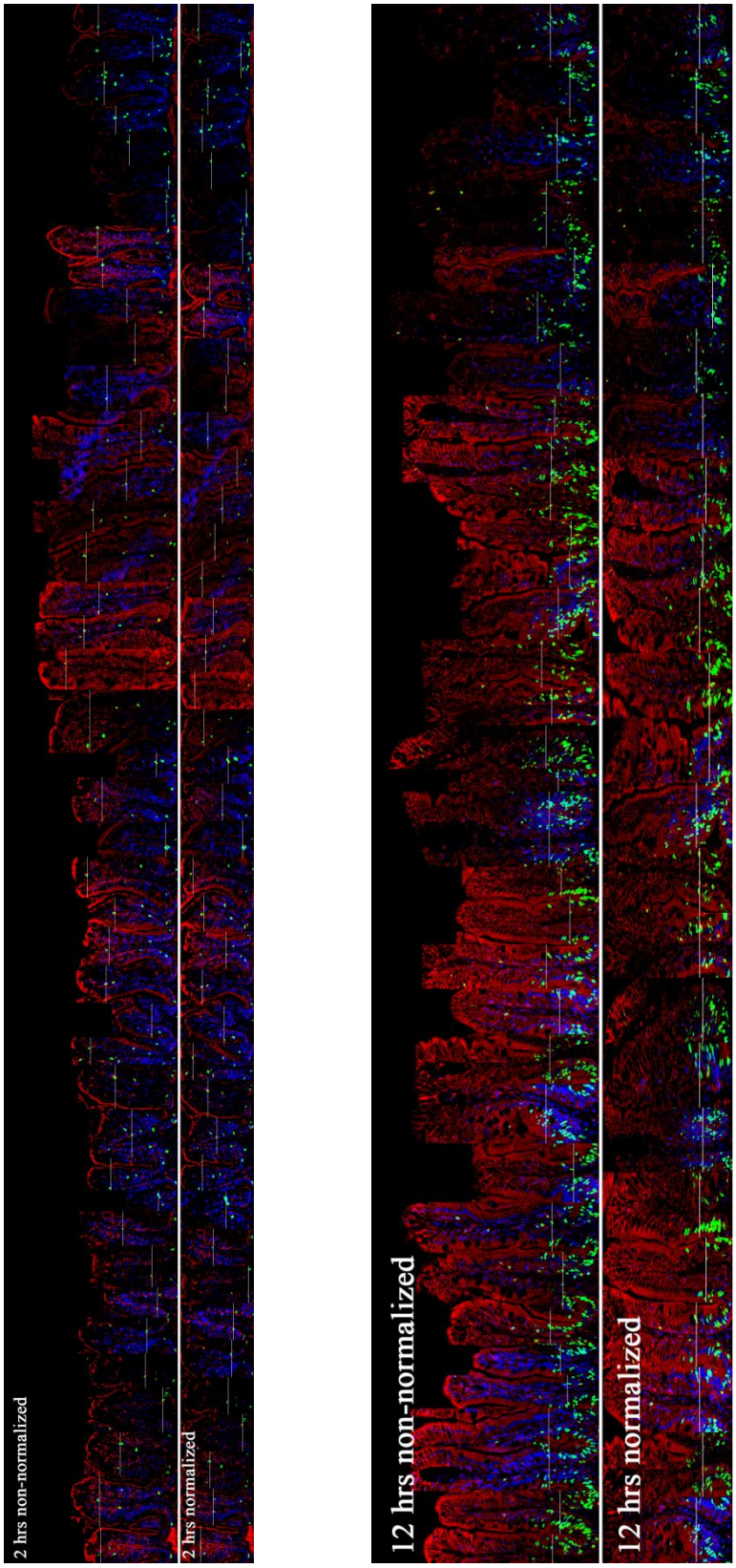

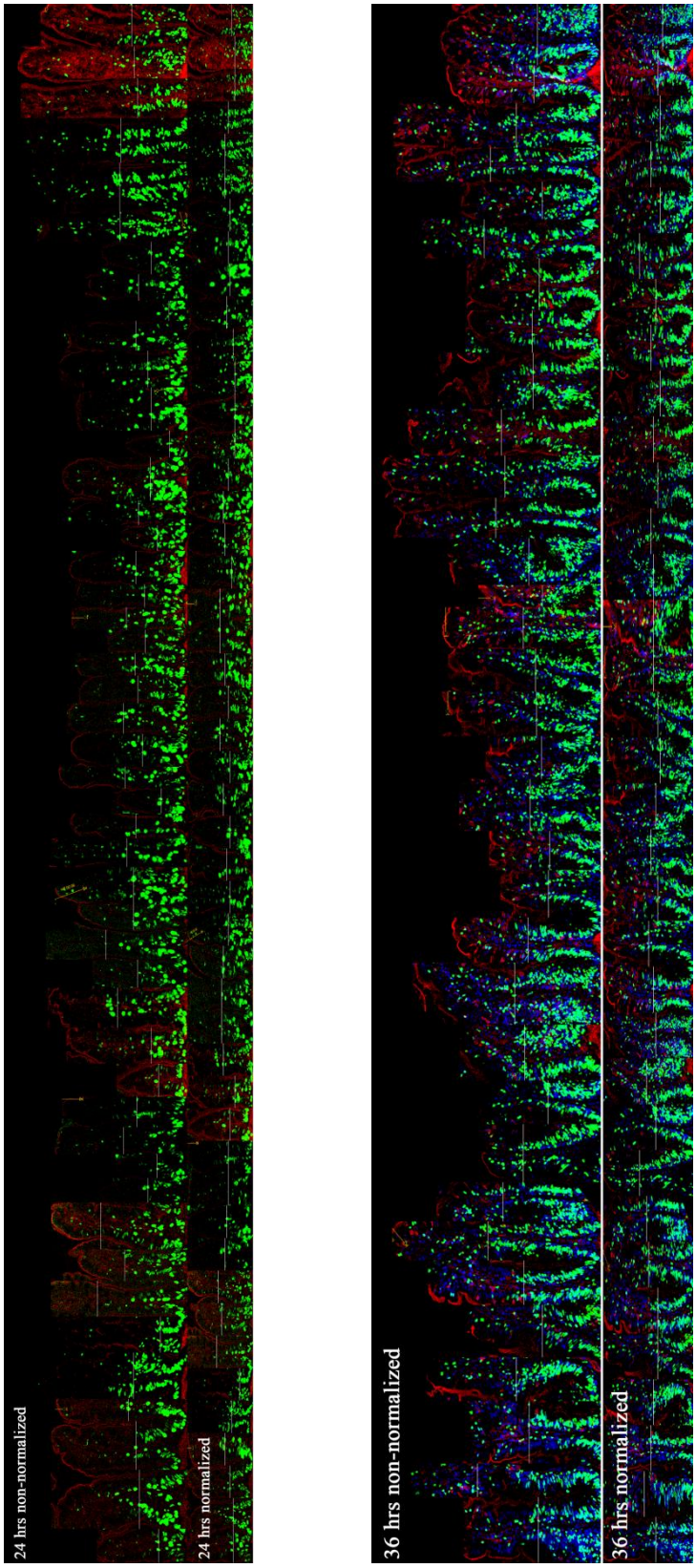
24 hrs non-normalized
24 hrs normalized
36 hrs non-normalized
36 hrs. normalized

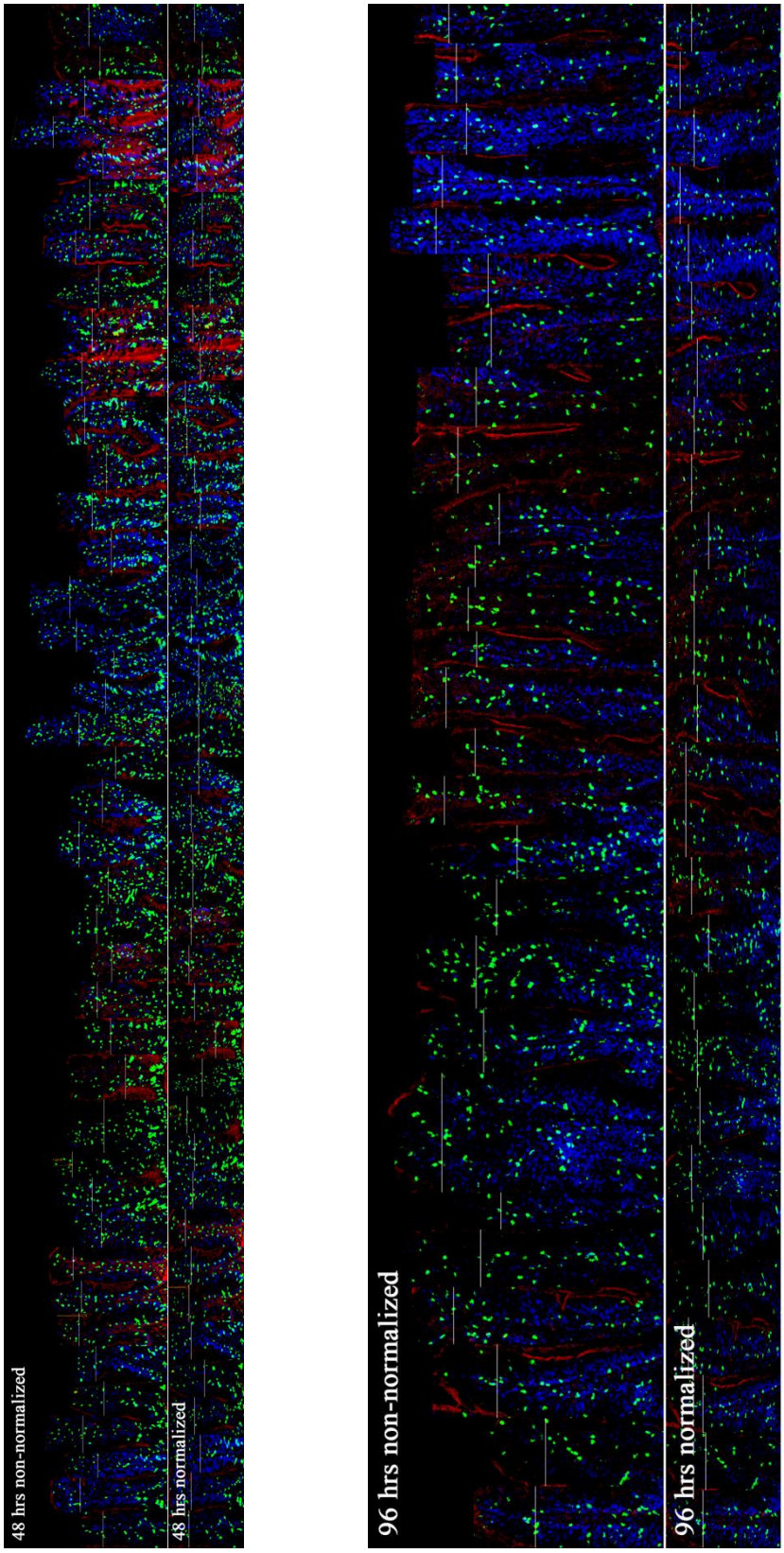
48 hrs non-normalized
48 hrs normalized
96 hrs non-normalized
96 hrs normalized

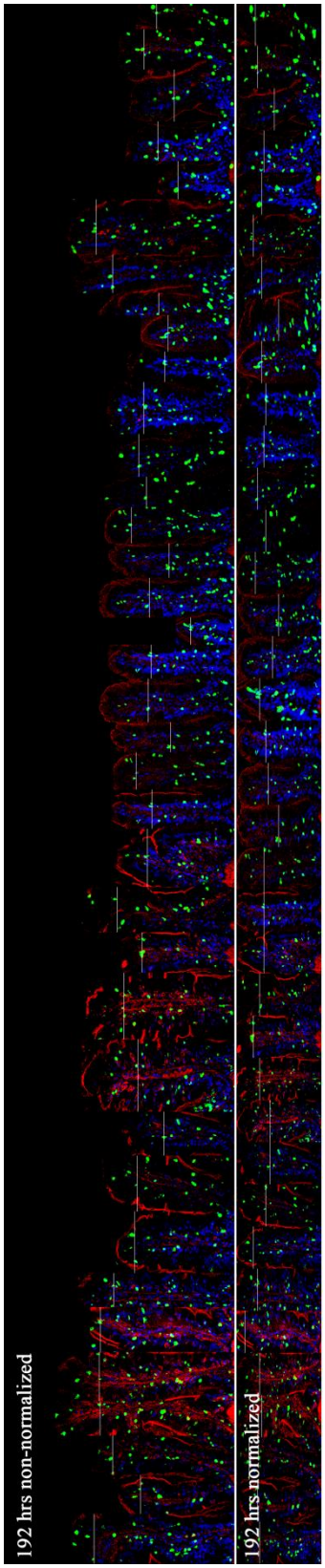
192 hrs non-normalized
192 hrs normalized

(B) STORM (STem cell mediated Optimal Renewal of epithelium Model)

matlab code:

```
c0 = 1;

betatwo = 10.7;

gamma = 2.0;


beta = betatwo;


minvalue = 1/0;

mins = 0;

mink4 = 0;


%function y = f(s, k4)

%y = -(s*(beta+gamma))/(2*beta) - 1/(2*(1+k4)) +
sqrt((s*(1+k4)*(beta+gamma)+beta)^2 -
4*s*beta*gamma*(1+k4)*(1+beta/gamma+s+s*k4))/(2*beta*(1+k4))


for s = 0:0.001:1

   for k4 = 0.001*(0:1:1000)

      sq = (s*(1+k4)*(beta+gamma)+beta)^2 -
4*s*beta*gamma*(1+k4)*(1+beta/gamma+s+s*k4);

      if (sq >= 0)

         value = -(s*(beta+gamma))/(2*beta) - 1/(2*(1+k4)) +
sqrt(sq)/(2*beta*(1+k4));

         if (value < minvalue)

           minvalue = value;
```

```
            mins = s;
            mink4 = k4;
          end
        end
    end
end

minvalue;
mins;
mink4;

alpha = c0/mins;
mins
beta = (1+1/alpha)*betatwo
```

Bibliography

Barker, N., & Clevers, H. (2010). Leucine-rich repeat-containing g-protein-coupled receptors as markers of adult stem cells. *Gastroenterology, 138*(5), 1681-1696. doi: 10.1053/j.gastro.2010.03.002

Barker, N., van de Wetering, M., & Clevers, H. (2008). The intestinal stem cell. *Genes & Development, 22*(14), 1856-1864. doi: 10.1101/gad.1674008

Barker, N., van Es, J. H., Kuipers, J., Kujala, P., van den Born, M., Cozijnsen, M., . . . Clevers, H. (2007). Identification of stem cells in small intestine and colon by marker gene lgr5. *Nature, 449*(7165), 1003-U1001. doi: 10.1038/nature06196

Barker, N., van Oudenaarden, A., & Clevers, H. (2012). Identifying the stem cell of the intestinal crypt: Strategies and pitfalls. *Cell Stem Cell, 11*(4), 452-460. doi: 10.1016/j.stem.2012.09.009

Bjerknes, M., & Cheng, H. (1981a). The stem-cell zone of the small intestinal epithelium .1. Evidence from paneth cells in the adult-mouse. *American Journal of Anatomy, 160*(1), 51-63.

Bjerknes, M., & Cheng, H. (1981b). The stem-cell zone of the small intestinal epithelium .5. Evidence for controls over orientation of boundaries between the stem-cell zone, proliferative zone, and the maturation zone. *American Journal of Anatomy, 160*(1), 105-112.

Bjerknes, M., & Cheng, H. (1999). Clonal analysis of mouse intestinal epithelial progenitors. *Gastroenterology, 116*(1), 7-14.

Buck, S. B., Bradford, J., Gee, K. R., Agnew, B. J., Clarke, S. T., & Salic, A. (2008). Detection of s-phase cell cycle progression using 5-ethynyl-2 '-deoxyuridine incorporation with click chemistry an alternative to using 5-

bromo-2 '-deoxyuridine antibodies. *Biotechniques, 44*(7), 927-929. doi: 10.2144/000112812

Buczacki, S. J., Zecchini, H. I., Nicholson, A. M., Russell, R., Vermeulen, L., Kemp, R., & Winton, D. J. (2013). Intestinal label-retaining cells are secretory precursors expressing lgr5. *Nature, 495*(7439), 65-69. doi: 10.1038/nature11965

Burgess, D. R. (1975). Morphogenesis of intestinal villi .2. Mechanism of formation of previllous ridges. *Journal of Embryology and Experimental Morphology, 34*(DEC), 723-740.

Cairns, J. (1975). Mutation selection and the natural history of cancer. *Nature, 255*(5505), 197-200.

Cappella, P., Gasparri, F., Pulici, M., & Moll, J. (2008). A novel method based on click chemistry, which overcomes limitations of cell cycle analysis by classical determination of brdu incorporation, allowing multiplex antibody staining. *Cytometry A, 73*(7), 626-636. doi: 10.1002/cyto.a.20582

Card, J. P., Kobiler, O., McCambridge, J., Ebdlahad, S., Shan, Z. Y., Raizada, M. K., . . . Enquist, L. W. (2011). Microdissection of neural networks by conditional reporter expression from a brainbow herpesvirus. *Proceedings of the National Academy of Sciences of the United States of America, 108*(8), 3377-3382. doi: 10.1073/pnas.1015033108

Cheng, H., & Leblond, C. P. (1974). Origin, differentiation and renewal of the four main epithelial cell types in the mouse small intestine v. Unitarian theory of the origin of the four epithelial cell types. *American Journal of Anatomy, 141*(4), 537–561.

Chia, L. A., & Kuo, C. J. (2010). The intestinal stem cell. In K. H. Kaestner (Ed.), *Development, differentiation, and disease of the luminal gastrointestinal tract* (Vol. 96, pp. 157-173).

Chung, K., Wallace, J., Kim, S. Y., Kalyanasundaram, S., Andalman, A. S., Davidson, T. J., . . . Deisseroth, K. (2013). Structural and molecular interrogation of intact biological systems. *Nature, 497*(7449), 332-+. doi: 10.1038/nature12107

Clarke, A. R. (2006). Wnt signalling in the mouse intestine. *Oncogene, 25*(57), 7512-7521. doi: 10.1038/sj.onc.1210065

Crosnier, C., Stamataki, D., & Lewis, J. (2006). Organizing cell renewal in the intestine: Stem cells, signals and combinatorial control. *Nature Reviews Genetics, 7*(5), 349-359. doi: 10.1038/nrg1840

Crosnier, C., Vargesson, N., Gschmeissner, S., Ariza-McNaughton, L., Morrison, A., & Lewis, J. (2005). Delta-notch signalling controls commitment to a secretory fate in the zebrafish intestine. *Development, 132*(5), 1093-1104. doi: 10.1242/dev.01644

Dahm, R. (2006). The zebrafish exposed. *American Scientist, 94*(5), 446-453. doi: 10.1511/2006.61.1006

Dalal, J., & Radhi, M. (2013). Intestinal stem cells: Common signal pathways, human disease correlation, and implications for therapies. *ISRN Stem Cells, 2013*, 6. doi: 10.1155/2013/372068

Dorland. (2011). *Dorland's illustrated medical dictionary*: Elsevier Health Sciences.

Erturk, A., Mauch, C. P., Hellal, F., Forstner, F., Keck, T., Becker, K., . . . Bradke, F. (2012). Three-dimensional imaging of the unsectioned adult spinal cord to assess axon regeneration and glial responses after injury. *Nature Medicine, 18*(1), 166-171. doi: 10.1038/nm.2600

Escobar, M., Nicolas, P., Sangar, F., Laurent-Chabalier, S., Clair, P., Joubert, D., . . . Legraverend, C. (2011). Intestinal epithelial stem cells do not protect their genome by asymmetric chromosome segregation. *Nat Commun, 2*, 258. doi: 10.1038/ncomms1260

Faro, A., Boj, S. F., & Clevers, H. (2009). Fishing for intestinal cancer models: Unraveling gastrointestinal homeostasis and tumorigenesis in zebrafish. *Zebrafish, 6*(4), 361-376. doi: 10.1089/zeb.2009.0617

Freeman, H. J. (2008). Crypt region localization of intestinal stem cells in adults. *World Journal of Gastroenterology, 14*(47), 7160-7162. doi: 10.3748/wjg.14.7160

Froese, R., & Pauly, D. (2011, 2011). Danio rerio. *FishBase*.

Gilbert, S. F. (2003). *Developmental biology* (Seventh Edition ed.): Sunderland (MA): Sinauer Associates.

Goldberg, I., & Williams, R. (1991). *Biotechnology and food ingredients*: Springer.

Gregorieff, A., & Clevers, H. (2005). Wnt signaling in the intestinal epithelium: From endoderm to cancer. *Genes & Development, 19*(8), 877-890. doi: 10.1101/gad.1295405

Grey, R. D. (1972). Morphogenesis of intestinal villi. I. Scanning electron microscopy of the duodenal epithelium of the developing chick embryo. *Journal of Morphology, 137*(2), 193-213. doi: 10.1002/jmor.1051370206

Gupta, V., & Poss, K. D. (2012). Clonally dominant cardiomyocytes direct heart morphogenesis. *Nature, 484*(7395), 479-U102. doi: 10.1038/nature11045

Hama, H., Kurokawa, H., Kawano, H., Ando, R., Shimogori, T., Noda, H., . . . Miyawaki, A. (2011). Scale: A chemical approach for fluorescence imaging and reconstruction of transparent mouse brain. *Nature Neuroscience, 14*(11), 1481-U1166. doi: 10.1038/nn.2928

Hans, H., & Hedrich, H. (2004). *The laboratory mouse*: Elsevier Science.

Hans, S., Freudenreich, D., Geffarth, M., Kaslin, J., Machate, A., & Brand, M. (2011). Generation of a non-leaky heat shock-inducible cre line for conditional cre/lox strategies in zebrafish. *Developmental Dynamics, 240*(1), 108-115. doi: 10.1002/dvdy.22497

Hans, S., Kaslin, J., Freudenreich, D., & Brand, M. (2009). Temporally-controlled site-specific recombination in zebrafish. *Plos One, 4*(2). doi: 10.1371/journal.pone.0004640

Heath, J. P. (1996). Epithelial cell migration in the intestine. *Cell Biology International, 20*(2), 139-146. doi: 10.1006/cbir.1996.0018

Howell, J. C., & Wells, J. M. (2011). Generating intestinal tissue from stem cells: Potential for research and therapy. *Regenerative Medicine, 6*(6), 743-755. doi: 10.2217/rme.11.90

Howlader, N., Noone, A. M., Krapcho, M., Neyman, N., Aminou, R., Altekruse, S. F., . . . Cronin, K. A. (2013). Seer cancer statistics review, 1975-2009 (vintage 2009 populations). from http://seer.cancer.gov/csr/1975_2009_pops09/

Humphries, A., & Wright, N. A. (2008). Colonic crypt organization and tumorigenesis. *Nature Reviews Cancer, 8*(6), 415-424. doi: 10.1038/nrc2392

Insel, P. (2010). *Nutrition*: Jones & Bartlett Learning.

Insel, P. M., Ross, D., McMahon, K., & Bernstein, M. (2013). *Discovering nutrition*: Jones & Bartlett Learning.

Ishizuya-Oka, A. (2007). Regeneration of the amphibian intestinal epithelium under the control of stem cell niche. *Development, Growth & Differentiation, 49*(2), 99-107. doi: 10.1111/j.1440-169X.2007.00913.x

Kapoor, B. G., Smit, H., & Verighina, I. A. (1975). *The alimentary canal and digestion in teleosts*.

Kiel, M. J., He, S. H., Ashkenazi, R., Gentry, S. N., Teta, M., Kushner, J. A., . . . Morrison, S. J. (2007). Haematopoietic stem cells do not asymmetrically segregate chromosomes or retain brdu. *Nature, 449*(7159), 238-U210. doi: 10.1038/nature06115

Kimmel, C. B., Ballard, W. W., Kimmel, S. R., Ullmann, B., & Schilling, T. F. (1995). Stages of embryonic-development of the zebrafish. *Developmental Dynamics, 203*(3), 253-310.

Kimmel, C. B., & Law, R. D. (1985). Cell lineage of zebrafish blastomeres .3. Clonal analyses of the blastula and gastrula stages. *Developmental Biology, 108*(1), 94-101. doi: 10.1016/0012-1606(85)90012-0

Koo, B.-K., Stange, D. E., Sato, T., Karthaus, W., Farin, H. F., Huch, M., . . . Clevers, H. (2012). Controlled gene expression in primary lgr5 organoid cultures. *Nature Methods, 9*(1), 81-U197. doi: 10.1038/nmeth.1802

Langnas, A. N., Goulet, O., Quigley, E. M. M., & Tappenden, K. A. (2009). *Intestinal failure: Diagnosis, management and transplantation*: Wiley.

Lansdorp, P. M. (2007). Immortal strands? Give me a break. *Cell, 129*(7), 1244-1247. doi: 10.1016/j.cell.2007.06.017

Leblond, C. P., & Stevens, C. E. (1948). The constant renewal of the intestinal epithelium in the albino rat. *The Anatomical Record, 100*(3), 357-377. doi: 10.1002/ar.1091000306

Lee, C., Goolsby, C. L., & Sensibar, J. A. (1994). Cell cycle kinetics in rat prostatic epithelia: Nuclear migration during g2 phase. *J Urol, 152*(6 Pt 2), 2294-2299.

Lessard, J., & Sauvageau, G. (2003). Bmi-1 determines the proliferative capacity of normal and leukaemic stem cells. *Nature, 423*(6937), 255-260. doi: 10.1038/nature01572

Li, V. S. W., & Clevers, H. (2012). In vitro expansion and transplantation of intestinal crypt stem cells. *Gastroenterology, 143*(1), 30-34. doi: 10.1053/j.gastro.2012.05.017

Li, Y. Q., Roberts, S. A., Paulus, U., Loeffler, M., & Potten, C. S. (1994). The crypt cycle in mouse small-intestinal epithelium. *Journal of Cell Science, 107*, 3271-3279.

Livet, J., Weissman, T. A., Kang, H. N., Draft, R. W., Lu, J., Bennis, R. A., . . . Lichtman, J. W. (2007). Transgenic strategies for combinatorial expression of fluorescent proteins in the nervous system. *Nature, 450*(7166), 56-+. doi: 10.1038/nature06293

Lopez-Garcia, C., Klein, A. M., Simons, B. D., & Winton, D. J. (2010). Intestinal stem cell replacement follows a pattern of neutral drift. *Science, 330*(6005), 822-825. doi: 10.1126/science.1196236

Lundgren, O., Jodal, M., Jansson, M., Ryberg, A. T., & Svensson, L. (2011). Intestinal epithelial stem/progenitor cells are controlled by mucosal afferent nerves. *Plos One, 6*(2), e16295. doi: 10.1371/journal.pone.0016295

Marshman, E., Booth, C., & Potten, C. S. (2002). The intestinal epithelial stem cell. *Bioessays, 24*(1), 91-98. doi: 10.1002/bies.10028

Maton, A., Hopkins, J., McLaughlin, C. W., Johnson, S., Warner, M. Q., LaHart, D., & Wright, J. D. (1993). *Human biology and health*: Englewood Cliffs, N.J. : Prentice Hall.

Matsudaira, P. T., & Burgess, D. R. (1982). Organization of the cross-filaments in intestinal microvilli. *Journal of Cell Biology, 92*(3), 657-664. doi: 10.1083/jcb.92.3.657

Mayden, R. L., Tang, K. L., Conway, K. W., Freyhof, J., Chamberlain, S., Haskins, M., . . . He, S. (2007). Phylogenetic relationships of danio within the order cypriniformes: A framework for comparative and evolutionary studies of a model species. *Journal of Experimental Zoology Part B-Molecular and Developmental Evolution, 308B*(5), 642-654. doi: 10.1002/jez.b.21175

Merzel, J., & Leblond, C. P. (1969). Origin and renewal of goblet cells in the epithelium of the mouse small intestine. *American Journal of Anatomy, 124*(3), 281-305.

Montgomery, R. K., & Breault, D. T. (2008). Small intestinal stem cell markers. *Journal of Anatomy, 213*(1), 52-58. doi: 10.1111/j.1469-7580.2008.00925.x

Mosimann, C., Kaufman, C. K., Li, P., Pugach, E. K., Tamplin, O. J., & Zon, L. I. (2011). Ubiquitous transgene expression and cre-based recombination driven by the ubiquitin promoter in zebrafish. *Development, 138*(1), 169-177. doi: 10.1242/dev.059345

Muncan, V., Faro, A., Haramis, A. P. G., Hurlstone, A. F. L., Wienholds, E., van Es, J., . . . Clevers, H. (2007). T-cell factor 4 (tcf712) maintains proliferative compartments in zebrafish intestine. *Embo Reports, 8*(10), 966-973. doi: 10.1038/sj.embor.7401071

Mundlos, S. (2009). Gene action: Developmental genetics *Vogel and motulsky's human genetics: Problems and approaches*.

Ng, A. N. Y., de Jong-Curtain, T. A., Mawdsley, D. J., White, S. J., Shin, J., Appel, B., . . . Heath, J. K. (2005). Formation of the digestive system in zebrafish: Iii. Intestinal epithelium morphogenesis. *Developmental Biology, 286*(1), 114-135. doi: 10.1016/j.ydbio.2005.07.013

Pack, M., Solnica-Krezel, L., Malicki, J., Neuhauss, S. C., Schier, A. F., Stemple, D. L., . . . Fishman, M. C. (1996). Mutations affecting development of zebrafish digestive organs. *Development, 123*, 321-328.

Pack, M., SolnicaKrezel, L., Malicki, J., Neuhauss, S. C. F., Schier, A. F., Stemple, D. L., . . . Fishman, M. C. (1996). Mutations affecting development of zebrafish digestive organs. *Development, 123*, 321-328.

Pan, Y. A., Livet, J., Sanes, J. R., Lichtman, J. W., & Schier, A. F. (2011). Multicolor brainbow imaging in zebrafish. *Cold Spring Harb Protoc, 2011*(1), pdb prot5546. doi: 10.1101/pdb.prot5546

Pinto, D., & Clevers, H. (2005). Wnt, stem cells and cancer in the intestine. *Biology of the Cell, 97*(3), 185-196.

Potten, C. S., & Ellis, J. R. (2006). Adult small intestinal stem cells: Identification, location, characteristics, and clinical applications. In J. Morser, S. I. Nishikawa & H. R. Schöler (Eds.), *Stem cells in reproduction and in the brain* (Vol. 60, pp. 81-98): Springer Berlin Heidelberg.

Potten, C. S., Owen, G., & Booth, D. (2002). Intestinal stem cells protect their genome by selective segregation of template DNA strands. *Journal of Cell Science, 115*(11), 2381-2388.

Radtke, F., & Clevers, H. (2005). Self-renewal and cancer of the gut: Two sides of a coin. *Science, 307*(5717), 1904-1909. doi: 10.1126/science.1104815

Rakic, P. (2002). Pre- and post-developmental neurogenesis in primates. *Clinical Neuroscience Research, 2*(1-2), 29-39. doi: 10.1016/s1566-2772(02)00005-1

Rando, T. A. (2007). The immortal strand hypothesis: Segregation and reconstruction. *Cell, 129*(7), 1239-1243. doi: 10.1016/j.cell.2007.06.019

Rombout, J., Stroband, H. W. J., & Tavernethiele, J. J. (1984). Proliferation and differentiation of intestinal epithelial-cells during development of barbus-conchonius (teleostei, cyprinidae). *Cell and Tissue Research, 236*(1), 207-216. doi: 10.1007/bf00216533

Sachan, D. (2009). Decoding the genome mystery. Retrieved July 5, 2009

Sakamori, R., Das, S., Yu, S., Feng, S., Stypulkowski, E., Guan, Y., . . . Gao, N. (2012). Cdc42 and rab8a are critical for intestinal stem cell division, survival, and differentiation in mice. *The Journal of Clinical Investigation, 122*(3), 1052-1065. doi: 10.1172/JCI60282

Salic, A., & Mitchison, T. J. (2008). A chemical method for fast and sensitive detection of DNA synthesis in vivo. *Proceedings of the National Academy of Sciences of the United States of America, 105*(7), 2415-2420. doi: 10.1073/pnas.0712168105

Sancho, E., Batlle, E., & Clevers, H. (2003). Live and let die in the intestinal epithelium. *Current Opinion in Cell Biology, 15*(6), 763-770. doi: 10.1016/j.ceb.2003.10.012

Sancho, E., Batlle, E., & Clevers, H. (2004). Signaling pathways in intestinal development and cancer. *Annual Review of Cell and Developmental Biology, 20*, 695-723. doi: 10.1146/annurev.cellbio.20.010403.092805

Sangiorgi, E., & Capecchi, M. R. (2008). Bmi1 is expressed in vivo in intestinal stem cells. *Nature Genetics, 40*(7), 915-920.

Sato, T., van Es, J. H., Snippert, H. J., Stange, D. E., Vries, R. G., van den Born, M., . . . Clevers, H. (2011). Paneth cells constitute the niche for lgr5 stem cells in intestinal crypts. *Nature, 469*(7330), 415-+. doi: 10.1038/nature09637

Sato, T., Vries, R. G., Snippert, H. J., van de Wetering, M., Barker, N., Stange, D. E., . . . Clevers, H. (2009). Single lgr5 stem cells build crypt-villus structures in vitro without a mesenchymal niche. *Nature, 459*(7244), 262-U147. doi: 10.1038/nature07935

Savin, T., Kurpios, N. A., Shyer, A. E., Florescu, P., Liang, H. Y., Mahadevan, L., & Tabin, C. J. (2011). On the growth and form of the gut. *Nature, 476*(7358), 57-+. doi: 10.1038/nature10277

Schmidt, G. H., Garbutt, D. J., Wilkinson, M. M., & Ponder, B. A. J. (1985). Clonal analysis of intestinal crypt populations in mouse aggregation chimeras. *Journal of Embryology and Experimental Morphology, 85*(FEB), 121-130.

Schmidt, G. H., Winton, D. J., & Ponder, B. A. (1988). Development of the pattern of cell renewal in the crypt-villus unit of chimaeric mouse small intestine. *Development, 103*(4), 785-790.

Schonhoff, S. E., Giel-Moloney, M., & Leiter, A. B. (2004). Neurogenin 3-expressing progenitor cells in the gastrointestinal tract differentiate into both endocrine and non-endocrine cell types. *Developmental Biology, 270*(2), 443-454. doi: 10.1016/j.ydbio.2004.03.013

Scoville, D. H., Sato, T., He, X. C., & Li, L. H. (2008). Current view: Intestinal stem cells and signaling. *Gastroenterology, 134*(3), 849-864. doi: 10.1053/j.gastro.2008.01.079

Sherwood, L. (2010). *Fundamentals of physiology*: Brooks/Cole, Cengage Learning.

Simons, B. D., & Clevers, H. (2011). Stem cell self-renewal in intestinal crypt. *Experimental Cell Research, 317*(19), 2719-2724. doi: 10.1016/j.yexcr.2011.07.010

Snippert, H. J., Schepers, A. G., Delconte, G., Siersema, P. D., & Clevers, H. (2011). Slide preparation for single-cell-resolution imaging of fluorescent proteins in their three-dimensional near-native environment. *Nature Protocols, 6*(8), 1221-1228. doi: 10.1038/nprot.2011.365

Snippert, H. J., van der Flier, L. G., Sato, T., van Es, J. H., van den Born, M., Kroon-Veenboer, C., . . . Clevers, H. (2010). Intestinal crypt homeostasis results from neutral competition between symmetrically dividing lgr5 stem cells. *Cell, 143*(1), 134-144. doi: 10.1016/j.cell.2010.09.016

Starr, C. (2013). *Human biology, 10th ed*: Brooks/Cole Cengage Learning.

Starr, C., Evers, C. A., & Starr, L. (2008). *Biology: Concepts & applications: Concepts and applications*: Thomson Brooks/Cole.

Tank, P. W., & Grant, J. C. B. (2012). *Grant's dissector*: Wolters Kluwer Health.

Theodosiou, N. A., & Tabin, C. J. (2003). Wnt signaling during development of the gastrointestinal tract. *Developmental Biology, 259*(2), 258-271. doi: 10.1016/s0012-1606(03)00185-4

Thisse, C., Thisse, B., Schilling, T. F., & Postlethwait, J. H. (1993). Structure of the zebrafish snail1 gene and its expression in wild-type, spadetail and no tail mutant embryos. *Development, 119*(4), 1203-1215.

van den Brink, G. R., & Hardwick, J. C. H. (2006). Hedgehog wnteraction in colorectal cancer. *Gut, 55*(7), 912-914. doi: 10.1136/gut.2005.085902

van der Flier, L. G., & Clevers, H. (2009). Stem cells, self-renewal, and differentiation in the intestinal epithelium *Annual review of physiology* (Vol. 71, pp. 241-260).

van der Flier, L. G., van Gijn, M. E., Hatzis, P., Kujala, P., Haegebarth, A., Stange, D. E., . . . Clevers, H. (2009). Transcription factor achaete scute-like 2 controls intestinal stem cell fate. *Cell, 136*(5), 903-912. doi: 10.1016/j.cell.2009.01.031

Walker, W. A. (2004). *Pediatric gastrointestinal disease: Pathophysiology, diagnosis, management*: BC Decker.

Wallace, K. N., Akhter, S., Smith, E. M., Lorent, K., & Pack, M. (2005). Intestinal growth and differentiation in zebrafish. *Mechanisms of Development, 122*(2), 157-173. doi: 10.1016/j.mod.2004.10.009

Wallace, K. N., & Pack, M. (2003). Unique and conserved aspects of gut development in zebrafish. *Developmental Biology, 255*(1), 12-29. doi: 10.1016/s0012-1606(02)00034-9

Wang, Z. Y., Du, J. G., Lam, S. H., Mathavan, S., Matsudaira, P., & Gong, Z. Y. (2010). Morphological and molecular evidence for functional organization along the rostrocaudal axis of the adult zebrafish intestine. *Bmc Genomics, 11*. doi: 392

10.1186/1471-2164-11-392

Wang, Z. Y., Matsudaira, P., & Gong, Z. Y. (2010). Storm: A general model to determine the number and adaptive changes of epithelial stem cells in teleost, murine and human intestinal tracts. *Plos One, 5*(11). doi: 10.1371/journal.pone.0014063

Warga, R. M., & Kimmel, C. B. (1990). Cell movements during epiboly and gastrulation in zebrafish. *Development, 108*(4), 569-580.

Warga, R. M., & Nusslein-Volhard, C. (1999). Origin and development of the zebrafish endoderm. *Development, 126*(4), 827-838.

Westerfield, M. (2007). The zebrafish book. A guide for the laboratory use of zebrafish (danio rerio). University of Oregon Press: Eugene.

Winton, D. J., Blount, M. A., & Ponder, B. A. J. (1988). A clonal marker induced by mutation in mouse intestinal epithelium. *Nature, 333*(6172), 463-466.

Woo, K., Shih, J., & Fraser, S. E. (1995). Fate maps of the zebrafish embryo. *Current Opinion in Genetics & Development, 5*(4), 439-443.

Yang, Q., Bermingham, N. A., Finegold, M. J., & Zoghbi, H. Y. (2001). Requirement of math1 for secretory cell lineage commitment in the mouse intestine. *Science, 294*(5549), 2155-2158. doi: 10.1126/science.1065718

Yu, Y. M., Arora, A., Min, W. X., Roifman, C. M., & Grunebaum, E. (2009). Edu incorporation is an alternative non-radioactive assay to h-3 thymidine uptake for in vitro measurement of mice t-cell proliferations. *Journal of Immunological Methods, 350*(1-2), 29-35. doi: 10.1016/j.jim.2009.07.008

Yui, S. R., Nakamura, T., Sato, T., Nemoto, Y., Mizutani, T., Zheng, X., . . . Watanabe, M. (2012). Functional engraftment of colon epithelium expanded in vitro from a single adult lgr5(+) stem cell. *Nature Medicine, 18*(4), 618-623. doi: 10.1038/nm.2695

Zaret, K. S. (2001). Hepatocyte differentiation: From the endoderm and beyond. *Current Opinion in Genetics & Development, 11*(5), 568-574. doi: 10.1016/s0959-437x(00)00234-3

Zeng, C. B., Pan, F. H., Jones, L. A., Lim, M. M., Griffin, E. A., Sheline, Y. I., . . . Mach, R. H. (2010). Evaluation of 5-ethynyl-2 '-deoxyuridine staining as a sensitive and reliable method for studying cell proliferation in the adult nervous system. *Brain Research, 1319*, 21-32. doi: 10.1016/j.brainres.2009.12.092